

國立交通大學

半導體材料與製程產業研發碩士專班

碩士論文

高耐熱透明聚醚醯亞胺之合成及其應用於可撓式元件
界面接著性探討

High Tg, transparent BAPP-ODPA polyimide for flexible
device applications: Its synthesis, properties, and ITO/PI
adhesion improvement

研究生：黃少農

指導教授：呂志鵬 博士

中華民國九十八年二月

高耐熱透明聚醚醯亞胺之合成及其應用於可撓式元件界面接著性探討

High T_g, transparent BAPP-ODPA polyimide for flexible device applications: Its synthesis, properties, and ITO/PI adhesion improvement

研究生：黃少農

Student : Shao-Nung Huang

指導教授：呂志鵬

Advisor : Dr. Jihperng (Jim) Leu



February 2009

Hsinchu, Taiwan, Republic of China

中華民國九十八年二月

高耐熱透明聚醯醯亞胺之合成及其應用於可撓式元件界面接著性探討

學生:黃少農

指導教授:呂志鵬 博士

國立交通大學半導體材料與製程產業研發碩士班

摘 要

隨著全球化跨國商務與旅遊驟增，消費者對產品之輕量性、機動性和多功能性等需求、已經帶動新世代 IC 產品組裝於軟性基板上，例如電子紙、衛星內可撓性的太陽能電池以及行動電話和數位相機的軟性電子組件等。雖然這些可撓性軟性基板材料具有不錯的性質，然而也有某些限制和問題急需克服，諸如過高的熱膨脹係數(CTE)、較低的玻璃轉換溫度(Tg)、較低的加工溫度、較高的氧氣和水穿透率、元件的老化以及其與障礙層、硬膜 (hard coat) 或者透明的導電層等多層結構的黏著力(adhesion)等。

因此本論文分為兩大部分: (一) 針對可撓性軟性基板因具較低的玻璃轉換溫度(Tg)而使得後續製程加工溫度受到限制之問題，使用兩種高分子單體(4,4'-oxydiphthalic anhydride, ODPa 和 2,2'-bis[4-(4-aminophenoxy)phenyl]propane, BAPP)開發具高穿透度、高玻璃轉換溫度和熱穩定性佳的聚亞醯醯胺薄膜，來克服可撓式元件當前所遭遇到的問題; (二) 可撓性產品因多層結構中彼此的材料性質迥異，如熱膨脹係數的差異，造成層與層間因黏著力不佳而發生彼此剝離的現象，此現象導致可撓性產品使用壽命與可靠度下降。所以提昇可撓性產品結構中層與層間的黏著性，是當前一個非常重要的課題。在本研究中利用氧氣電漿改質新穎聚亞醯醯胺薄膜表面的方法，改變新穎聚亞醯醯胺薄膜表面之化學鍵結狀態與組成成分，藉此提升透明導電層(氧化銻錫)與所合成之新穎聚亞醯醯胺兩者間的界面黏著性，提高可撓式產品之使用壽命與可靠度。

研究結果顯示，由於因共軛而互相堆疊的苯環會吸收可見光的藍光波段，造成聚亞醯醯胺薄膜呈現出黃褐顏色，但此現象也造成聚亞醯醯胺鏈間彼此相互吸引，使得聚亞醯醯胺具有良好的物性。本研究中所選用的高分子單體 BAPP 與 ODPa，它

們分別具有丙烷基與醚基，藉此可以達到降低或消除苯環間電荷轉移(Charge Transfer)的現象和提升材料之可撓性，使得其所聚合成之新穎聚亞醯胺薄膜在厚度為 80um 時，其透光度可達到 98%以及 230°C 和 495°C 的玻璃轉換溫度和熱裂解溫度。

在第二部份裡，本研究利用 X 射線光電子能譜(XPS)鑑定聚亞醯胺薄膜表面的化學狀態改變。並使用四點彎曲抗折儀器(four-point bending)來量測氧化銻錫與新穎聚亞醯胺界面黏著性。研究結果顯示，聚亞醯胺的表面經過氧氣電漿改質過後，新穎聚亞醯胺表面的 C-OH 鍵結成分大幅增加，因而提供孤對電子(lone pair)作為載體(donor)，與氧化銻錫中的金屬原子(銻、錫)形成共軛共價鍵，而使得其與氧化銻錫界面的黏著力由未處理時之 3.01 J/m^2 提升至 8.7 J/m^2 。因而證實氧氣電漿的表面改質方法確實提升了可撓式產品的壽命與可靠度。



High Tg, transparent BAPP-ODPA polyimide for flexible device applications: Its synthesis, properties, and ITO/PI adhesion improvement

Student: Shao-Nung Huang

Advisor: Dr. Jihperng (Jim) Leu

Industrial Technology R&D Master Program on Semiconductor Materials and Processes

National Chiao Tung University

Abstract

As the progress of globalization makes the world flat, the desire for lightweight, mobility, and versatility has energized a sleuth of new IC products mounted onto flexible substrates, such as e-paper, flexible solar cell in satellite, or key components using plastic substrate sin cell phones and digital cameras. While these materials offer many attractive features, they also impose limitations and challenges such as high CTE, lower Tg, low processing temperatures, problematic adhesion strength in the multiple film stacking (with barrier, hard coat, or conductive transparent oxides), high O₂ and water permeation, and device degradation.

Thus, there are two objections in this thesis: (1) To develop a novel flexible, polyimide substrate with high Tg in order to enable higher processing temperatures for better electric performance. A novel and transparent polyimide has been synthesized by using 4,4'-oxydiphthalic anhydride (ODPA) and 2,2'-bis[4-(4-aminophenoxy)phenyl]propane (BAPP). (2) Due to dissimilar materials properties (E, CTE and Poisson ratio), flexible devices may induce to delaminate between layers. The behavior will decrease the lifetime of devices and low the reliability. Therefore, the adhesion of multiple-layered structure used in the typical flexible devices

is a critical reliability issue. In this thesis, oxygen plasma was used to modify the surface chemical states of BAPP-ODPA polyimide. The surface modification method had enhanced the adhesion at ITO and BAPP-ODPA polyimide interface. For purpose, it could improve the lifetime and reliability of flexible devices.

According to the research, the coloration of polyimide had higher light absorption at 400 nm due to the conjugation of benzene rings in stacked packing. However, the transparency of the BAPP-ODPA polyimide in the visible region was found to be 98 % because the ether linkage and bulky group in BAPP and ODPA monomers destroyed benzene stacking to minimize or eliminate charge transfer. Moreover, the BAPP-ODPA polyimide demonstrated superior thermal stability with Td at 495 °C and a glass transition temperature of 230 °C.

In the second part, the surface of BAPP-ODPA polyimide was modified by oxygen plasma and the changes of surface chemical states were characterized by X-ray Photoelectron Spectroscopy (XPS). The interfacial adhesive strength was determined by four-point bending system. According to the XPS results, the component ratio of C-OH increased in a great quantity by oxygen plasma. The adhesive strength of un-treatment polyimide/ITO was 3.01 J/m². After oxygen plasma treatment, the interfacial adhesion had obviously increased to 8.7 J/m². We could suggest that the adhesion of ITO/BAPP-ODPA polyimide improved with the increase of C-OH. The force of coordinate covalent bond was explained to help the improvement of interfacial adhesion. Because the oxygen element in C-OH bond provided a lone pair as donor to attract the metal elements in ITO structure (In, Sn), the interfacial adhesive strength between ITO and BAPP-ODPA polyimide had definitively improved by oxygen plasma treatment.

Acknowledgements

終於可以換我寫誌謝了，時間真的過的很快，才一轉眼已經來這間實驗室兩年多了，首先最感謝呂志鵬老師不厭其煩的教導，沒有你的砥礪沒有今天站在這裡的我，真的發自內心的感謝。並感謝清大廖建能教授與交大潘福民教授於口試期間，細心且親切的指正本論文疏失缺漏之處，並提供許多寶貴意見，使本論文更加完整。

在這兩年多的研究生活中，誠摯感謝國源學長與幸玲學姊不厭其煩的指導我，讓對有機化學一竅不通的我，能略窺門徑。感謝 NIP 實驗室同甘共苦的夥伴們，昱涵學長、泰印學長、牧龍學長、明義學長、弘恩學長、王智學長和柏村學長的陪伴與胡鬧，還有林宏洲實驗室的梁宗琦學長，我會記得每次熬夜奮鬥與球場熱血的日子，以及施雅學妹、茹瑛學妹、晉誠學弟、婉婷學妹、柏政學弟及瑜修學弟的沒幫上什麼忙，但至少帶給我歡樂。這裡真的很友善也很親切，大家都像一家人，只是這次剛好換我離開，不過我知道這不是一個結束，因為還有你們。

最後，我要特別給我的家人與女友詩盈一個大大的擁抱，沒有你們一路默默支持，我無法完成這篇論文，除了謝謝與感恩，沒有更美好的形容詞了，在此我附上我最真摯的感激。

Contents

摘 要	iii
Abstract	v
Acknowledgements.....	vii
Contents	viii
List of Tables.....	x
List of Figures	xii
Chapter 1 Introduction	1
1.1 Background	1
1.2 Overview	5
Chapter 2 Literature Review	6
2.1 Introduction of Flexible Devices	6
2.1.1 Varieties of Flexible Substrates.....	8
2.1.2 Requirements of Polymer substrates.....	11
2.1.3 Synthesis of High Tg, Transparent Polyimide Substrate.....	13
2.1.3.1 Polyimide of alicyclic dianhydride and aliphatic diamine.....	13
2.1.3.2 Polyimide of aliphatic dianhydride and alicyclic diamine.....	15
2.1.3.3 Polyimide of aromatic dianhydride and diamine [37]	18
2.3 Methods to Improve the Reliability of Flexible Devices	20
2.3 Analysis of thin-film interfacial strength	23
Chapter 3 Experimental	28
3.1 Sample Preparation	28
3.1.1 Synthesis of Polyimide	28
3.1.2 Plasma Surface Modification of Polyimide	32
3.1.3 Indium tin oxide layer deposition	32
3.1.4 Samples preparation for four-point bending adhesion test	34
3.2 Experimental Procedures	38
3.3 Instrumentation	40
3.3.1 Fourier-Transform Infrared Spectroscopy (FT-IR).....	40

3.3.2 Differential Scanning Calorimetry (DSC)	40
3.3.3 Thermo-Gravimetric Analysis (TGA)	42
3.3.4 Ultraviolet-Visible (UV-Vis) spectroscopy	43
3.3.5 Reactive Ionic Etching (RIE).....	43
3.3.6 X-ray Photoelectron Spectroscopy (XPS)	44
3.3.6.1 Surface Chemical States Analysis of BAPP-ODPA Polyimide by XPS.....	46
3.3.7 Four-Point Bending System.....	48
Chapter 4 Results and Discussion	50
4.1 Synthesis and Characterization of Polyimide	50
4.1.1 ODPA purity.....	50
4.1.2 The effects of solvent of anhydrous or hydrous DMAc for film-forming ability	50
4.1.3 Structural Analysis by FTIR Spectroscopy.....	52
4.1.4 Transmittance in UV-Vis.....	54
4.1.5 Thermal Properties of BAPP-ODPA Polyimide	56
4.1.5.1 The glass transition temperature (T _g) measured by differential Scanning Calorimetry (DSC).....	56
4.1.5.2 Thermo-Gravimetric Analysis (TGA)	57
4.2 XPS analysis of surface chemical states of BAPP-ODPA polyimide	59
4.3 Adhesion of ITO/Polyimide Interface	72
Table 4.10 The critical loads and adhesion strength of various ITO/BAPP-ODPA polyimide samples (untreated and plasma-treated) based on 5 valid measurement data	75
4.4 Discussion	76
4.4.1 Characteristic properties of BAPP-ODPA polyimide	76
4.4.1.1 Transparency	76
4.4.1.2 Thermal stability	77
4.4.1.3 Transparency vs. Thermal stability	78
4.4.2 Surface chemical states of BAPP-ODPA polyimide.....	79
4.4.3 Surface chemical states vs. interfacial adhesion	84
Chapter 5 Conclusions	86

List of Tables

Table 2.1 Properties of typical polymeric films as plastic substrates.	12
Table 2.2 The thermal and optical properties of polyimides based on CBDA and alicyclic dianhydride.....	16
Table 2.3 Glass transition temperatures (T _g) and initial thermal decomposition temperatures (T _d) of alicyclic polyimides.....	18
Table 2.5 Values of the pull strength, surface roughness and increased chemical states in copper/polyimides samples.....	21
Table 3.1 Chemical structures and transmission of two transparent polyimides.....	29
Table 3.2 Chemical structures and molecular weights of ODPA and BAPP monomers	30
Table 3.3 Experimental conditions for oxygen plasma pre-treatment of BAPP-ODPA polyimide films.....	32
Table 3.4 Experimental parameters for ITO film deposition.....	33
Table 4.1 Absorption peak positions of four types of chemical bonds.....	52
Table 4.2 Main components and their binding energies in C 1s and O 1s XPS signals of BAPP-ODPA polyimide.....	62
Table 4.3 Experimental conditions for plasma pre-treatment surface of BAPP-ODPA polyimides.....	62
Table 4.4 Carbon 1s spectrum: binding energies and composition quantification of untreated BAPP-ODPA polyimide film.....	63
Table 4.5 Carbon 1s spectrum: binding energies and composition quantification of BAPP-ODPA polyimide film modified by oxygen plasma at a RF Power of 50W.	63
Table 4.6 Carbon 1s spectrum: binding energies and composition quantification of BAPP-ODPA polyimide film modified by oxygen plasma at a RF Power of 100W.	64
Table 4.7 Oxygen 1s spectrum: binding energies and composition quantification of untreated BAPP-ODPA polyimide film.....	68
Table 4.8 Oxygen 1s spectrum: binding energies and composition quantification of BAPP-ODPA polyimide film modified by oxygen plasma at a RF Power of 50W.	68
Table 4.9 Oxygen 1s spectrum: binding energies and composition quantification of BAPP-ODPA polyimide film modified by oxygen plasma at a RF Power of 100W.	68
Table 4.11 The average and standard deviation values for three different ITO/PI samples.....	76
Table 4.12 The component ratios of BAPP-ODPA polyimide surface of untreated film and modified films under various conditions in carbon 1s.....	81

Table 4.13 The component ratios of BAPP-ODPA polyimide surface of un-treat film and modified films under various conditions in oxygen 1s..... 81

Table 4.14 Binding energies of typical chemical bonds. 82

Table 4.14 The component ratios of C-OH in C and O 1s versus adhesion strength 85



List of Figures

Figure 1.1 The charge transfer occurred in a traditional polyimide. Dash line indicated inter-molecular charge transfer, while solid line illustrated intra-molecular charge transfer.	2
Figure 1.2 Delamination was occurred between layers due to the residual stress.....	4
Figure 2.1 Global flexible display revenues forecast	7
Figure 2.2 Sony’s flexible, full-color OLED Display.....	7
Figure 2.3 TFT/OLED were on the steel foil substrate.	9
Figure 2.4 Device structure of the plastic solar cell and its substrate was glass	10
Figure 2.5 Structure of TTFT fabricated on PET substrate	10
Figure 2.6 The synthesized of polyimides from aliphatic diamine and alicyclic diahydride	14
Figure 2.7 The synthetic of polyimides from aliphatic diahydride and alicyclic diamine	17
Figure 2.8 Synthesis of the fluorinated polyimides and various aromatic dianhydrides	19
Figure 2.9 Peel strength of sputtered copper to (a) unmodified and argon plasma–modified Kapton E(N) and (b) unmodified and argon plasma–modified Upilex S plotted with various duration times for argon plasma modification.....	22
Figure 2.10 Effect of Ar plasma-pretreatment time of the PTFT film on the graft concentration and the T-peel adhesion strength of the ITO/GMA/PTFE assembly.	23
Figure 2.11 The common techniques for measuring the interfacial strength.....	25
Figure 2.12 Three different fracture modes	25
Figure 2.13 Macroscopic adhesion of fracture	26
Figure 2.14 Adhesion depending on the fracture phase angle	27
Figure 3.1 Reaction steps in the synthesis of BAPP-ODPA polyimide.....	31
Figure 3.2 PVD sputtering system for the deposition of ITO films.....	33
Figure 3.3 Preparation process steps of a sandwich sample for 4-point bending test	35
Figure 3.4 C-clamp and small clamps for fixing the sample	36
Figure 3.5 The stacking structure of sandwich sample for measuring the adhesion of ITO/polyimide interface.....	36
Figure 3.6 (a) Schematic drawing of four-point bend test sample and (b) a typical load vs. displacement curve for four-point bend test.	37
Figure 3.7 Flow-chart of experimental procedures.....	39
Figure 3.8 Heat Flux DSC	41
Figure 3.9 Power Compensation DSC.....	42

Figure 3.10 The principle of photoelectron generation	45
Figure 3.11 The XPS instrument and its principle. (Not clear to me about the principles)	46
Figure 3.12 The XPS Peak Fitting program	47
Figure 3.13 Schematic diagram of sandwich sample for four-point bending test	49
Figure 3.14 Schematic diagram of micro-mechanical test system	49
Figure 4.1 ODPA reacted easily with moisture in the atmosphere to form a dicarboxylic acid.....	50
Figure 4.2 The BAPP-ODPA polyimide was brittle when a hydrous DMAc solvent was used.....	51
Figure 4.3 The BAPP-ODPA polyimide was tough and useful when an anhydrous DMAc solvent was used.....	51
Figure 4.4 The FT-IR spectra of BAPP-ODPA polyimides cured at low (60 °C) and high temperature (250 °C).....	53
y-axis: Absorbance (arb. unit).....	53
Figure 4.5 The BAPP-ODPA poly(amic acid) was dehydrated to form polyimide upon heating.....	54
Figure 4.6 The photographs of traditional polyimide and BAPP-ODPA polyimide illustrating their difference in transmission rate	55
Figure 4.7 The UV-visible spectra of BAPP-ODPA and traditional polyimide films at 80 m	56
Figure 4.8 DSC curves of BAPP-ODPA polyimide in two heating scans. Tg was determined in 2nd heating scan at a 20 °C/min heating/cooling rate.....	57
Figure 4.9 The TGA curve of BAPP-ODPA polyimide under nitrogen at a heating rate of 20 °C/min.....	58
Figure 4.10 Binding states of the (a) carbon and (b) oxygen atoms in the repeating unit of BAPP-ODPA.....	61
Figure 4.11 The XPS C 1s spectra of untreated BAPP-ODPA polyimide films.....	65
Figure 4.12 The XPS C 1s spectra of BAPP-ODPA polyimide film plasma modified at a RF power of 50W.....	66
Figure 4.13 The XPS C 1s spectra of BAPP-ODPA polyimide film plasma modified at a RF power of 100W.....	67
Figure 4.14 The XPS O 1s spectra of untreated BAPP-ODPA polyimide films	69
Figure 4.15 The XPS O 1s spectra of BAPP-ODPA polyimide film at a RF power of 50W.....	70
Figure 4.16 The XPS O 1s spectra of BAPP-ODPA polyimide film at a RF power of 100W.....	71
Figure 4.17 Load-displacement graph of ITO/untreated PI sample under 4-point bending	

test.....	73
Figure 4.18 Surface morphology of (a) ITO (b) BAPP-ODAP polyimide thin film (c) Epoxy resin in samples after 4-point bending test.....	74
Figure 4.19 Adhesion strength values for ITO/untreated BAPP-ODPA and for ITO/plasma-treated BAPP-ODPA samples.....	75
Figure 4.20 The different molecular structures between commercial and transparent PI.	77
Figure 4.20 Proposed surface reaction mechanisms in BAPP-ODPA polyimide thin films were modified by oxygen plasma.	83



Chapter 1 Introduction

1.1 Background

Recently, flexible devices had received more attentions due to their advantages such as light weight, smaller size, high mobility, and low cost. Their applications had emerged in many new territories such as solar cell [1], flexible display, e-paper, or RFID [2] based on polymer or metal substrate. The requirements of flexible substrate typically included bendability, thermal stability, and reliability. In terms of low cost, polymeric substrate was preferred over metal foil due to its ease in fabrication based on roll-to-roll process. Among the candidate materials such as polyethylene terephthalate (PET), polyethylene naphthalate (PEN), polycarbonate (PC), polyethersulfone (PES), or polyimide (PI), PET and PEN were often used as flexible substrates for their low-cost and ease of fabrication. While these materials offer many attractive features, they also impose limitations and challenges such as high coefficient of thermal expansion (CTE), lower glass transition temperature (T_g), low processing temperatures, dubious adhesive strength in multiple films stacking (with barrier, hard coat, or conductive transparent oxides), high O_2 and water permeation, and device degradation. In order to acquire excellent electric resistivity of indium tin oxide (ITO) onto flexible polymer substrate, its processing temperature typically is higher than 200°C . Thus, PET and PEN could not survive these high temperature processing steps due to their lower glass transition temperature ($<150^\circ\text{C}$). As a result, the development of transparent polymer substrate with high glass transition temperature and excellent thermal stability has been fervently engaged in the past few years. [3, 4]

Among all high-temperature polymers, polyimides (PI) in particular had received most attention. Typically, polyimides possessed rigidity and excellent high-temperature resistance, mechanical strength and superior electrical properties due to the chemical

structure of imide link in the molecular main chain of polyimide. [5] Therefore, polyimides could be processed and exposed in rigorous working circumstances such as high processing temperature and hard-wearing. However, traditional polyimide could not be used in the optical devices because its transmittance was low ($< 60\%$). The key factors affecting the coloration of polyimide were two folds: (1) The charge of π electrons in diamine was transferred to dianhydride inter-molecularly and intra-molecularly as illustrated by Figure 1.1 and (2) It had higher light absorption at 400 nm due to the conjugation of benzene rings in stacked packing. [6] In order to fabricate colorless polyimide, one had to minimize or eliminate the benzene rings stacking and low charge transfer. [7]

Hence, one of the objectives in the thesis is to develop a colorless polyimide as substrate for flexible devices applied.

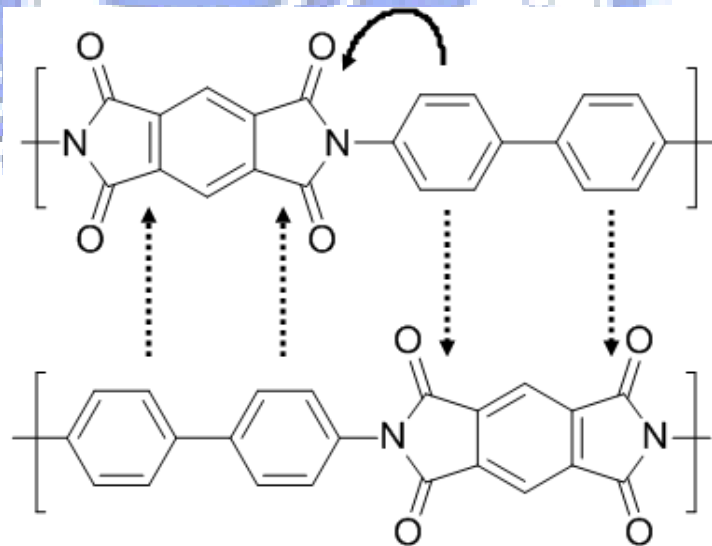
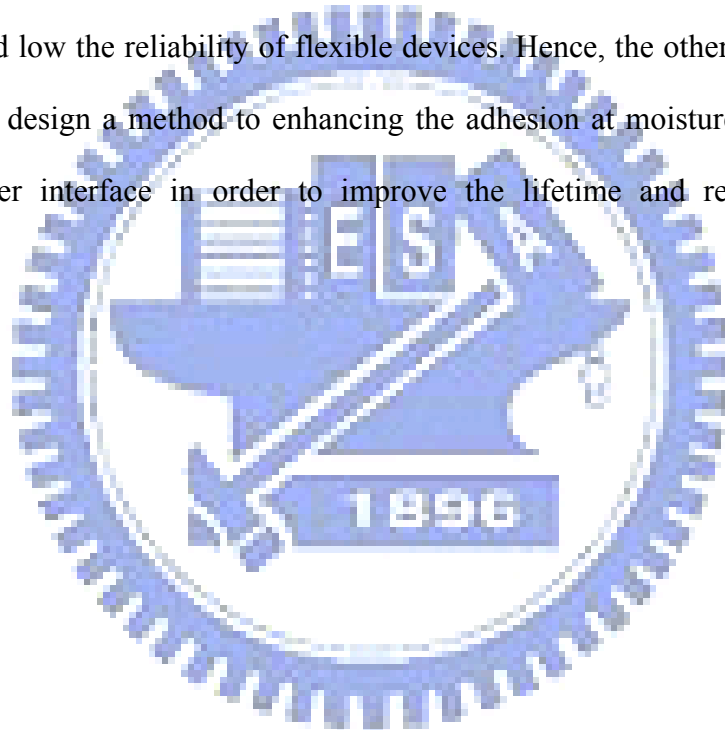


Figure 1.1 The charge transfer occurred in a traditional polyimide. Dash line indicated inter-molecular charge transfer, while solid line illustrated intra-molecular charge transfer.

On the other hand, the adhesion of multiple-layered structure used in the typical flexible devices is a critical reliability issue. V. Teixeira [8] reported that residual stress affected the integrity of PVD coatings. The stress induced the failures into device due to the effect of thermal expansion misfit. The multiple layered structures were delaminated as illustrated by Figure 1.2. According to the past research, delamination, buckling or catastrophic failure might be induced owing to mechanical integrity of the multiple layered structure with dissimilar materials properties such as Young's modulus, coefficient of thermal expansion and Poisson ratio. The behavior will decrease the lifetime and low the reliability of flexible devices. Hence, the other of objectives in the thesis is to design a method to enhancing the adhesion at moisture barrier/polymer or ITO/polymer interface in order to improve the lifetime and reliability of flexible devices.



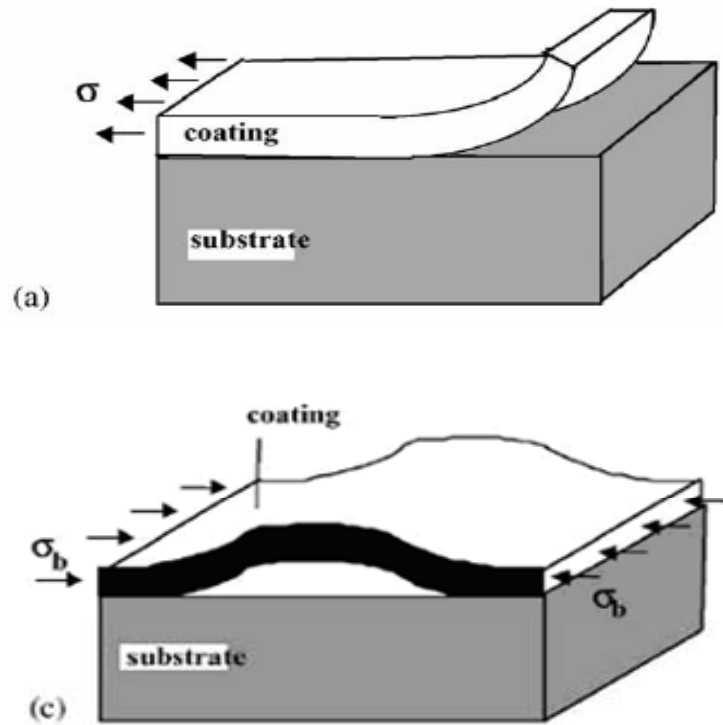


Fig. 5. Failure modes of a thin coating under residual stress : (a) delamination (coating under tensile stress and “weak” interface, adherence); (c) buckling (coating under compressive stress)

Figure 1.2 Delamination was occurred between layers due to the residual stress

1.2 Overview

This thesis was organized into five chapters. Following a concise introduction in Chapter 1, Chapter 2 reviewed the synthesis of transparent polyimide, the key factors affecting the coloration of polyimide, and methods for improving the reliability of devices. Chapter 3 described the synthesis processes of BAPP-ODPA polyimide, sample preparation, experimental procedures of the plasma treatment, instrumentation and how to calculate the interface strength. Chapter 4 described key results and discussion. Specifically, the characteristic properties of BAPP-ODPA polyimide were investigated. The correlation between surface chemical states of BAPP-ODPA polyimide and the interfacial adhesion improvement of ITO/BAPP-ODPA polyimide were examined and proposed. Then key results and conclusion of this thesis were summarized in Chapter 5.



Chapter 2 Literature Review

2.1 Introduction of Flexible Devices

With the advancement of technology, people sought for products with mobility and convenience. Flexible plastic substrates are the focus of increasing attention due to their broad, potential applications in portable devices such as cellular phones, personal digital assistants (PDAs), notebook computers, and ultra mobile personal computers (UMPC), etc., which require light weight, transportability, good impact resistance, and mechanical durability. [9] iSuppli forecasts that the total flexible display market will reach US\$2.8 billion by 2013, a 35-times expansion from about US\$80 million in 2007 as shown in Figure 2.1. [10] Clearly, flexible devices will be one of the next great emerging products with huge market potential. Many international corporations have invested vast resource in the R&D of flexible electronic devices for a long time. For example, Sony Corporation successfully developed a flexible, full-color OLED display as shown in Figure 2.2. [11] Although flexible devices had many advantages such as its light weight, thin thickness and small size, their broad adoption had been hindered by several issues; namely (1) low processing temperature and (2) poor thermal stability and reliability due to dissimilar materials properties (E, CTE and Poisson ratio). Hence, it is a critical issue to develop a novel flexible substrate that can overcome problems such as low T_g and low processing temperatures. Among various flexible substrates (stainless steel foil, ultrathin glass sheet, and polymer thin films), polymer substrates had received more attention because of its low cost, excellent optical characteristic, and easier production based on roll-to-roll technology.

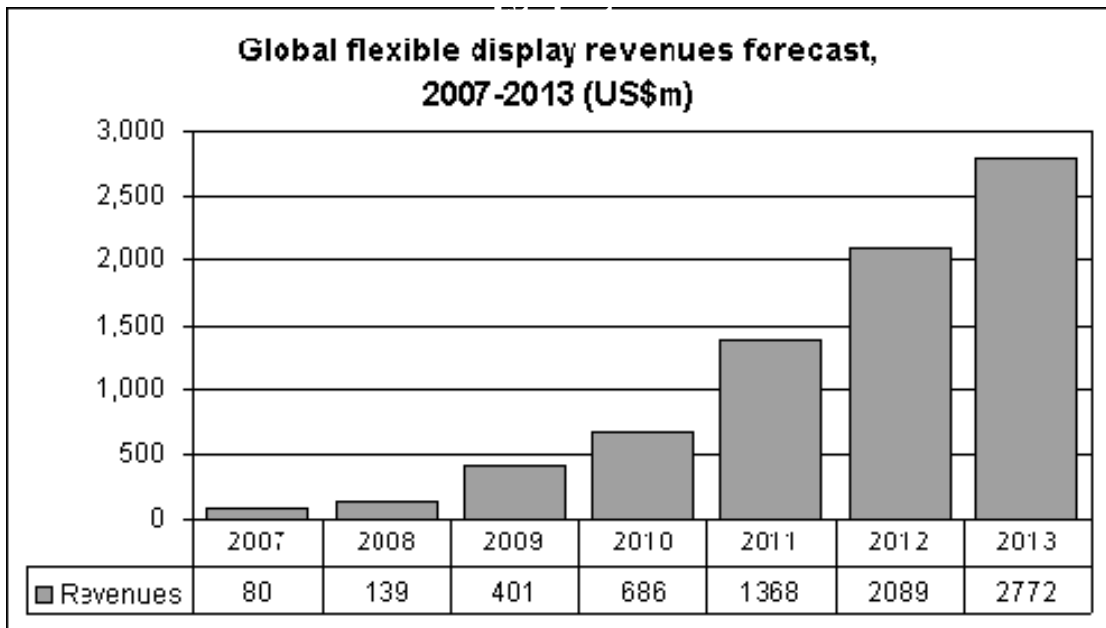


Figure 2.1 Global flexible display revenues forecast



Figure 2.2 Sony's flexible, full-color OLED Display

2.1.1 Varieties of Flexible Substrates

In the past few years, stainless steel foil shown in Figure 2.3 [12], ultrathin glass sheet shown in Figure 2.4 [13], and a variety of plastic polymer films as shown in Figure 2.5 [14] have been considered as possible substrate choices for flexible device. [15]

Steel foil had excellent properties as a barrier layer to overcome water and oxygen transmission, but it was hard to handle multiple bends. Due to its T_g over 900°C , steel foil had good thermal stability. Therefore, steel foil could sustain high processing temperature. Another problem was that the weight of stainless steel foil was too heavy to fabricate big size products because these substrates could not be conveniently conveyed.

Ultrathin glass substrates with polymer coating might be suitable for displays with good performance, but it had been limited by its flexibility in use. Moreover, glass substrates were not suitable for some specific applications such as electronic maps and smart cards. The issues of flexibility, weight, and safety were important in glass substrates because glass substrates were very brittle and could not be easily deformed. Flexible polymer substrates, for example, polyethylene terephthalate (PET) and polyethylene naphthalate (PEN), had been used for flexible devices due to their low cost, easier to produce, more robust, compact, and lighter weight than glass substrates. While they were very hopeful products, the plastic polymer substrates, however, were limited by their low processing temperature, low T_g ($< 150^\circ\text{C}$) [16], high heat-induced shrinkage, high moisture and oxygen permeability, and low chemical resistance. [17] For instance, high temperature pre-deposition thermal annealing ($\geq 200^\circ\text{C}$) of the transparent conducting oxide (TCO) as the transparent electrode was typically employed in the fabrication of organic light-emitting devices. But, TCO on the plastic

polymer substrate usually exhibited lower transparency, higher resistance and poorer adhesion compared to that on the glass substrate. [17] Thus, However, commercial polyimide (PI) had excellent potential to use for flexible devices because it had possession of high glass transition temperature ($T_g > 250\text{ }^\circ\text{C}$) [18], inherent toughness, mechanical strength and remarkable thermal stability. A major drawback of polyimide for the optical applications had been the poor transparency ($< 60\%$) [19] in the visible light range because it had higher light absorption at 400 nm due to conjugation of benzene rings in stacked packing. [20] The approaches of improving transmittance of polyimides were to destroy the benzene rings stacking and/or to decrease the charge transfer to make them colorless [19, 20], which will be discussed further in Chapter 3. According to above the studies, the requirements of polymer substrate were lighter weight, thinner, high transparent, easily carried and good thermal stability.

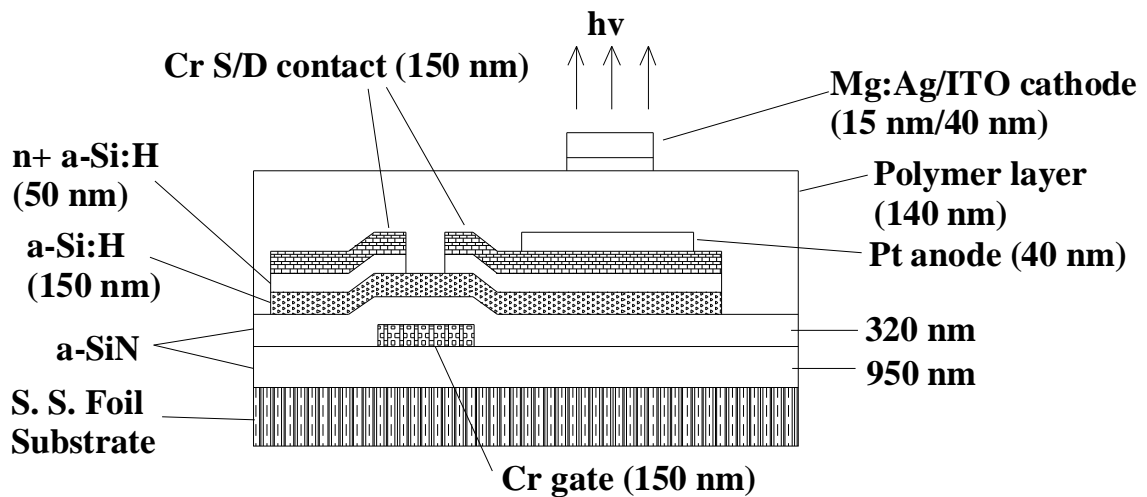


Figure 2.3 TFT/OLED were on the steel foil substrate.

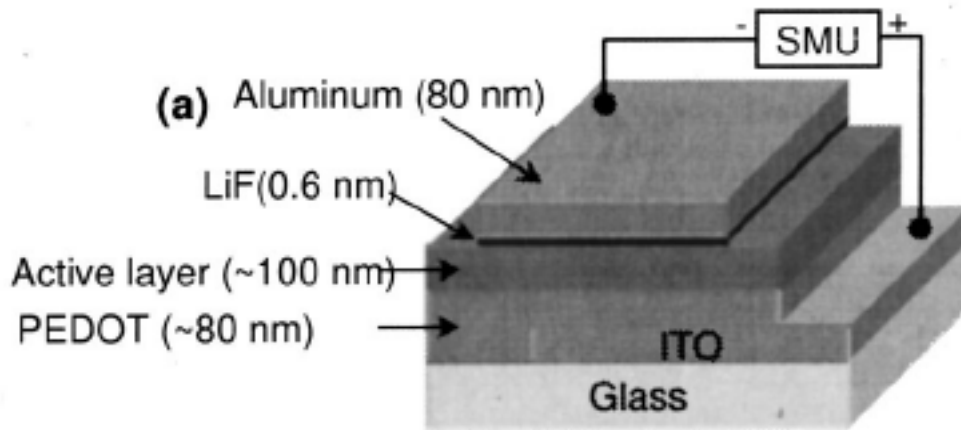


Figure 2.4 Device structure of the plastic solar cell and its substrate was glass

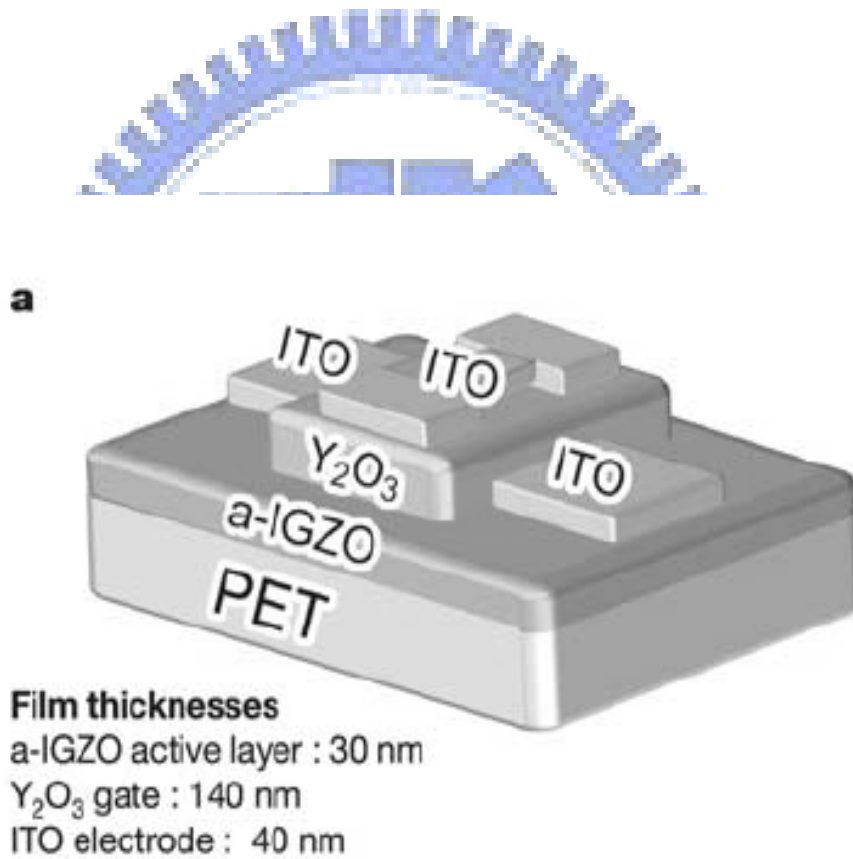


Figure 2.5 Structure of TFT fabricated on PET substrate

2.1.2 Requirements of Polymer substrates

Recently, flexible devices using polymer substrates had received a lot of attention because these flexible devices had advantages of being thinner, light weight, flexible, thermal stability and tough. Furthermore, polymer substrates provided a possibility of cost reduction since these devices were fabricated in roll-to-roll processing and printing technology. Therefore, polymer materials were the best choice as the substrates for flexible devices. Table 2.1 [21] showed the material properties such as transmittance, refractive index, glass transition temperature (T_g), coefficient of thermal expansion (CTE), and etc. of commercial films for applications as the flexible substrates. Although polycarbonate (PC) and cyclic olefin co-polymer (COC) had high light transmittance, the coefficient of thermal expansion (CTE) of these polymers and thermal stability could not meet the requirements for flexible devices. The CTE of PC and COC about 70-75 ppm/°C was much greater than those of inorganic materials such as ITO, Si_3N_4 , SiO_2 , at about 5 ppm/°C or that of Al metal, 5 ppm/°C. [22, 23] When polymer substrate was stacked with inorganic materials such as Si_3N_4 as diffusion barrier or indium tin oxide as the transparent conducting electrode, or their combination in the flexible devices, large thermal stress was induced in the multi-layered structure upon thermal cycling due to their CTE mismatch in thermal expansion. Tensile stress in the deposited film may cause through-thickness microcracking while compressive stress tended to promote microcrack propagation along the interface. [24] Buckling can occur when there was a pre-existing flaw at the organic/inorganic interface and when the in-plane compressive stress exceeded a critical value. [25] Such behavior and phenomena arisen either as-deposit or upon thermal cycling may result in catastrophic failure of flexible devices. Thus, it was a critical issue to address the

thermo-mechanical integrity of the functional coated components [24] or mutli-layered structure in flexible devices.

In terms of the requirements on the thermal properties, polymer substrates had to possess excellent thermal resistance at temperature above 200°C, because they were exposed to the high temperature (> 200 °C) during the deposition of TCO with a low resistance and high transmittance. Consequently, even though PET and PEN had superior CTE than PC and COC, they were still not preferred to be used as flexible substrates due to their lower glass transition temperatures, < 150 °C, although a post-treatment step may improve its thermal and electric properties. In contrast, polyimide (PI) had exceptional glass transition temperature (> 300 °C) and low coefficient of thermal expansion (< 20 ppm/°C). But it was not suitable for transparent, flexible device products due its yellowish-brown coloration and low light transmittance. (< 60 %) [19] Therefore, the first objective of this work is to develop a novel, high Tg (> 200 °C) and transparent (transmittance > 90%) polyimide substrate for flexible device applications.

Table 2.1 Properties of typical polymeric films as plastic substrates.

	PET	PEN	PC	COC	PES	PI
Thickness (mm)	0.1	0.1	0.1	0.1	0.1	0.1
Total light transmittance (%)	90.4	87.0	92.0	94.5	89.0	30–60
Retardation (nm)	Large	Large	20	7	<10	Large
Refractive index	1.66	1.75	1.59	1.51	1.6	—
Glass transition temperature (°C)	80	150	145	164	223	300 <
Coefficient of thermal expansion (ppm/°C)	33	20	75	70	54	8–20
Water absorption ratio (%)	0.5	0.4	0.2	<0.2	1.4	2.0–3.0
H ₂ O barrier (g m ⁻² day ⁻¹)	9	2	50	—	80	—

2.1.3 Synthesis of High Tg, Transparent Polyimide Substrate

Polyimides had been widely used in microelectronics industries because they had excellent thermal, mechanical, and electronic properties. [25] However, the applications of polyimides in optical devices were limited due to their color in yellow to deep brown. The main reasons causing the coloration of polyimide were the intra-molecular and inter-molecular charge transfer interactions between alternating electron-donor (diamine) and electron-acceptor (dianhydride). [26-28] In order to overcome these issues, several series of linear aromatic polyimide films had been synthesized and characterized with the objective of obtaining maximum optical transparency. The major and common method was to vary the molecular structure so as to reduce charge transfer interactions between polymer chains to lower the intensity of color in the resulting polymer films. Therefore, the strategy was to use dianhydrides of lower electron-acceptability and diamines of lower-donatability as monomers for weakening the charge transfer interactions. The high-temperature stability of polyimides was sacrificed by using alicyclic dianhydride or diamine monomers due to the incorporation of less stable aliphatic segments. [29-33] In the following sections, the synthesis of polyimides based on different alicyclics and aliphatics anhydride /or amine will be reviewed.

2.1.3.1 Polyimide of alicyclic dianhydride and aliphatic diamine

M. Goyal *et al.* [34] synthesized aliphatic polyimides (P-XBTA) as shown in Figure 2.6, by a high-pressure polycondensation of the salt monomers, consisting of aliphatic diamines with various methylene chain lengths ($x=4-12$) and 3,3',4,4'-benzophenonetetracarboxylic acid (BTA), under 200-250 MPa at 200-320 °C. However, the salt monomers with odd numbered methylene chains were more susceptible to thermally induced cross-linking than their even-numbered counterparts.

The melting temperatures of the polyimides decreased with increasing aliphatic chain length, which can be attributed to the observed increase in susceptibility toward cross linking.

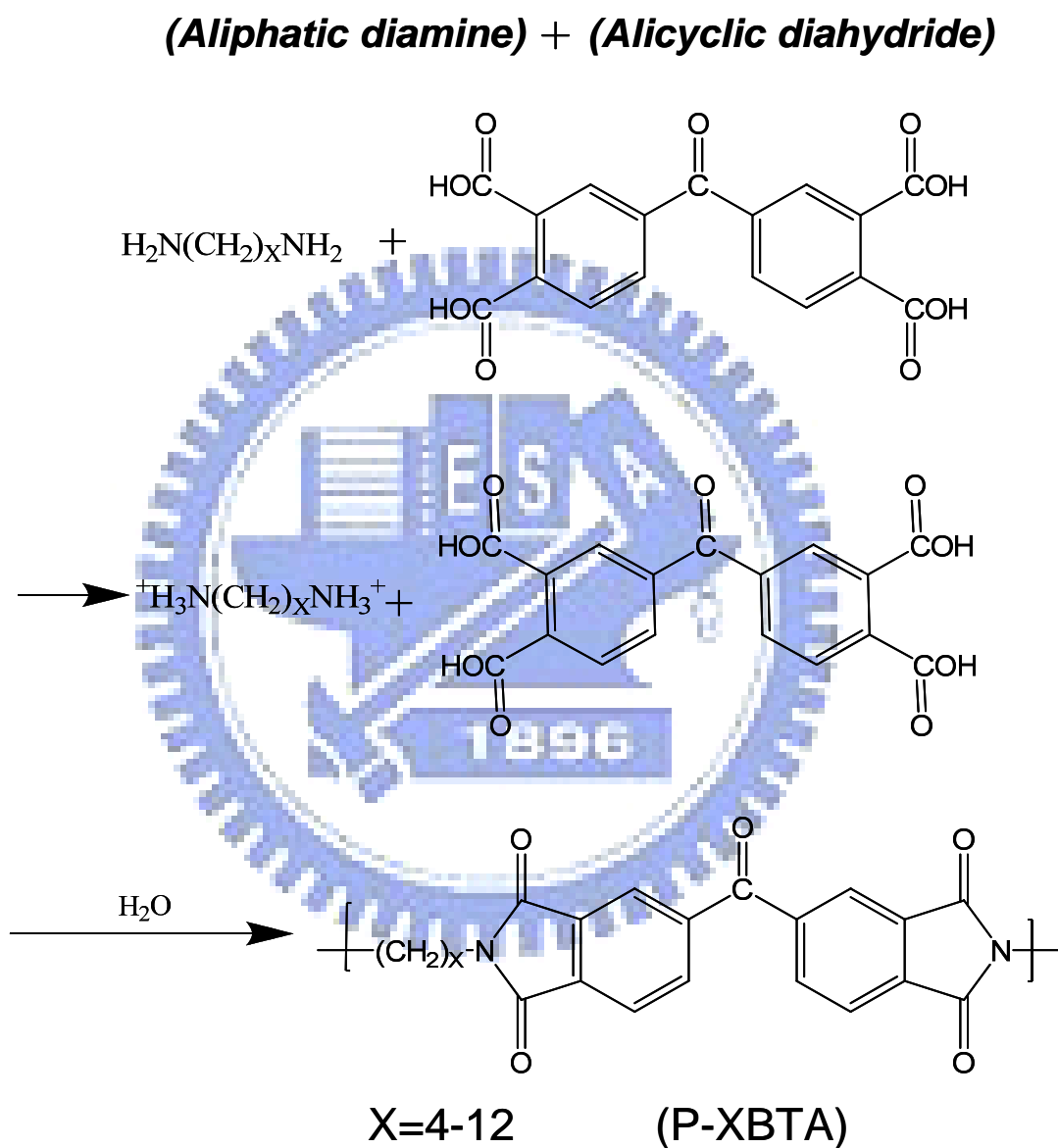


Figure 2.6 The synthesized of polyimides from aliphatic diamine and alicyclic dianhydride

2.1.3.2 Polyimide of aliphatic dianhydride and alicyclic diamine

Hideo Suzuki *et al.* [35] had investigated the temperature resistance and light transmission rate of polyimide films. The polyimides were synthesized using cyclobutane-1,2,3,4-tetracarboxylic dianhydride (CBDA) and several kinds of aromatic diamine. As indicated in Table 2.2, the films of 2, 3, 4, and 5 had a transmittance, at least 80 %, whereas the films of 6 and 7 exhibited transmittances as low as 63.9 and 48 %, respectively. These results indicated that the films based on CBDA and aromatic diamines had better transparencies than those entirely based on alicyclic monomers. It is interesting that a random polymer (5) prepared from a mixture of CBDA and benzophenone tetracarboxylic dianhydride in a 9:1 molar ratio with diaminodiphenylether shows a higher thermal stability than that of 3 while still keeping a high transmittance.

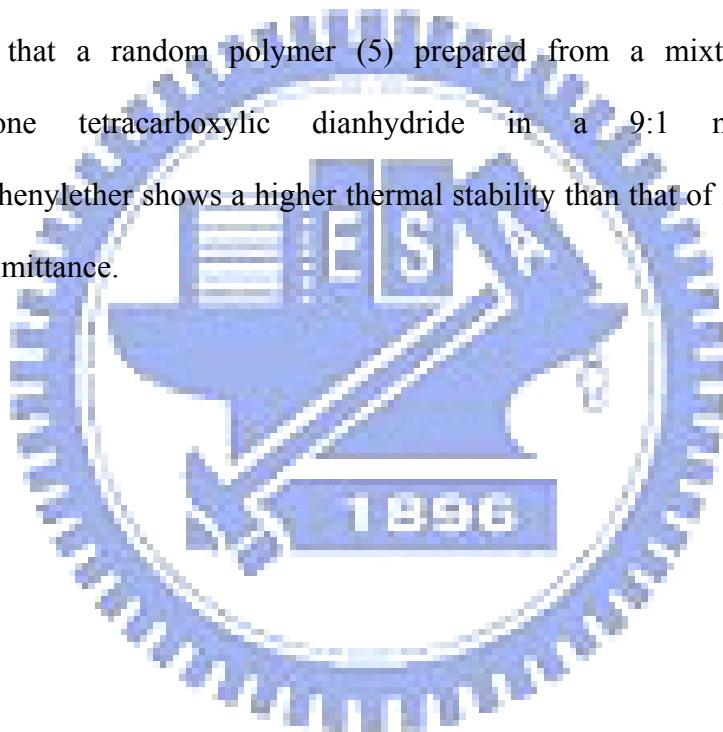
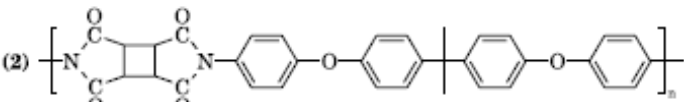
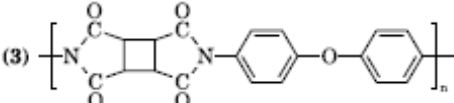
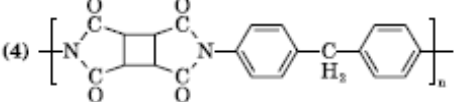
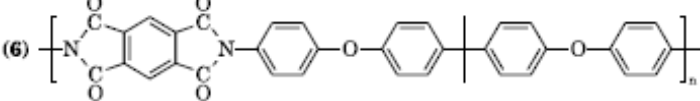
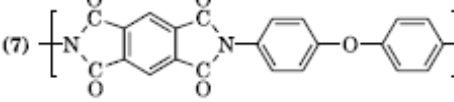


Table 2.2 The thermal and optical properties of polyimides based on CBDA and alicyclic dianhydride

Polyimides	Percent Transmission (%)	Thermal Decomposition Temperature (°C)
(2) 	85.8	454
(3) 	82.1	456
(4) 	81.0	452
(5) $\left\{ \begin{array}{l} \left[\text{N} \begin{array}{c} \text{O} \\ \diagup \diagdown \\ \text{C} \quad \text{C} \\ \diagdown \diagup \\ \text{O} \end{array} \begin{array}{c} \text{O} \\ \diagup \diagdown \\ \text{C} \quad \text{C} \\ \diagdown \diagup \\ \text{O} \end{array} \text{N} \begin{array}{c} \text{C}_6\text{H}_4 \\ \\ \text{O} \\ \\ \text{C}_6\text{H}_4 \end{array} \end{array} \right]_m + \\ \left[\text{N} \begin{array}{c} \text{O} \\ \diagup \diagdown \\ \text{C} \quad \text{C} \\ \diagdown \diagup \\ \text{O} \end{array} \begin{array}{c} \text{O} \\ \diagup \diagdown \\ \text{C} \quad \text{C} \\ \diagdown \diagup \\ \text{O} \end{array} \text{N} \begin{array}{c} \text{C}_6\text{H}_4 \\ \\ \text{C} \\ \\ \text{C}_6\text{H}_4 \end{array} \end{array} \right]_n \end{array} \right\}$ $\Sigma m / \Sigma n = 9 / 1$	80.2	478
(6) 	63.9	473
(7) 	48.0	530

* All films were 50 μm thick.



The preparation of polyimides based on an alicyclic dianhydride, 3-carboxyl-methylcyclopentane-1,2,4-tricarboxylic acid dianhydride, and three conventional aromatic diamines, and the characterization of their solubility, optical properties, and thermal properties were investigated by Jie Yin *et al.* [36] Their synthesis processes were illustrated in Figure 2.7. It was reported that all three alicyclic polyimides exhibited low glass transition temperature (T_g : about 180 °C). This clearly indicated that the alicyclic group possessed much higher flexibility than the aromatic

group. Furthermore, three alicyclic polyimides have almost identical glass transition temperature. This identity in T_g of polyimides based on diamines with different rigidity may also indicate that the alicyclic group in polyimides exhibits much greater flexibility and plays a deciding role in the possibility of segment motion. The UV-Vis spectra showed that PI-1, PI-2, and PI-3 were transparent compared to yellow-brownish in commercial polyimides. The absorptions of the alicyclic polyimides were quite low, not only in the visible light range (400–700 nm), but also in the near-UV range (300–400 nm). Thus, PI-1, PI-2, and PI-3 films were almost transparent and colorless.

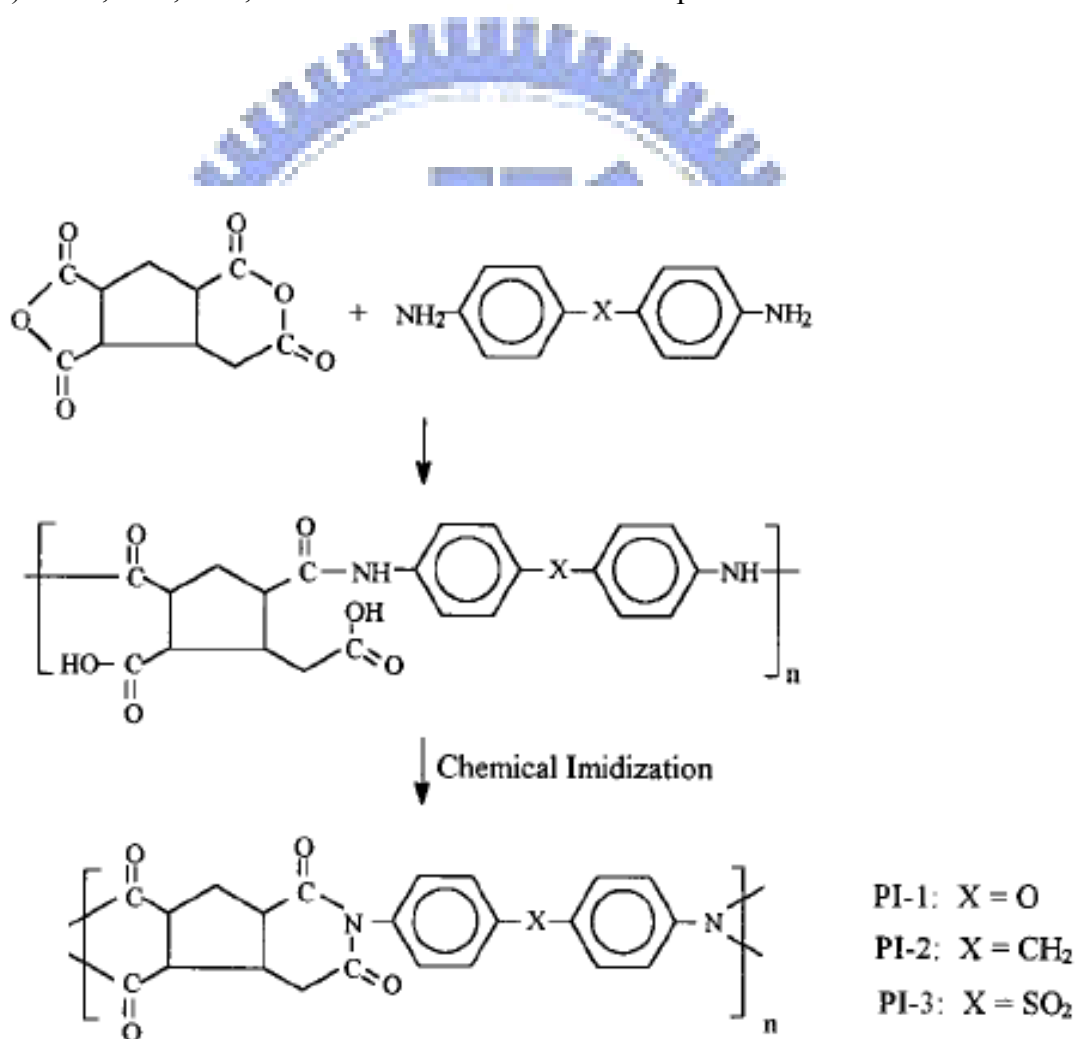


Figure 2.7 The synthetic of polyimides from aliphatic dianhydride and alicyclic diamine

Table 2.3 Glass transition temperatures (T_g) and initial thermal decomposition temperatures (T_d) of alicyclic polyimides

Samples	PI-1	PI-2	PI-3
T_g ($^{\circ}\text{C}$) ^a	182.2	180.8	180.8
T_d ($^{\circ}\text{C}$) ^b	447.6	441.8	477.4

^a Scan rate: 20 $^{\circ}\text{C}/\text{min}$

^b Scan rate: 20 $^{\circ}\text{C}/\text{min}$; N_2 protection.

2.1.3.3 Polyimide of aromatic dianhydride and diamine [37]

Yang *et al.* [37] had investigated the organosoluble and light-colored fluorinated polyimides from 4,4'-Bis(4-amino-2-trifluoromethylphenoxy)biphenyl and various aromatic dianhydrides. The reaction steps for the synthesis of fluorinated polyimides 5a–5f were illustrated in Figure 2.8. The T_g values of these polyimides were in the 247–313 $^{\circ}\text{C}$ range, depending on the structure of the dianhydride component and decreasing with the increasing flexibility of the polymer backbones. As expected, the polyimide (5e) obtained from ODPA showed the lowest T_g due to the presence of a flexible ether linkage between the phthalimide units, and the polyimide (5a) derived from PMDA exhibited the highest T_g due to the rigid pyromellitimide unit. In Table 2.5, the 6FDA and ODPA produced fairly transparent and almost colorless polyimide films, in contrast to other dianhydrides. These results were attributed to the reduction of the intermolecular charge-transfer complex (CTC) between alternating electron-donor (diamine) and electron-acceptor (dianhydride) moieties. The light colors of the polyimides with the 3F groups in their diamine moieties can be explained by the reduced intermolecular interactions. The bulky and electron-withdrawing 3F group in diamine 2 was effective in decreasing CTC formation between polymer chains through

steric hindrance and the inductive effect (by decreasing the electron-donating property of diamine moieties).

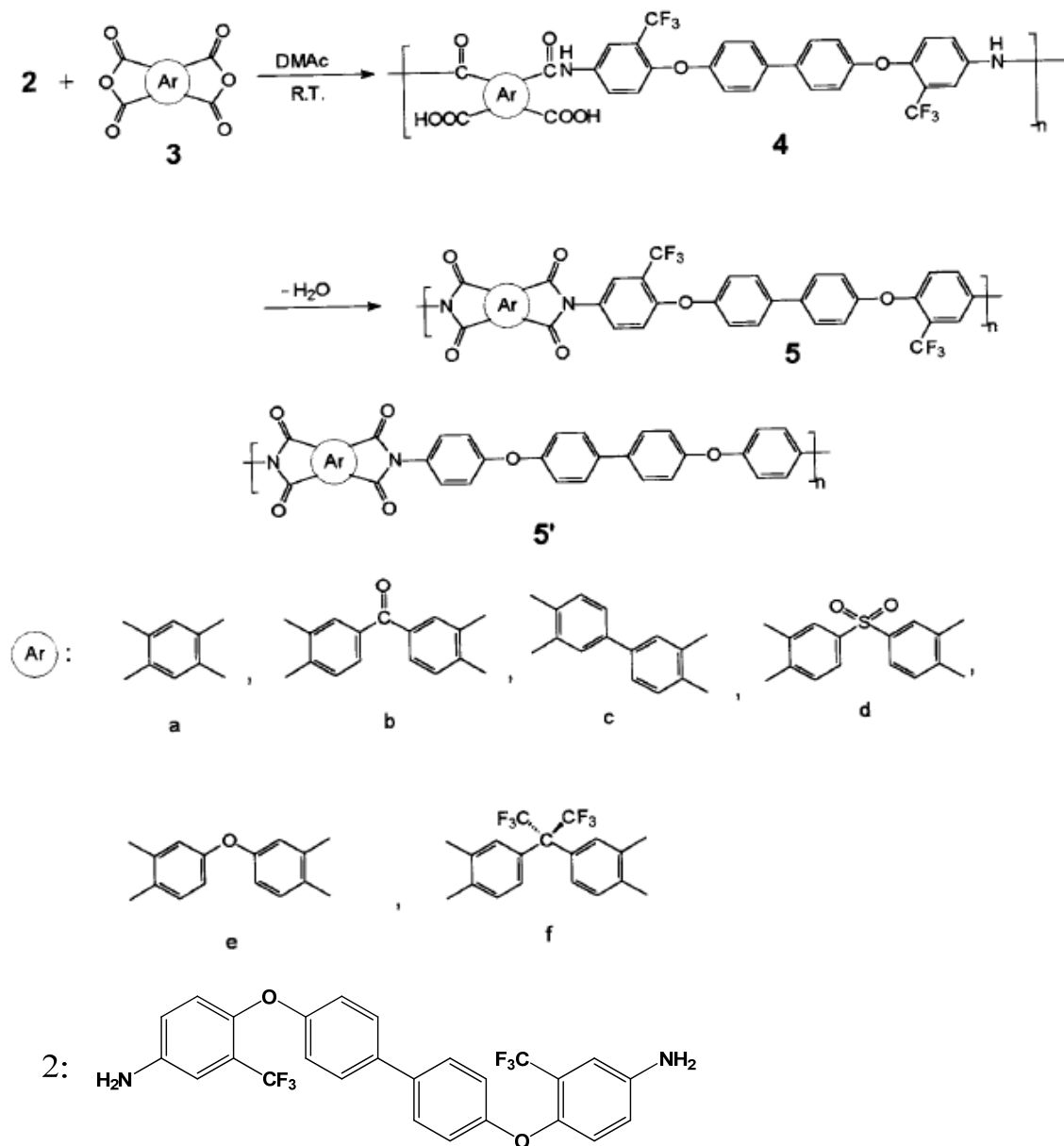


Figure 2.8 Synthesis of the fluorinated polyimides and various aromatic dianhydrides

2.3 Methods to Improve the Reliability of Flexible Devices

The study of inorganic/organic materials interfacial adhesive strength has received considerable interest in recent years. Industrial application of such compound systems covers a wide range, from decorative coatings to microelectronics. In these applications, plasma modification is an empirically established procedure for improving the adhesion strength between the inorganic and organic materials, which is one of the key properties for the technological use of these compound systems. [38]

The influence of the surface chemistry and morphology of polymer thin films such as polyimides and poly(tetrafluoroethylene) (PTFE) on the adhesive strength had been widely investigated and discussed. Sanda *et al.* [39] investigated two model systems of polyimide and found that copper interacts with the ether group. Haight *et al.* [40] reported a complex formation between copper and the delocalized π -electrons of the polyimide, but excluded the fact that the ether group is involved in the interaction. Nakamura *et al.* [41] reported that oxygen plasma etching changed the chemical state of the polyimide surface. Table 2.4 showed the changes in surface chemical states. The main influence of improved adhesion was attributed to C-O bonding not surface roughness as illustrated in Table 2.5. Lin *et al.* [42] found that polyimide surface roughness affected its adhesion strength with copper. Figure 2.9 had demonstrated that argon plasma modification was a good method that greatly increased the strength of the adhesion of copper to polyimide.

For ITO/polymer system, Jinzhu *et al.* [43] found that the T-peel adhesion strength between the graft-modified PTFE and sputtered ITO increased with the graft concentration up to an optimal graft concentration. The adhesion was further enhanced by thermal post-treatment of the laminates after ITO metallization as illustrated by

Figure 2.10. The strong adhesion in the present ITO/graft-modified PTFE laminates arose from the strong interaction between the sputtered ITO and the functional groups of the graft chains, as well as the fact that the graft chains were covalently tethered on the PTFE surfaces.

Table 2.4 Measured and calculated concentration of various chemical states in C 1s spectrum.

Bonding	Treatment (%)		
	As-received	Oxygen plasma etching	Dipped into water after oxygen plasma etching
C=O	13.6	5.9	5.8
C-OH	0	10.5	22.4
C-O	30.4	44.3	34.3

Table 2.5 Values of the pull strength, surface roughness and increased chemical states in copper/polyimides samples.

	Oxygen plasma etching for 3 min	Dipped into water after oxygen plasma etching
Pull strength (MPa)	30.4	14.7
Roughness Ra (nm)	8	29
Increased chemical component	C-O	C-OH

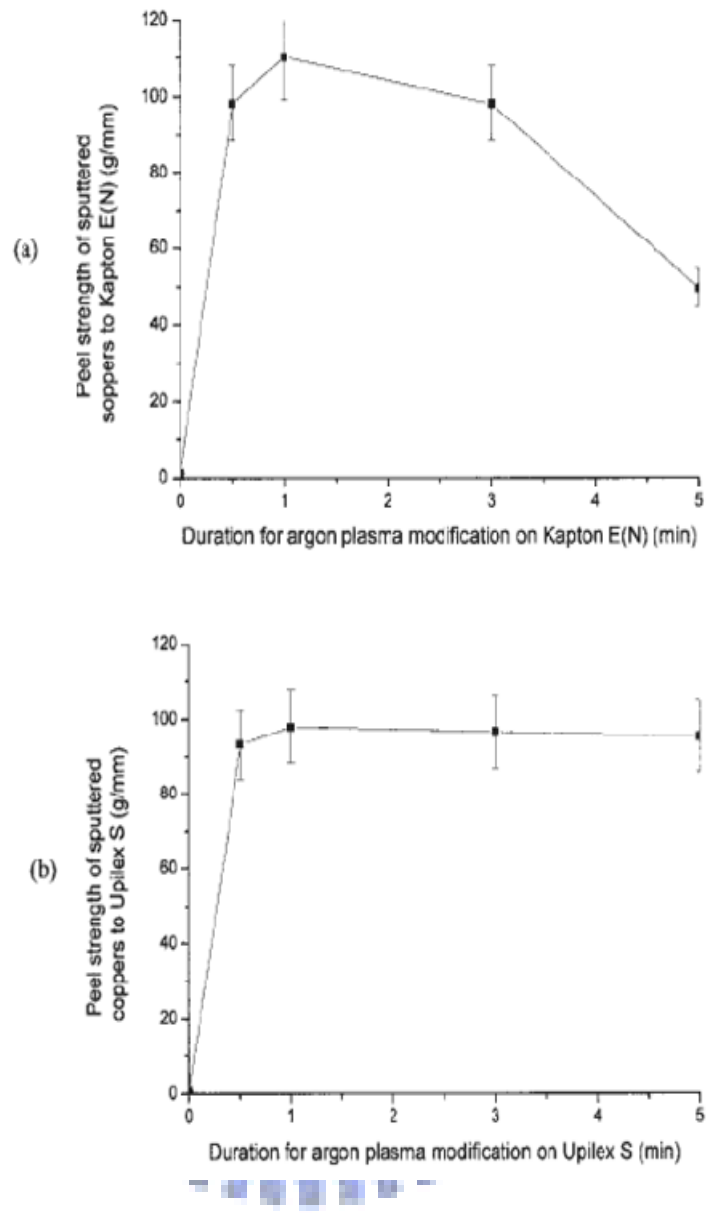


Figure 2.9 Peel strength of sputtered copper to (a) unmodified and argon plasma–modified Kapton E(N) and (b) unmodified and argon plasma–modified Upilex S plotted with various duration times for argon plasma modification.

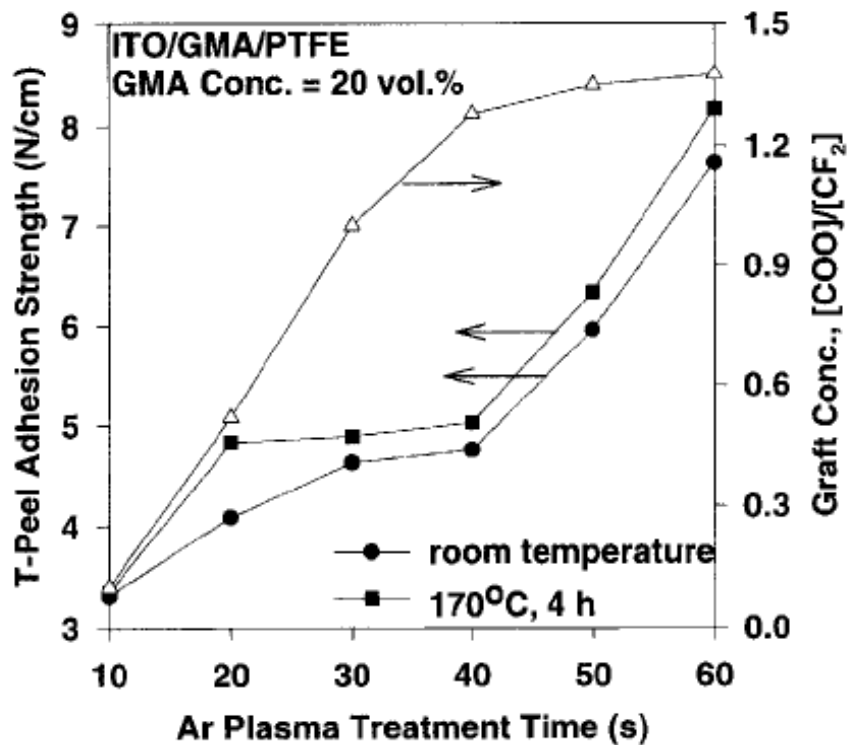


Figure 2.10 Effect of Ar plasma-pretreatment time of the PTFT film on the graft concentration and the T-peel adhesion strength of the ITO/GMA/PTFE assembly.

2.3 Analysis of thin-film interfacial strength

Mittal *et al.* [44] reported that there were about 300 techniques to measure the interfacial strength between multi-layers. Apparently, there was no single technique which would apply in every situation because different samples needed a suitable technique to obtain the correct interfacial strength. Nevertheless, the common techniques included stud pull [45], scotch tap [46], and scratch test [47] as shown in Figure 2.11. The scotch tape test could not measure a quantitative value. Meanwhile, the large plastic energy induced by stud-pull and shear test that could not measure the true adhesion at the interface. Especially for adhesion at thin film interface, traditional methods are very difficult to induce the crack at thin film interface. In contrast,

techniques such as superlayer test, four-point bending test, and nanoindentation test [48] have been widely employed to measure adhesion in recent years due to their capability of quantitative measurement. Among these adhesion tests, four-point bending test was the best choice as the technique to determine interfacial adhesive strength because it had at least two advantages:

- (1) It had a fixed fracture mode and a fracture phase angle $\Psi \sim 43^\circ$. [49]
- (2) A quantitative fracture-energy value, G_c was obtained based on the sensitive value of energy release rate.

In general, there were three different fracture modes based on the different surface displacement modes including tensile mode (mode I), in-plane shearing mode (mode II) and tearing mode (mode III). The different modes had the different fracture phase angle Ψ as shown in Figure 2.12 [50] The mode-mixity can be quantified using the fracture phase angle Ψ and associated with stress intensity factor K . In this study, two test systems were loaded in two-dimensional plane under mode I and mode II fracture contributions. The fracture phase angle ranges from 0° for pure mode I fracture to 90° pure mode II fracture. The fracture phase angle can be determined by Eq. (2.1) :

$$\Psi = \tan^{-1}\left(\frac{K_{II}}{K_I}\right) \quad (2.1)$$

The relationship between stress intensity factor K and energy release rate G under three fracture modes can be written as following Eq. (2.2) :

$$G = \frac{K_I^2}{E'} + \frac{K_{II}^2}{E'} + \frac{K_{III}^2(1+\nu)}{E'} \quad (2.2)$$

where K_I , K_{II} , K_{III} : stress intensity factor of three fracture modes

E : Young's modulus ν : Poisson's ratio

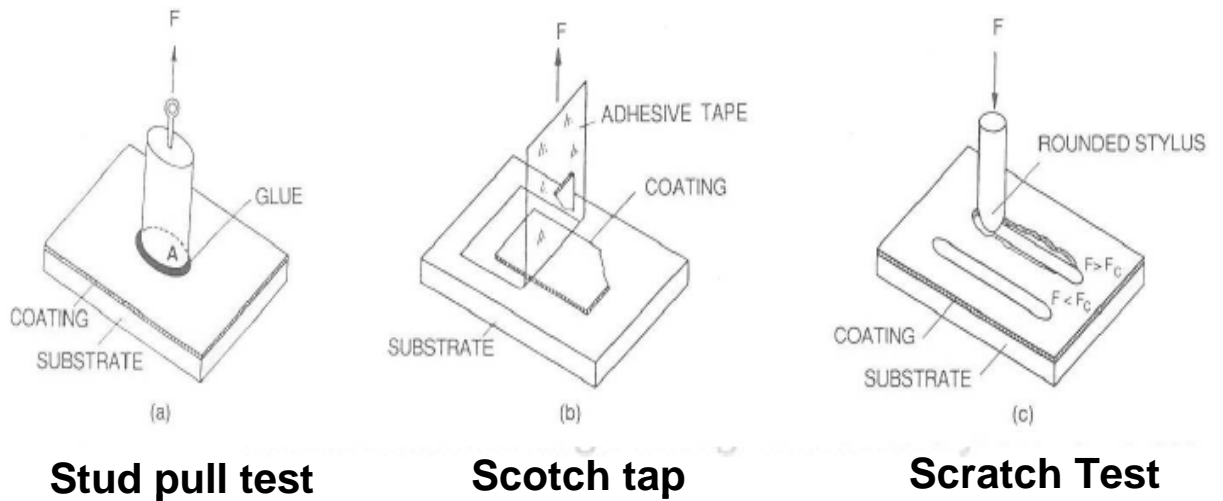


Figure 2.11 The common techniques for measuring the interfacial strength

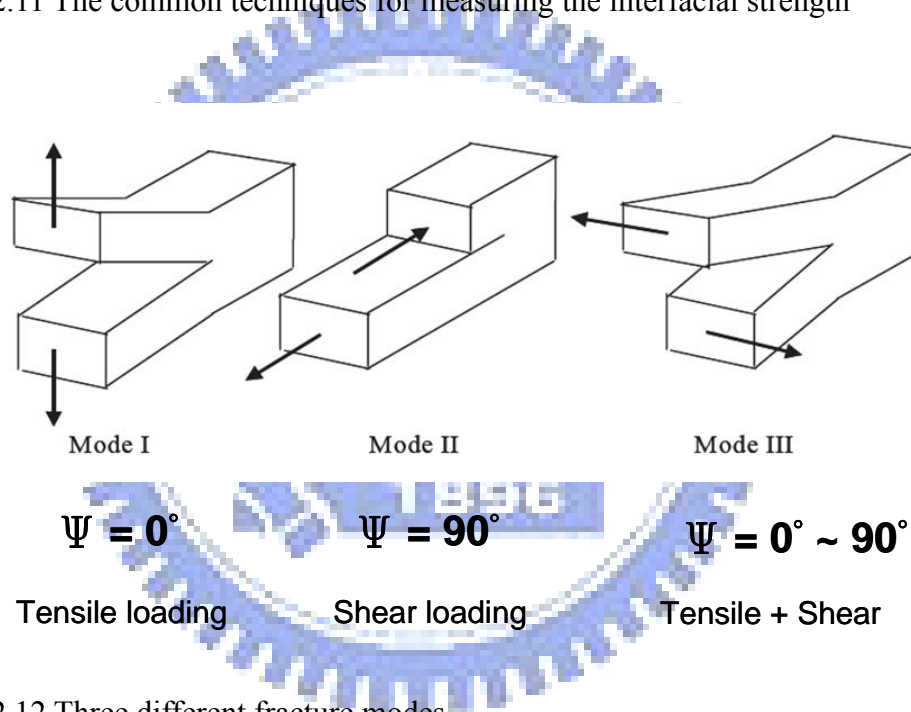


Figure 2.12 Three different fracture modes

However, the intrinsic adhesion strength G_0 can be regarded as the energy to rupture chemical bonds at the fracture interface. But larger changes may result in macroscopic adhesion G_c because of other energy-absorbing processes. The relationship between intrinsic adhesion G_0 and macroscopic adhesion G_c can be indicated by Eq. (2.3) and as shown in Figure 2.13 [51] :

$$G_c = (\xi + \chi + \zeta) G_0 \quad (2.3)$$

where ξ : contribution of surface creation

χ : parameter of surface roughness

ζ : dissipation of plastic energy

Different fracture mode has different contribution to macroscopic adhesion as shown in Figure 2.14 [51]. Interface fracture under pure mode I fracture has the most closed macroscopic adhesion to intrinsic but large increasing is induced under mode II fracture. The increase of adhesion may be attributed to the contributions of plasticity and surface roughness.

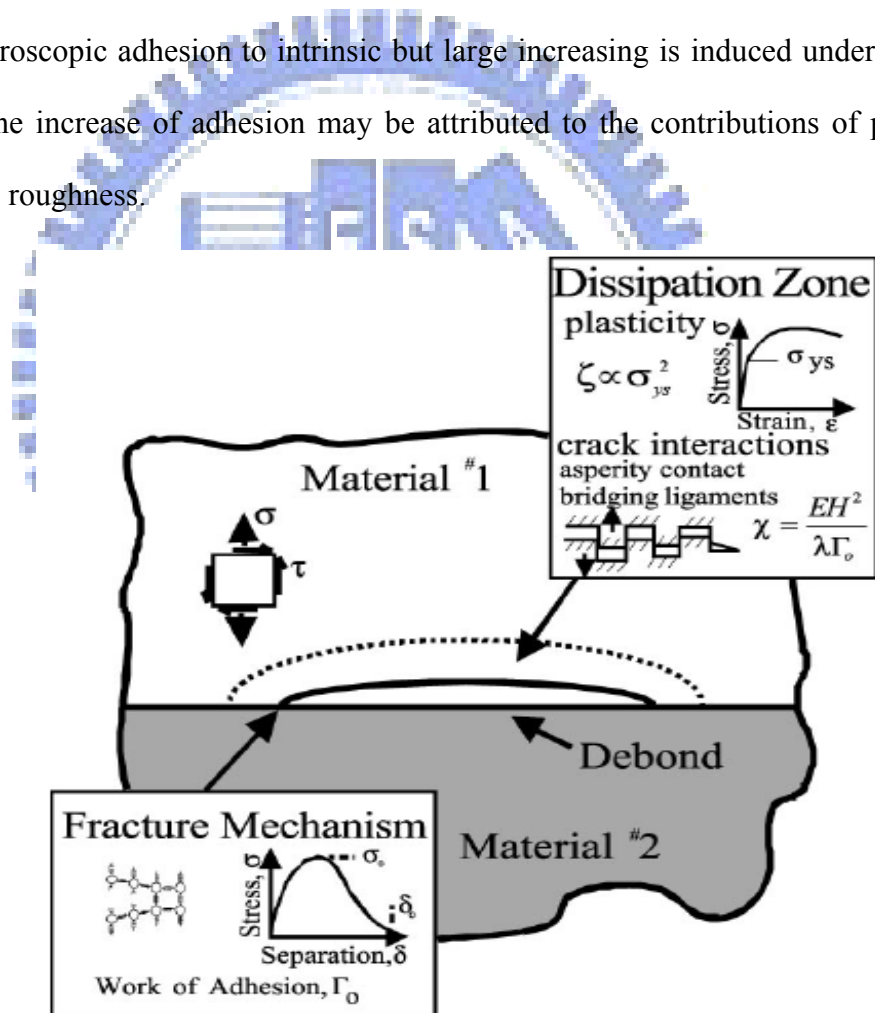


Figure 2.13 Macroscopic adhesion of fracture

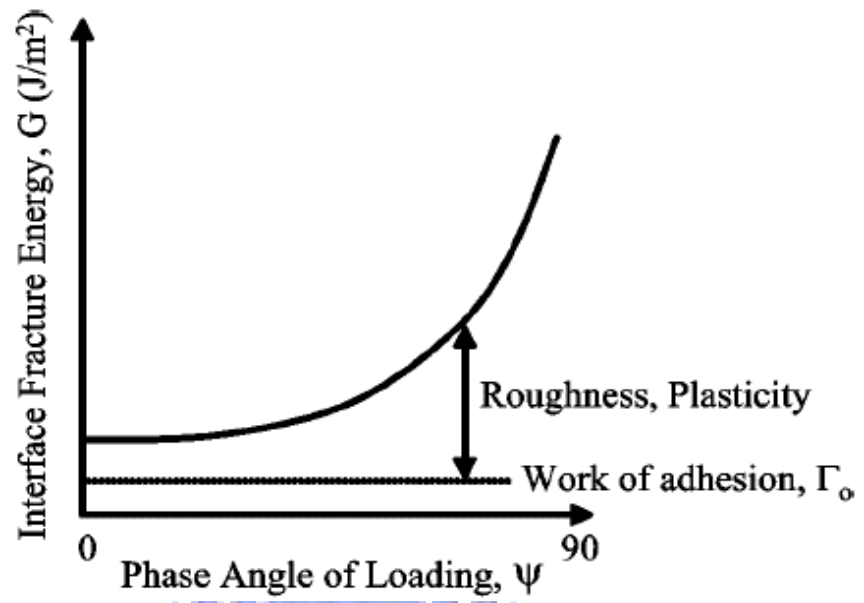


Figure 2.14 Adhesion depending on the fracture phase angle



Chapter 3 Experimental

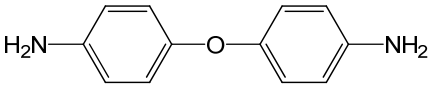
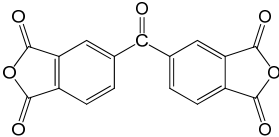
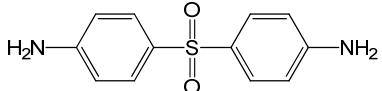
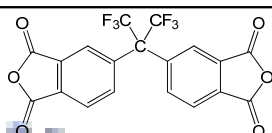
3.1 Sample Preparation

3.1.1 Synthesis of Polyimide

Nowadays, to the common approach of synthesizing transparent polyimides was to design the molecular structures of diamine and dianhydride so as to separate the stacking of benzene structures and reduce electronic interactions between polymer chains to lower the intensity of color in the resulting polyimides films. [52]

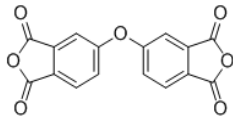
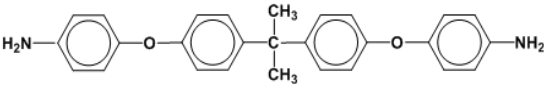
As previously described in Chapter 2, Hasanain *et. al* [53] studied two kinds of polyimides; namely, ODA-BTDA polyimide and DDS-6FDA polyimide. The transmission rate of ODA-BTDA polyimide reached 80 % because the ODA had the ester linkage to decrease charge transfer and, thereby improved the transparency. In contrast, DDS-6FDA polyimide exhibited a transmission rate of 87 % because the 6FDA monomers had the bulky group ($F_3C-C-CF_3$), which decreased the stacking degree of benzene structures and increased the transparency. It was understood that ester linkage eliminated the charge transfer, while bulky group diminished the stacking degree of benzene structures. In this thesis, BAPP and ODPA monomers were chosen for the synthesis of high T_g , transparent polyimide. The BAPP monomer had alkyl group (H_3C-C-C_3H), whose bulky group can reduce the stacking degree of benzene structures. The ODPA monomer had ester linkage to eliminate the charge transfer. It is expected that the BAPP-ODPA polyimide could possess a high transmittance without much sacrifice of the high T_g characteristics of polyimide.

Table 3.1 Chemical structures and transmission of two transparent polyimides

Amine	Anhydride	Transmission (%) (amine + anhydride)
ODA	BTDA	80
		
DDS	6FDA	87
		

4,4'-oxydiphthalic anhydride (ODPA) and 2,2'-bis[4-(4-aminophenoxy)phenyl]propane (BAPP) monomers, whose chemical structures and molecular weights were listed in Table 3.2, were chosen for the synthesis of high T_g, transparent ODPA-BAPP polyimide. N,N-dimethyl-acetamide (DMAc) and acetic anhydride (Ac₂O) were purchased from Sigma-Aldrich. 4,4'-oxydiphthalic anhydride (ODPA) was re-crystallized from acetic anhydride (Ac₂O) before use. The DMAc solvents had two different forms: anhydrous and hydrous. The film-forming ability of BAPP-ODPA polyimide was affected by the state of DMAc solvents, which will be discussed in Chapter 4 of this thesis. The effect of different curing temperature on the transmittance BAPP-ODPA polyimide will be further investigated and reported in Chapter 4.

Table 3.2 Chemical structures and molecular weights of ODPA and BAPP monomers

Monomer	Structure	Molecular weight
ODPA [C ₁₆ H ₆ O ₇]		310
BAPP [C ₂₇ H ₂₆ N ₂ O ₂]		410

Polyimide was typically synthesized from the polycondensation of a diamine and a dianhydride through either a two-step polymerization including the formation of poly(amic-acid) and subsequent thermal or chemical imidization, or a direct one-step solution polycondensation at high temperature. The former method was adopted in this study to synthesize polyimide, whose reaction schemes were comprehensively described in Figure 3.1.

During synthesis, BAPP was added in the DMAc and stirred at the room temperature until BAPP was completely dissolved. Then, ODPA was added into the solution and stirred overnight (for ca. 12 h) to prepare a highly viscous solution. Then, the poly(amic acid) solution was poured into a glass culture dish and heated in an oven from room temperature to 250 °C to form a polyimide film with a thickness of 80 μm. The synthesis of BAPP-ODPA polyimide was confirmed by FTIR analysis of BAPP-ODPA thin films prepared by spin-coating.

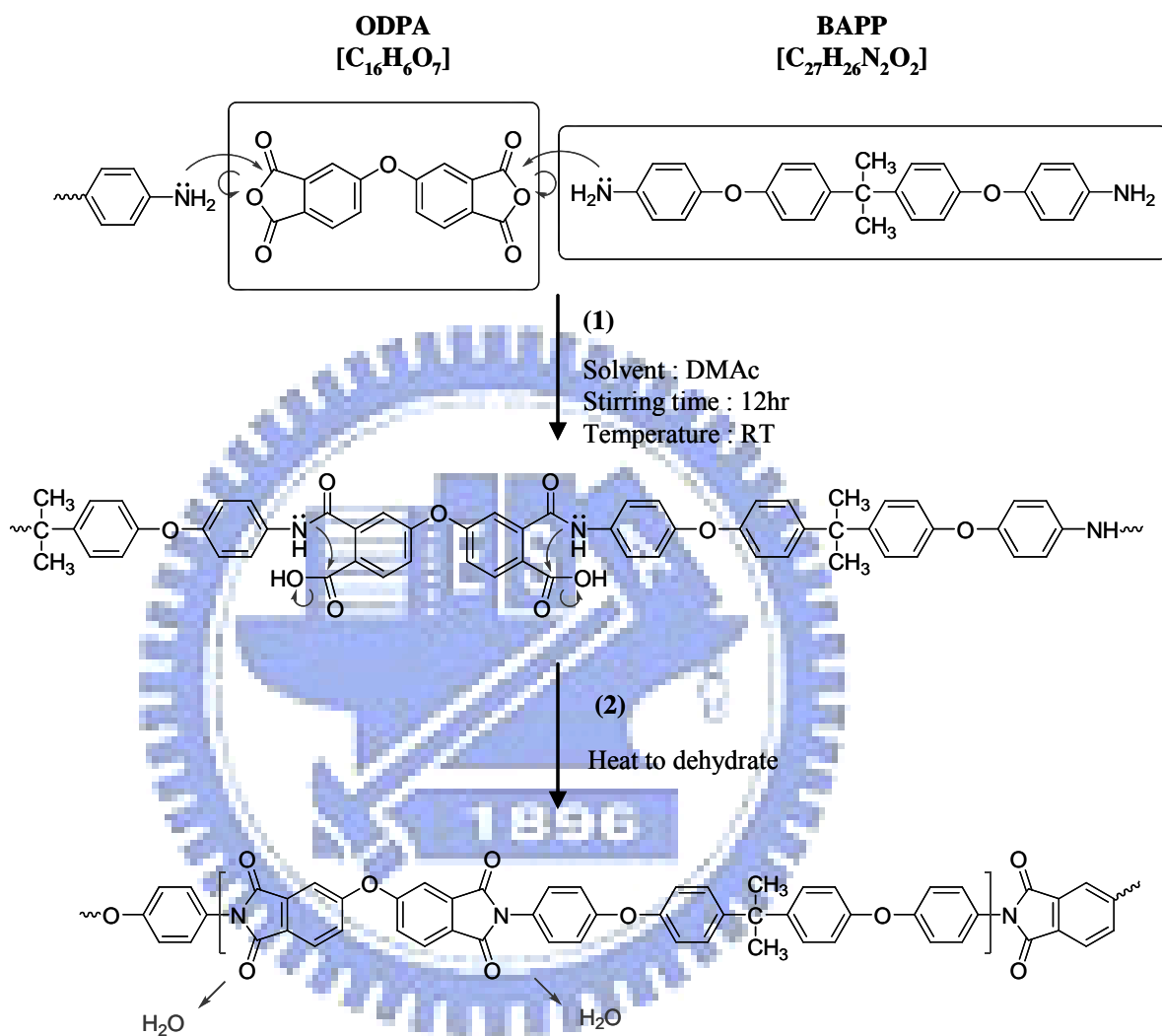


Figure 3.1 Reaction steps in the synthesis of BAPP-ODPA polyimide.

3.1.2 Plasma Surface Modification of Polyimide

BAPP-ODPA polyimide films with a thickness of 2 μm were produced by spin-coating on a silicon wafer prior to the plasma surface modification. The sizes of samples were $1 \times 1 \text{ cm}^2$ for XPS measurements and $7 \times 7 \text{ cm}^2$ for ITO/ BAPP-ODPA polyimide interface adhesion test. Before plasma treatment, the samples were heated up to $100 \text{ }^\circ\text{C}$ in a oven for 1 hour in order to remove absorbed water then the surface of samples was clean by argon gas. Table 3.3 showed in detail the experimental conditions of oxygen plasma pre-treatment. In this case, reactive ion etching (RIE) [54] was as the source of plasma treatment.

Table 3.3 Experimental conditions for oxygen plasma pre-treatment of BAPP-ODPA polyimide films

Gas	Flow rate (sccm)	Pressure (mtorr)	Power (W)	Time (min)
Oxygen	20	50	100	5
	20	50	50	5

3.1.3 Indium tin oxide layer deposition

Indium tin oxide (ITO) thin films were deposited onto unheated polyimide films on silicon substrate by sputtering ceramic ITO target. The schematic diagram of the physical-vapor-deposition (PVD) sputtering system was illustrated by Figure 3.2. In general, ITO film should have (1) good optical transmission, (2) low stress in the film, (3) good thickness uniformity, and (4) low sheet resistance. The deposition parameters that affect the above characteristics of the ITO film were identified as (1) temperature of the deposition chamber, (2) total gas flow, (3) power, and (4) oxygen percentage in Ar. Table 3.4 summarized the experimental parameters the deposition of ITO film in this

study.

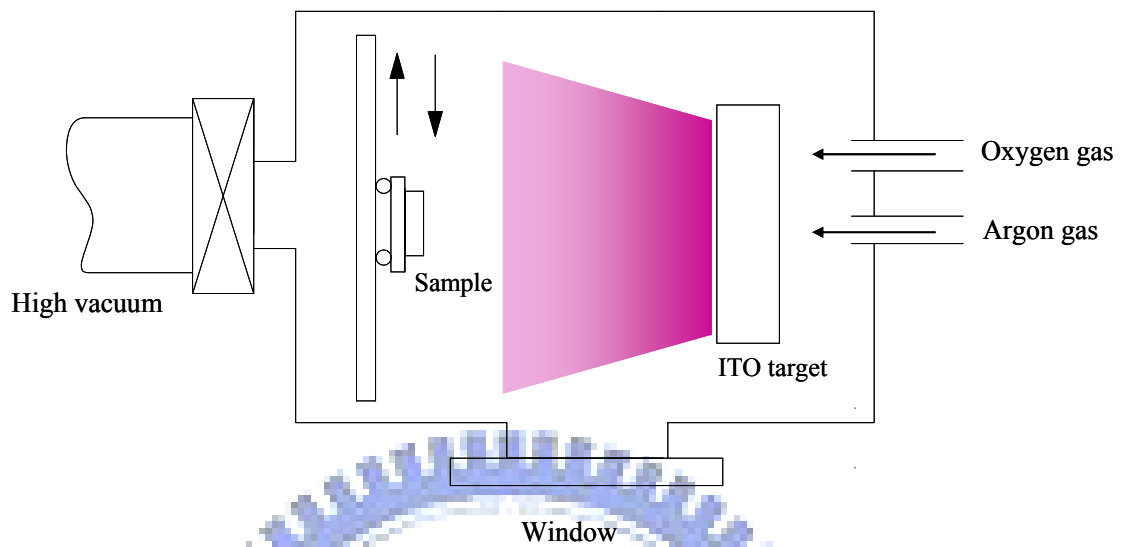


Figure 3.2 PVD sputtering system for the deposition of ITO films

Table 3.4 Experimental parameters for ITO film deposition

Deposition parameters	Conditions
DC power	1000 W
Base pressure	5×10^{-6} Torr
Working pressure	2.74 mTorr
Argon flow rate	300 sccm
Oxygen flow rate	5 sccm
Thickness	140 nm
Substrate temperature	RT

3.1.4 Samples preparation for four-point bending adhesion test

A sandwich sample was prepared as illustrated by the sequential steps shown in Figure 3.3. The epoxy resin (Epotek 375TM) was laid on the blank silicon wafer at 5000 rpm to control the thickness below 2 μm by spin-coating. A sandwich sample was clamped by using C-clamp as shown in Figure 3.4. Thick Si wafers and small clamps were used to distribute the applied force by C-clamp. The sandwich sample was then heated in an oven at 100°C for 3 hours to make the sample and blank wafer inseparable. After the sandwich sample was cooled down to room temperature in an oven, it was cut into the size of 7 \times 0.5 cm² to fit for four-point bending test. A 400~500 μm pre-notch was created in the middle by using a diamond saw. Figure 3.5 illustrated the structure of final sample prior to four-point bending adhesion measurement. Figure 3.6 shows the typical load-displacement graph of four-point bending test. The pre-notch was extended to the interface at first, and then crack growth at the weakest interface under critical load. [55] The critical load, P_c , was obtained from the load-displacement curve. Therefore, the fracture resistance of the interface, G_c , could be calculated using Eq. 3.1.

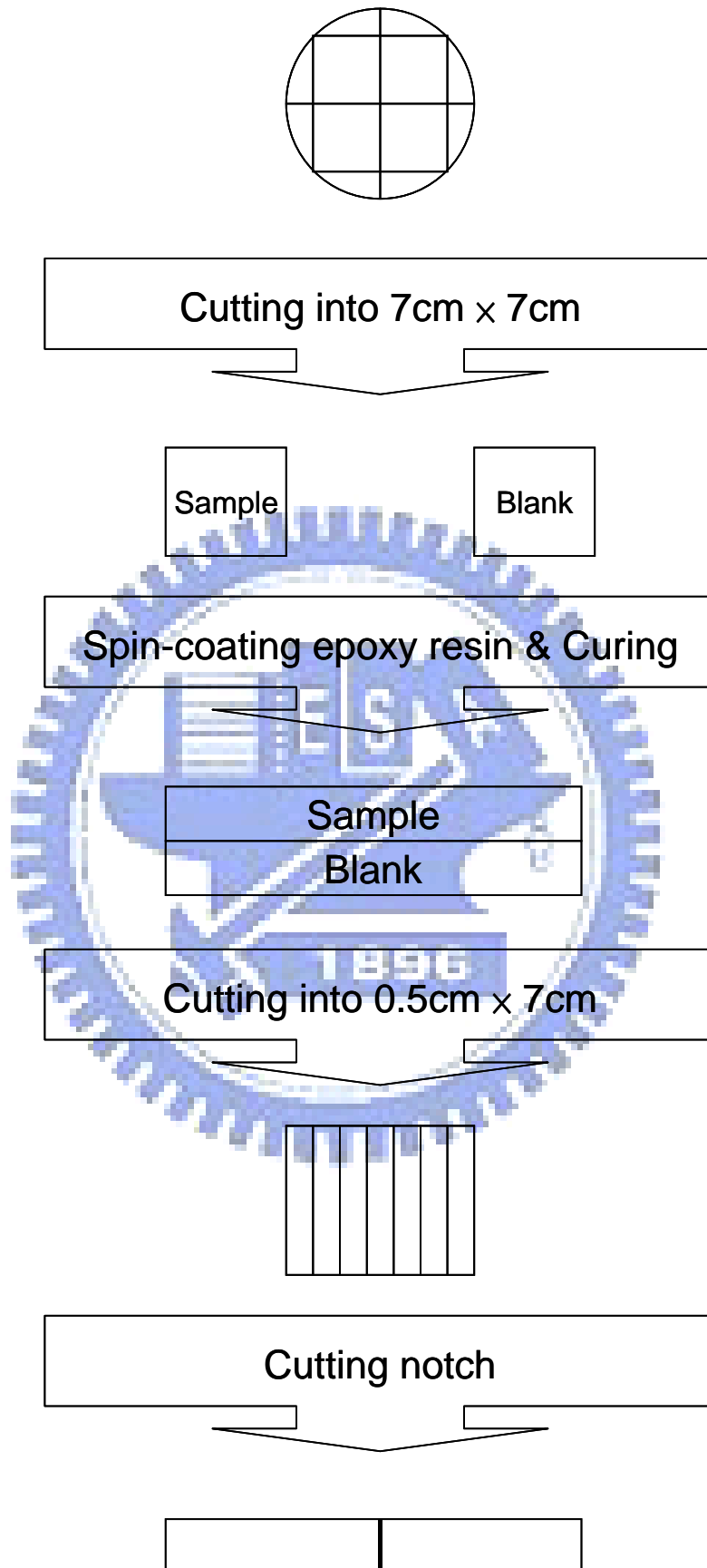


Figure 3.3 Preparation process steps of a sandwich sample for 4-point bending test



Figure 3.4 C-clamp and small clamps for fixing the sample

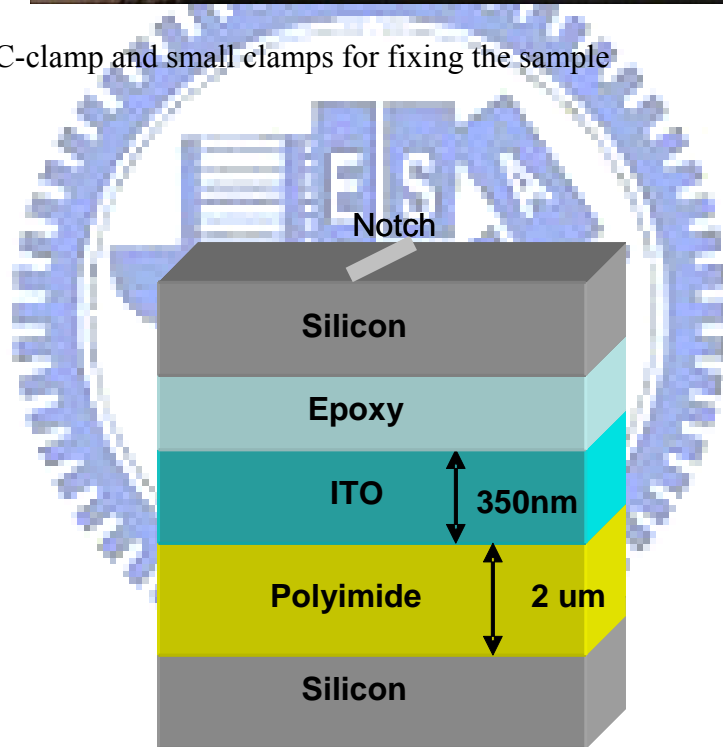


Figure 3.5 The stacking structure of sandwich sample for measuring the adhesion of ITO/polyimide interface.

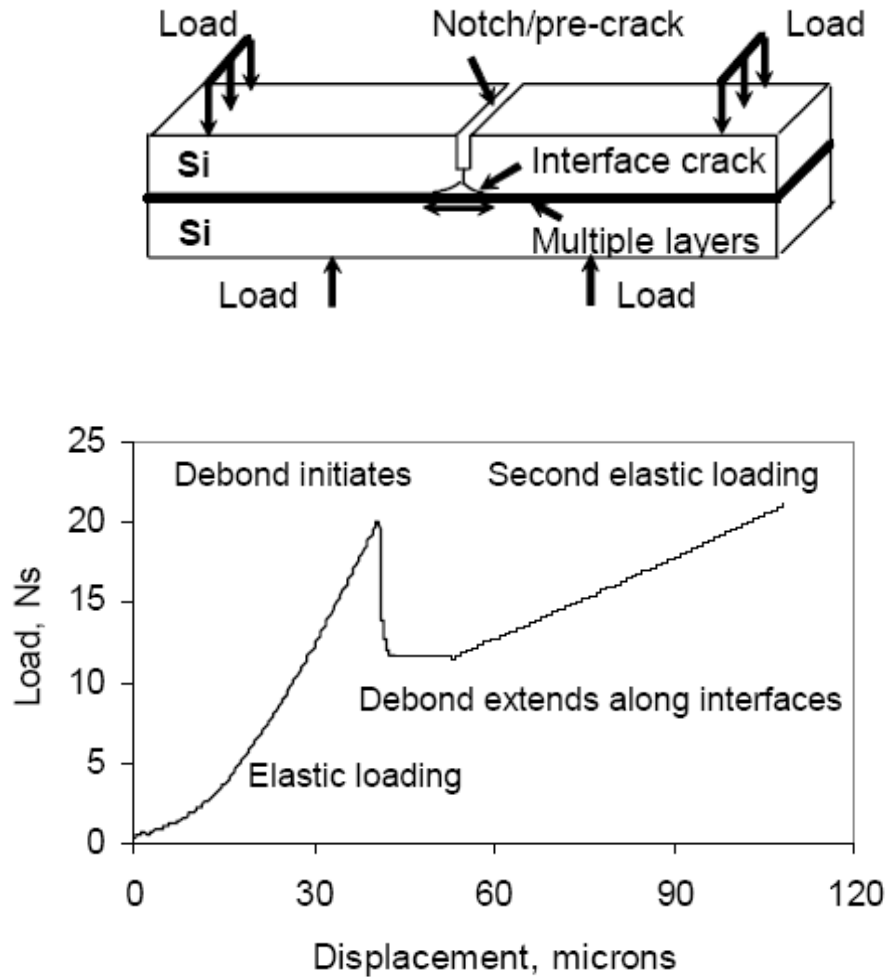


Figure 3.6 (a) Schematic drawing of four-point bend test sample and (b) a typical load vs. displacement curve for four-point bend test.

$$G_C = \frac{21(1-\nu^2)P_c^2 L^2}{16EB^2 h^3} \quad (3.1)$$

where P_c : critical load

L : distance between outer and inner load points

E : modulus of Si

ν : poisson's ratio of Si

B : width of sample

h : thickness of wafer

3.2 Experimental Procedures

As illustrated by the flow chart shown in Figure 3.7, Fourier transform infrared (FT-IR) spectra were collected using a Nicolet 360 FT-IR spectrometer. IR spectra was used to verify if poly(amic-acid) was completely transformed into polyimide. The glass transition temperature (T_g) and enthalpies of phase transitions were determined by differential scanning calorimetry (DSC, model: Perkin Elmer Pyris 7) at a heating and cooling rate of 20 °C/min under nitrogen. Ultraviolet-visible (UV-Vis) spectra of the polymer films were recorded on a HP G1103A spectrophotometer. Reactive ion etching (RIE, model: AST Cire-200) was used to modify the surface chemical states of polyimide. The chemical states and composition of the polyimide thin films were investigated using x-ray photoelectron spectroscopy (XPS) (ULVAC-PHI, PHI Quantera SXM2). Interface adhesion of ITO/polyimide interface was measured by a home-built four-point bending system.

In the following section, the fundamentals of analytic instrumentation such as FTIR, DSC, TGA, UV-vis, XPS, RIE, and four-point bending adhesion test would be briefly described in the following sections.

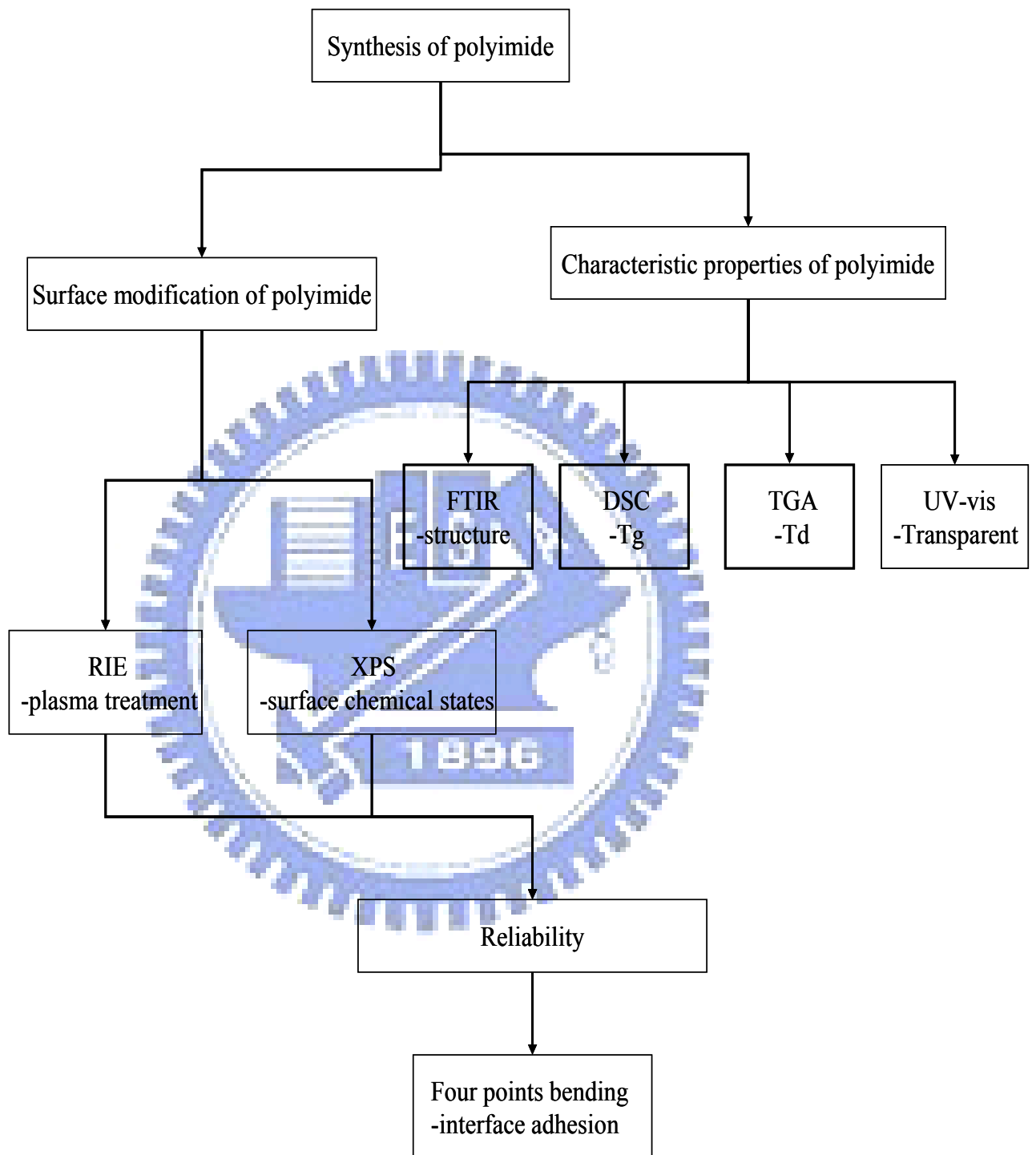


Figure 3.7 Flow-chart of experimental procedures.

3.3 Instrumentation

3.3.1 Fourier-Transform Infrared Spectroscopy (FT-IR)

Fourier-Transform Infrared Spectroscopy was a measurement technique whereby spectra were collected based on measurements of the temporal coherence of a radiative source, using time-domain measurements of the electromagnetic radiation or other type of radiation. Fourier transform infrared (FT-IR) spectra were collected using a Nicolet 360 FT-IR spectrometer. IR spectroscopy was employed to examine the chemical make and structural information of characteristic C-N-C imide ring. [56] The infrared spectra were collected in $500\text{-}4000\text{ cm}^{-1}$ range with a resolution of 4 cm^{-1} .

3.3.2 Differential Scanning Calorimetry (DSC)

The principle of differential scanning calorimetry (DSC) was to measure the energy variation of the sample affected by temperature. However, there are two types of differential scanning calorimetry (DSC) according to different designed modes:

1. Heat Flux DSC [57]

The designed mode of heat flux DSC is shown in Figure 3.8. There is a temperature difference (ΔT) between the sample and reference during heating or cooling due to the endothermic or exothermic reactions of the sample. Heat flux DSC measures the ΔT continuously and transforms ΔT into the energy variation (ΔQ) to show. The ΔQ inaccuracy of heat flux DSC is within $\pm 5\%$.

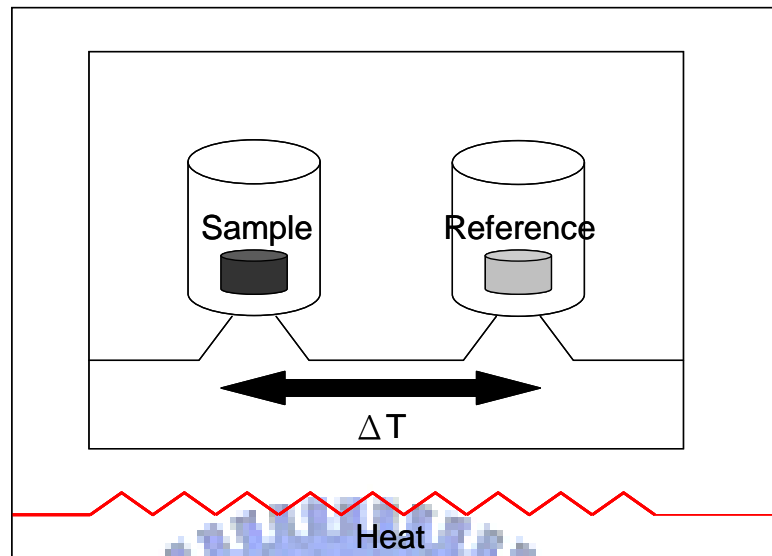


Figure 3.8 Heat Flux DSC

2. Power Compensation DSC [58]:

Figure 3.9 is the designed mode of power compensation DSC. The sample and reference are put in two individual Pt-Lr heating furnaces. The furnaces have individual Pt heating wires and Pt resistance temperature detector (PRTD). Pt heating wires offers energy precisely and fast. PRTD has linear relationship between resistance (Ω) and temperature ($-250^{\circ}\text{C}\sim 900^{\circ}\text{C}$). PRTD can measure the temperature of the sample and reference by measured Ω . There is a resistance difference ($\Delta\Omega$) between the sample and reference during heating or cooling due to the endothermic or exothermic reactions of the sample. Subsequently, Pt heating wires offer additional energy (ΔQ) fast to compensate the energy difference and make the sample and reference have the same Ω . The ΔQ inaccuracy of power compensation DSC was about $\pm 1\%$.

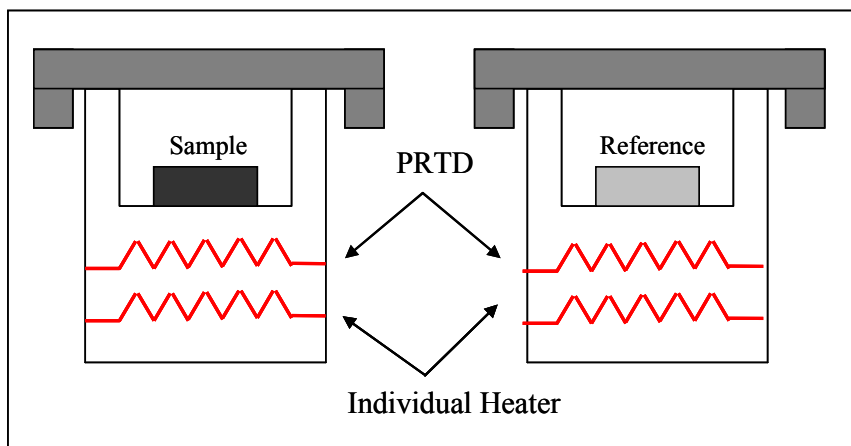


Figure 3.9 Power Compensation DSC

In this thesis, DSC was employed to measure the T_g of polyimide materials. The polyimide materials samples (5~10 mg) was placed in a Pt holder for DSC measurement using a PerkinElmer Diamond DSC in power compensation mode. The T_g was read as the midpoint of the heat capacity jump and was derived from the heating scan after heating from 50 °C to 350 °C.

3.3.3 Thermo-Gravimetric Analysis (TGA)

Thermo-gravimetric Analysis was a type of testing that was performed on samples to determine changes in weight in relation to change in temperature. Such analysis relied on a high degree of precision in three measurements: weight, temperature, and temperature change. TGA was commonly employed in research and testing to determine characteristics of materials such as polymers, to determine degradation temperatures, inorganic and organic components in materials, and solvent residues.

In the thesis, the thermal stability of the polyimide evaluated by dynamic TGA conducted at a heating rate of 20 °C/min. The temperature of 5 % weight loss was defined as decomposition temperature (T_d). Based on TGA measurement, the T_d value

of BAPP-ODPA polyimide was determined from the heating scan up to 900 °C.

3.3.4 Ultraviolet-Visible (UV-Vis) spectroscopy

An analytical technique for the measurement of wavelength-dependent attenuation of ultraviolet, visible and near-infrared light and used in the detection, identification and quantification of atomic and molecular species. UV/VIS Spectrophotometry was used to determine the absorption or transmission of UV/VIS light (180 to 820 nm) by a sample. It could also be used to measure concentrations of absorbing materials based on developed calibration curves of the material. Ultraviolet-visible (UV-vis) spectra of the polymer films were recorded on a HP G1103A spectrophotometer.

3.3.5 Reactive Ionic Etching (RIE)

Plasma was a collection of positive, negative and neutral particles. When an energetic electron struck a neutral reaction gas molecule, it could cause the dissociation to form free radicals, ionization, excitation and radiation. In the above mechanisms, two main types of species involved in reactive ion etching were the reactive neutral chemical species and the ions. In the dissociation process, reactive gas molecules were broken into free radicals. Free radicals were neutral atoms or collections of atoms with incomplete bonding. Because they were neutral, they were not affected by the electrical field induced in the reaction chamber and diffused to the target surface in random directions. Radicals were chemically reactive and the most important species in the plasma for the surface chemistry. On the other hand, ions were strongly affected by the electrical field induced in the chamber and were driven to the bottom powered electrode. Ions were not responsible for chemical reactions and they played a major role in etch

rate and anisotropy.

Reactive ion etching (RIE) was a plasma-based dry etching technique characterized by a combination of physical sputtering with the chemical activity of reactive species. RIE was used to generate plasma by different gas sources and causes different reactions to samples. In this thesis, RIE was used to modify the surface of polyimide under different treatment conditions.

3.3.6 X-ray Photoelectron Spectroscopy (XPS)

The fundamental principle of X-ray Photoelectron Spectroscopy (XPS) is the photoelectric effect, where an X-ray beam illuminates a solid surface, causing electrons to be emitted. The kinetic energy of these photoelectrons is measured, and from this, the binding energy of the electrons is determined, which identifies the element and its chemical state. The binding energy of elements can be calculated using Equation 3.2.

$$E(1s) = h\nu - E_e \quad (3.2)$$

Where E: binding energy in 1s orbit

$h\nu$: the energy of x-ray or UV

E_e : the energy of photoelectron

When an atom is illuminated by X-rays, the X-ray energy is greater than the electron binding energy of the innermost shell (L shell), and electrons are ionized to become free electrons, known as photoelectrons. The principle of photoelectron generation is illustrated in Figure 3.10. [59] Figure 3.11 shows a schematic diagram of XPS instrumentation. [60] (Need to re-arrange your text)

The composition and chemical bonding of the polyimide thin films were

investigated using XPS (ULVAC-PHI, PHI Quantera SXM2). The photoelectron emission spectra were obtained using an Al X-ray source (? eV) striking the surface of the sample. The analyzer resolution was fixed at 0.01 eV. Ar⁺ ion was used to remove adsorbed surface contaminants for 5 seconds before analysis. The insulating properties of these deposits caused surface charging effects, resulting in electron lines being shifted to lower kinetic energies. [61] However, the electronic-gun in the XPS could be neutralization and diminished the surface charge effects. The peak positions were calibrated with respect to the position of C 1s carbon contamination peak usually located at about 285 eV.

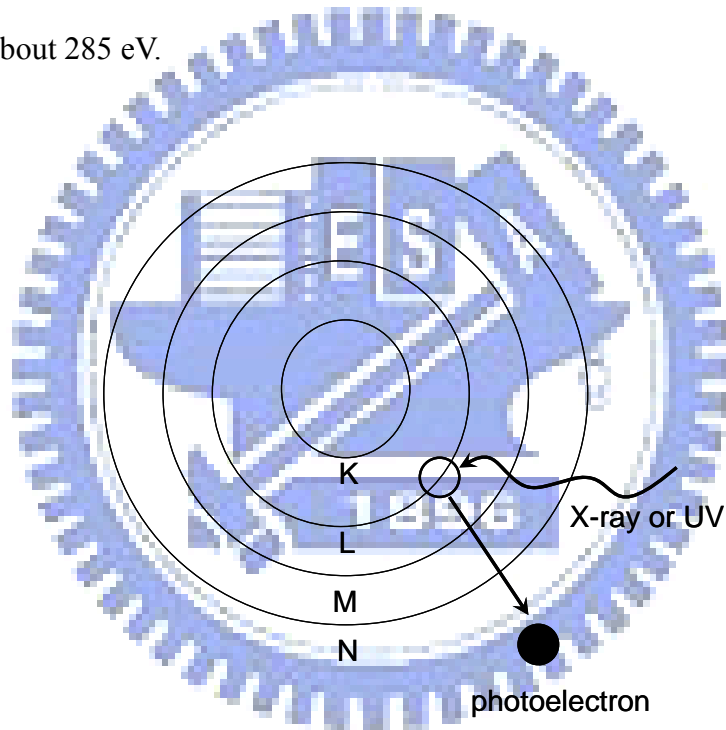


Figure 3.10 The principle of photoelectron generation

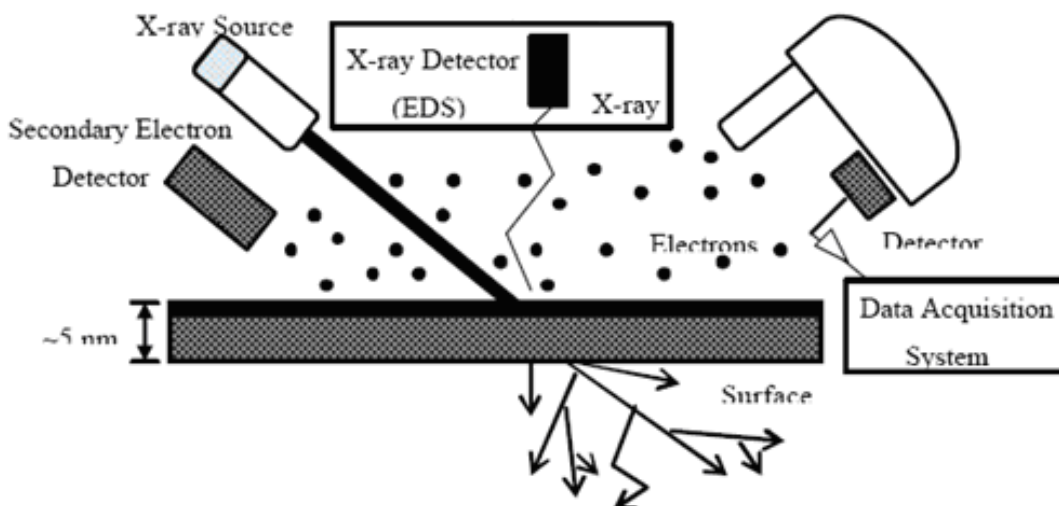


Figure 3.11 The XPS instrument and its principle. (Not clear to me about the principles)

3.3.6.1 Surface Chemical States Analysis of BAPP-ODPA Polyimide by XPS

The analysis of XPS spectra have been carried out using the XPS peak fitting program for WIN95/98 XPSPEAK Version 4.1 that have been created by Raymond W. M. Kwok. [62] The surface chemical states analysis of BAPP-ODPA polyimide had been illustrated by Figure 3.12. Two parameters were needed for this peak fitting software, such as the peak position assignment and the selection of distribution statistics. The Gaussian distribution was used for the calculation of each specific peak and the value of Gaussian distribution had been fixed at zero as seen in Figure 3.12 to obtain the symmetrical peaks. The full width at half maximum (FWHM) for the optimal de-convolution and the area of the peaks were calculated with the XPSPEAK 95 de-convolution software and the values of FWHM had been fixed to obtain the factual chemical states change as shown in Figure 3.12. The main algorithm used in this software is Newton's method for optimization, while Shirley and Linear background

was employed. Only the peak position was assigned by an operator, and the same values for all other parameters were used for every XPS chart to investigate the consistent intensity of the functional groups.

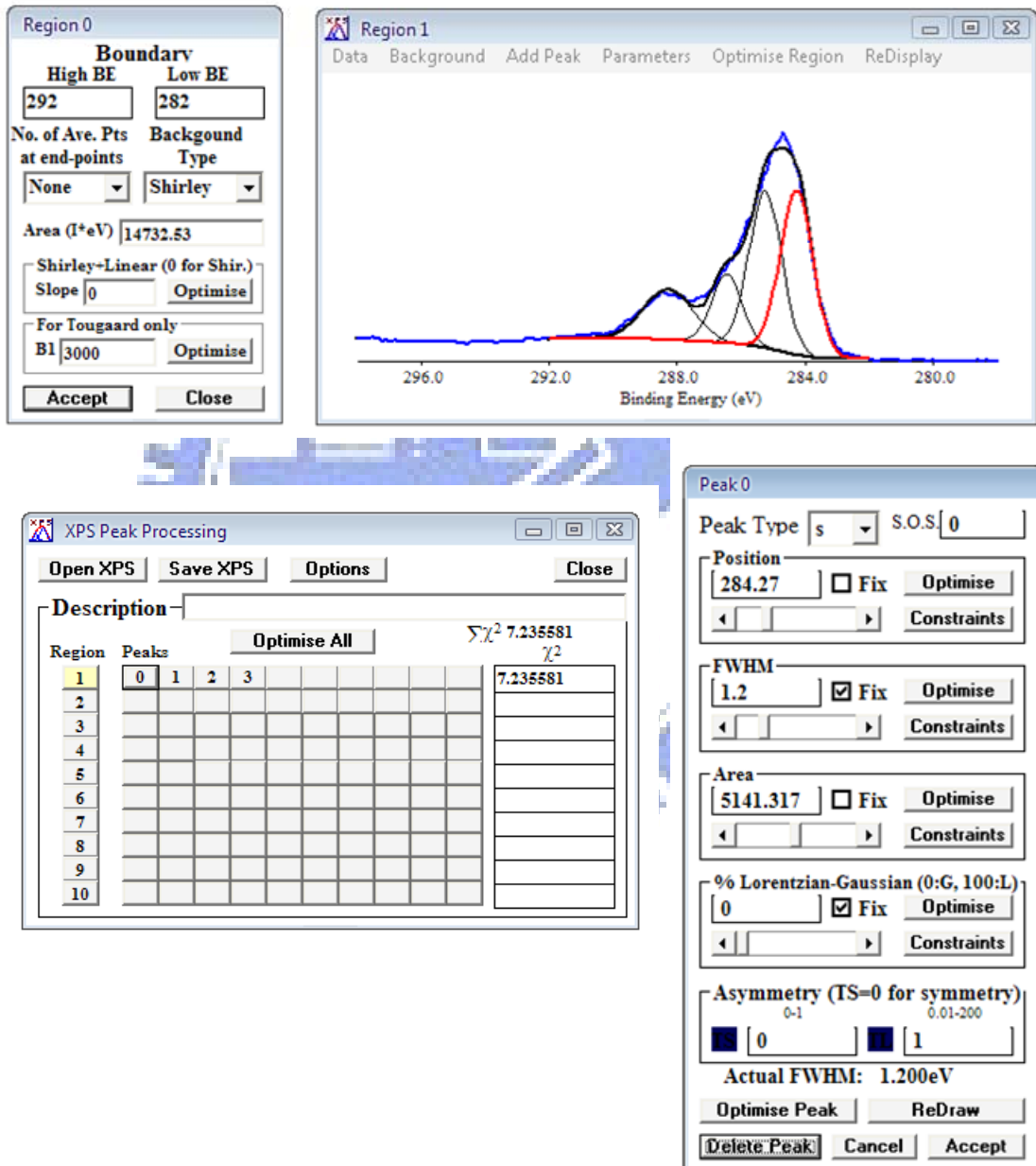


Figure 3.12 The XPS Peak Fitting program

3.3.7 Four-Point Bending System

Figure 3.13 showed the schematic diagram of sandwich sample for four-point bending test. The sandwich sample was loaded at four-points and crack was occurred at interface by the applied bending moment. Special stacks of sandwich sample were prepared for controlling the crack interface as wish. The loading condition of sandwich sample was under approximate equal stress of tensile and shears, which was mode-mixity fracture having a fracture phase angle $\Psi \sim 43^\circ$. [49] Because the compliance of sandwich sample increased linearly with crack length, the critical energy release rate of four-point bending test could be calculated to be quantitative analysis as the interface adhesive strength.

Figure 3.14 showed the micro-mechanical test system established in this study. Sandwich samples of four-point bending test were pulled by the linear motorized actuator. The displacement of load point was controlled by motion control card at range of velocity from 0.1 $\mu\text{m/s}$ to 200 $\mu\text{m/s}$ which had the sensitivity in 0.1 μm . The load cells with the capacities of 20N and 100N are used to measure the output of load. The test system is operated using Labview software, and the displacement and output of load are recorded. The critical load is measured to calculate the critical energy release rate G_c under steady growth state of crack at interface.

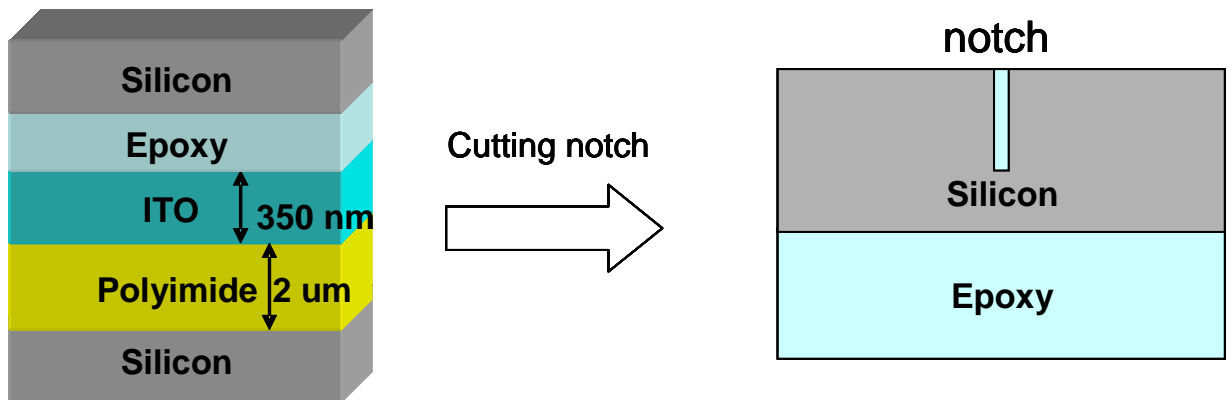


Figure 3.13 Schematic diagram of sandwich sample for four-point bending test

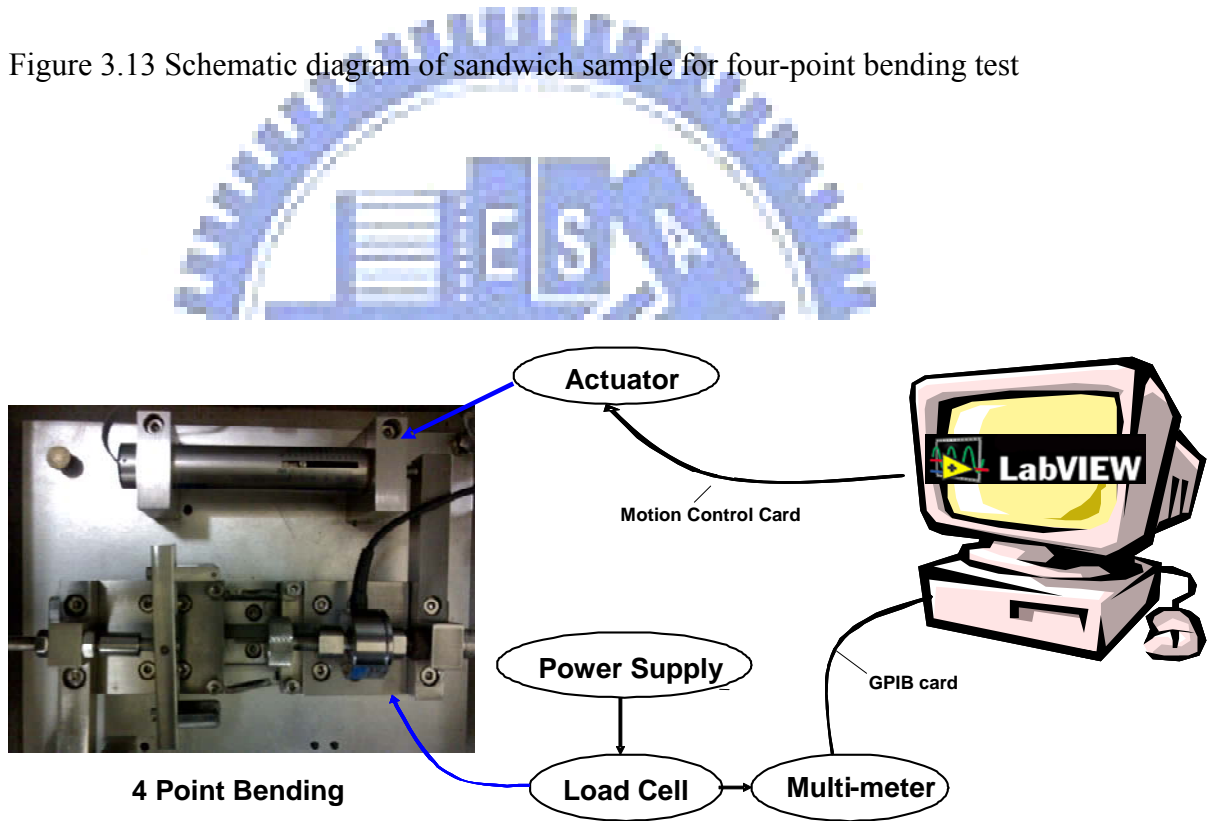


Figure 3.14 Schematic diagram of micro-mechanical test system

Chapter 4 Results and Discussion

4.1 Synthesis and Characterization of Polyimide

4.1.1 ODPA purity

Two pretreatment steps were taken to ensure complete condensation reaction. First, ODPA was re-crystallized from acetic anhydride at 120 °C to remove the moisture because ODPA could be easily hydrolyzed by moisture in the atmosphere to form a dicarboxylic acid as illustrated in Figure 4.1, which in turn reduced the activity of the polycondensation. Secondly, solvent was dried to avoid the hydrolysis of anhydride to acid.

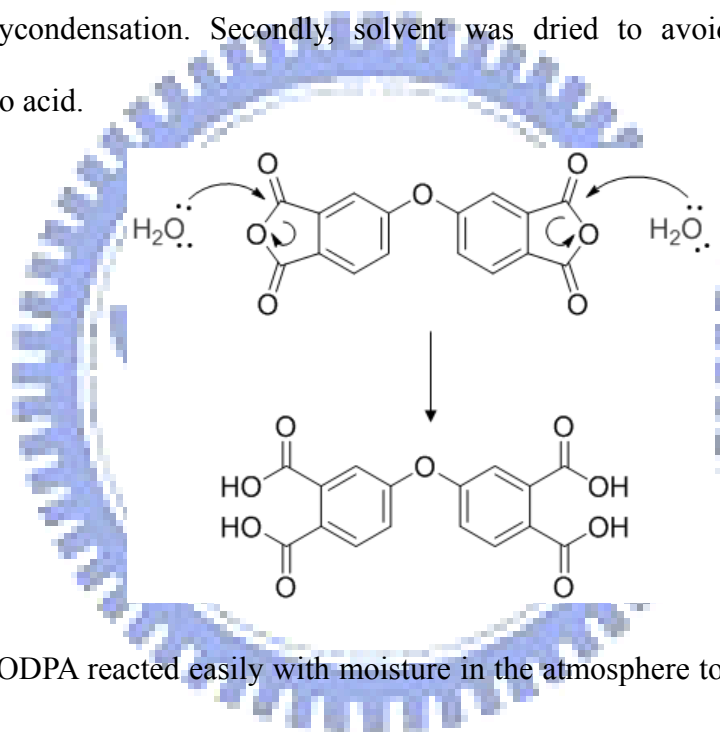


Figure 4.1 ODPA reacted easily with moisture in the atmosphere to form a dicarboxylic acid.

4.1.2 The effects of solvent of anhydrous or hydrous DMAc for film-forming ability

The moisture content in DMAc solvent affected the film-forming ability as illustrated by the photographs shown in Figure 4.2, showing that BAPP-ODPA polyimide film was very brittle. However, when an anhydrous DMAc was used in the synthesis process, film-forming ability was excellent as shown by photographs in Figure

4.3. It was believed that the moisture in DMAc solvent reacted with the ODPA forming a dicarboxylic acid, which reduced the activity of the polycondensation of BAPP and ODPA. This also resulted in BAPP-ODPA polyimide with less repeating units, i.e. lower molecule weight, which made this polyimide film very brittle.



Figure 4.2 The BAPP-ODPA polyimide was brittle when a hydrous DMAc solvent was used.



Figure 4.3 The BAPP-ODPA polyimide was tough and useful when an anhydrous DMAc solvent was used.

4.1.3 Structural Analysis by FTIR Spectroscopy

The degree of imidization of BAPP-ODPA polyimide was confirmed by FTIR spectroscopy using a 2 μm thick BAPP-ODPA thin film on silicon wafer prepared by spin coating. Figure 4.4 showed infrared spectra of BAPP-ODPA poly(amic acid) cured at different process temperatures. It was found that the di-anhydroxyl and di-amide bonds were significantly reduced when cure temperature was increased from 60 to 250 $^{\circ}\text{C}$. The film cured at 250 $^{\circ}\text{C}$ exhibited characteristic imide ring group absorptions around 1375 cm^{-1} (C-N-C stretching), 1730 cm^{-1} (typical of imide carbonyl asymmetrical and symmetrical stretching), 1500~1600 cm^{-1} (-NH decreased due to polycondensate), and 2800~3500 cm^{-1} (-OH decreased due to dehydrate), which were also listed in Table 4.1. [63] Based on the reduction of -OH/-NH and the appearance of C-N-C/imide ring in the film cured at 250 $^{\circ}\text{C}$, the evidences indicated a complete conversion of the poly(amic acid) precursor into BAPP-ODPA polyimide. The schematic diagram in Figure 4.5 showed that the C-N-C imide ring group in polyimide was formed by dehydrating BAPP-ODPA poly(amic acid) into a polyimide.

Table 4.1 Absorption peak positions of four types of chemical bonds.

Characteristic vibrational bands	Absorption Peak Position (cm^{-1})
C-N-C	1375
C-N (imide carbonyl)	1730
N-H	1500-1600
-OH	2800-3500

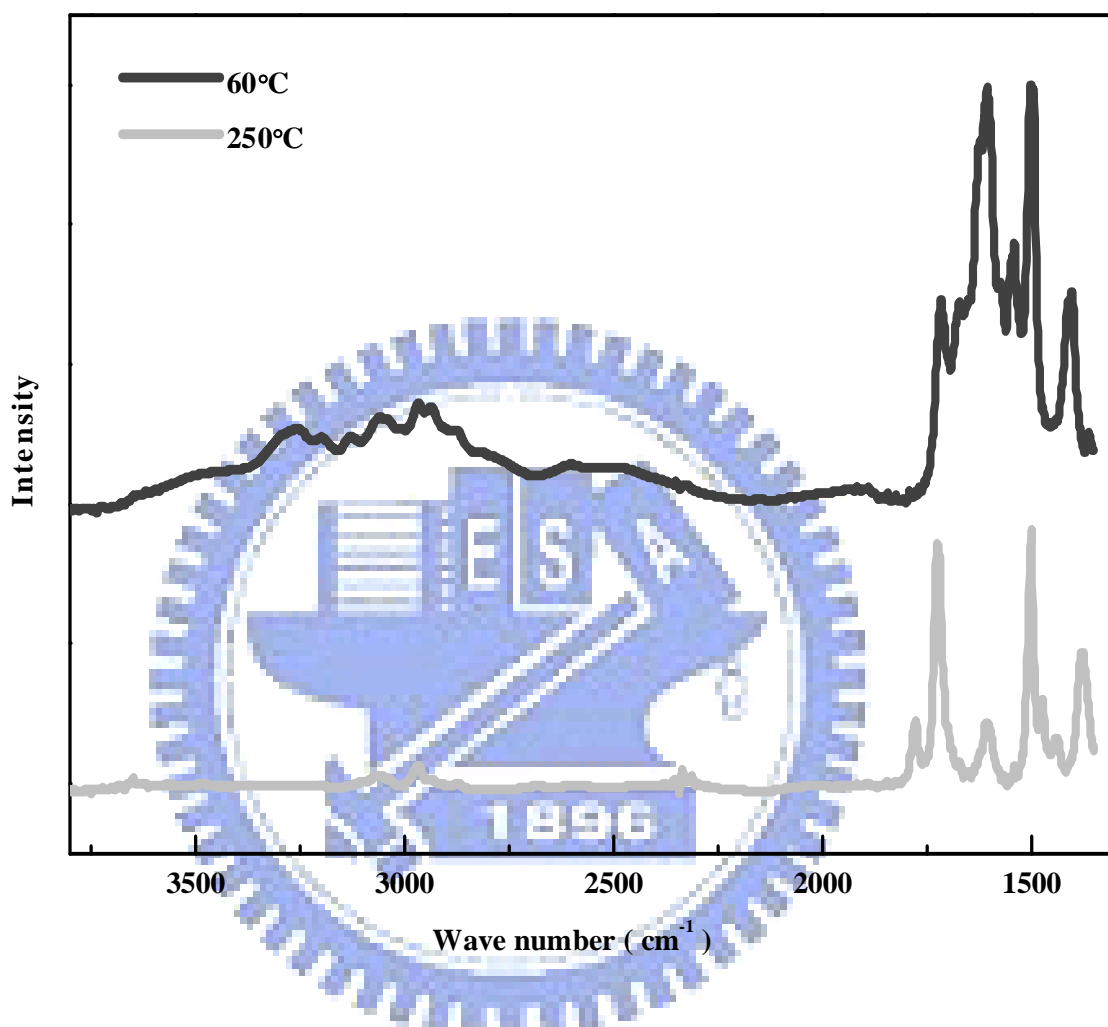


Figure 4.4 The FT-IR spectra of BAPP-ODPA polyimides cured at low (60 °C) and high temperature (250 °C).

y-axis: Absorbance (arb. unit)

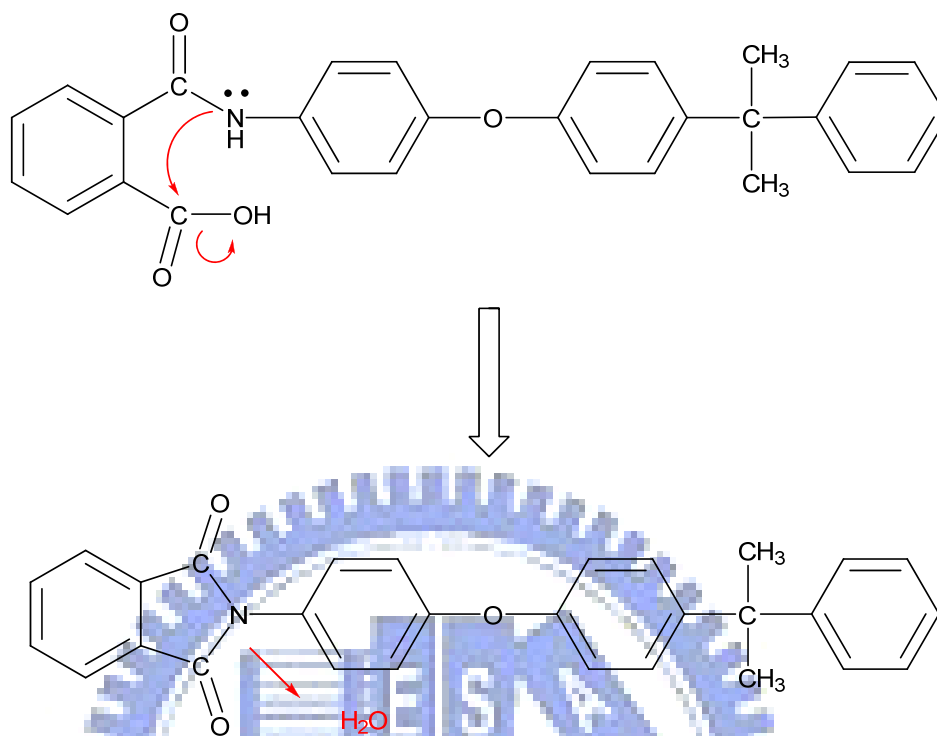


Figure 4.5 The BAPP-ODPA poly(amic acid) was dehydrated to form polyimide upon heating

4.1.4 Transmittance in UV-Vis

The difference in the light transmittance between commercial polyimide and BAPP-ODPA polyimide were clearly illustrated by the photographs shown in Figure 4.6. BPPA-ODPA polyimide showed much higher transparency. Next, the transmittance of BPAA-ODPA polyimide with a thickness of 80 μm was measured by using UV-Vis spectroscopy and compared to that of commercial polyimide as shown in Figure 4.7. In the visible light range (400~700 nm), the transmission rate of BAPP-ODPA polyimide reached 98 % at wavelength of 430 nm. Hasanain *et al.* [53] reported two kinds of transparent polyimides, DDS-6FDA and ODA-BTDA polyimides. The transmission rate

of DDS-6FDA polyimide reached 87 % because the 6FDA monomers had a bulky group to reduce the stacking degree of benzene structures. The transmission rate of ODA-BTDA polyimide was 80 % because the ester linkage in ODA decreased the charge transfer and improved the transparency. Compared to these two polyimides, BAPP-ODPA synthesized in this study exhibited a much higher transmission rate, which can be attributed to the hindrance and decreased stacking degree and charge transfer resulting from the insertion of the bulky group or side chain in BAPP monomers.

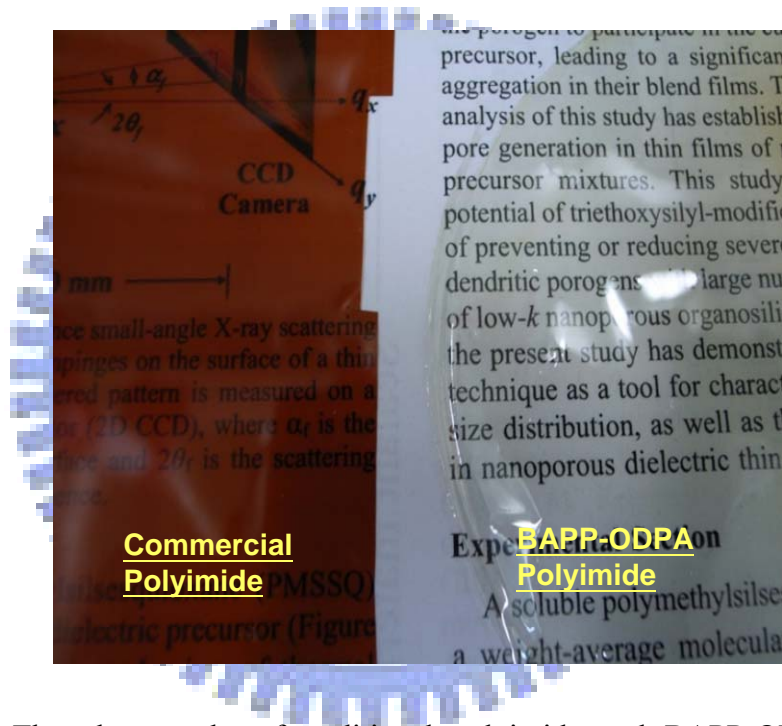


Figure 4.6 The photographs of traditional polyimide and BAPP-ODPA polyimide illustrating their difference in transmission rate

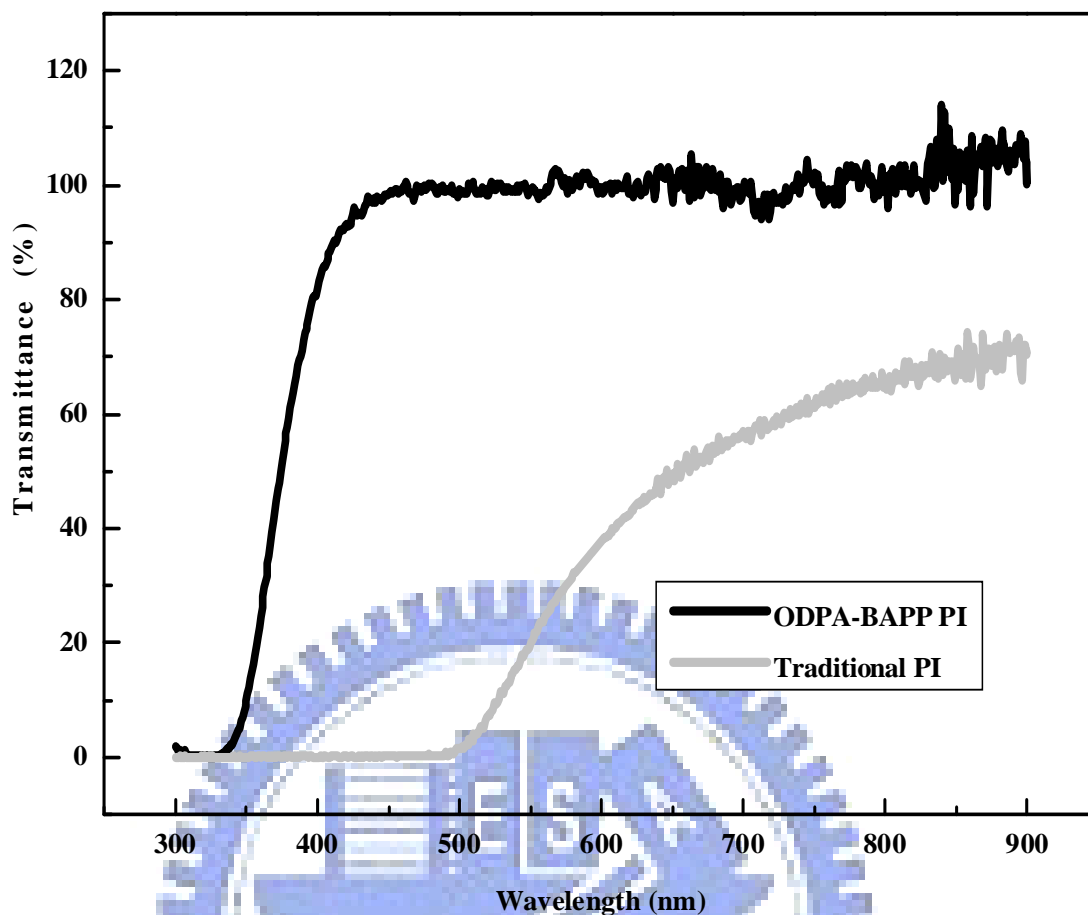


Figure 4.7 The UV-visible spectra of BAPP-ODPA and traditional polyimide films at 80 μm

4.1.5 Thermal Properties of BAPP-ODPA Polyimide

4.1.5.1 The glass transition temperature (T_g) measured by differential Scanning Calorimetry (DSC)

DSC measurement was conducted at a heating/cooling rate of 20 $^{\circ}\text{C}/\text{min}$ from 50 $^{\circ}\text{C}$ to 350 $^{\circ}\text{C}$ under nitrogen. The glass transition temperature of BAPP-ODPA polyimide film was determined in the 2nd heating scan as 230 $^{\circ}\text{C}$ as shown in Figure 4.8. Compared to the T_g of commercial polyimide (>300 $^{\circ}\text{C}$), BAPP-ODPA polyimide film possessed a slightly lower T_g (230 $^{\circ}\text{C}$), presumably due to the flexibility of molecular structure by the use of ether linkage and alkyl group. Nevertheless, the T_g of

BAPP-ODPA is still much higher than those of PET and PEN ($< 150\text{ }^{\circ}\text{C}$). BAPP-ODPA can meet the requirements of ITO deposition at $T > 200\text{ }^{\circ}\text{C}$ readily if its thermal stability is not an issue.

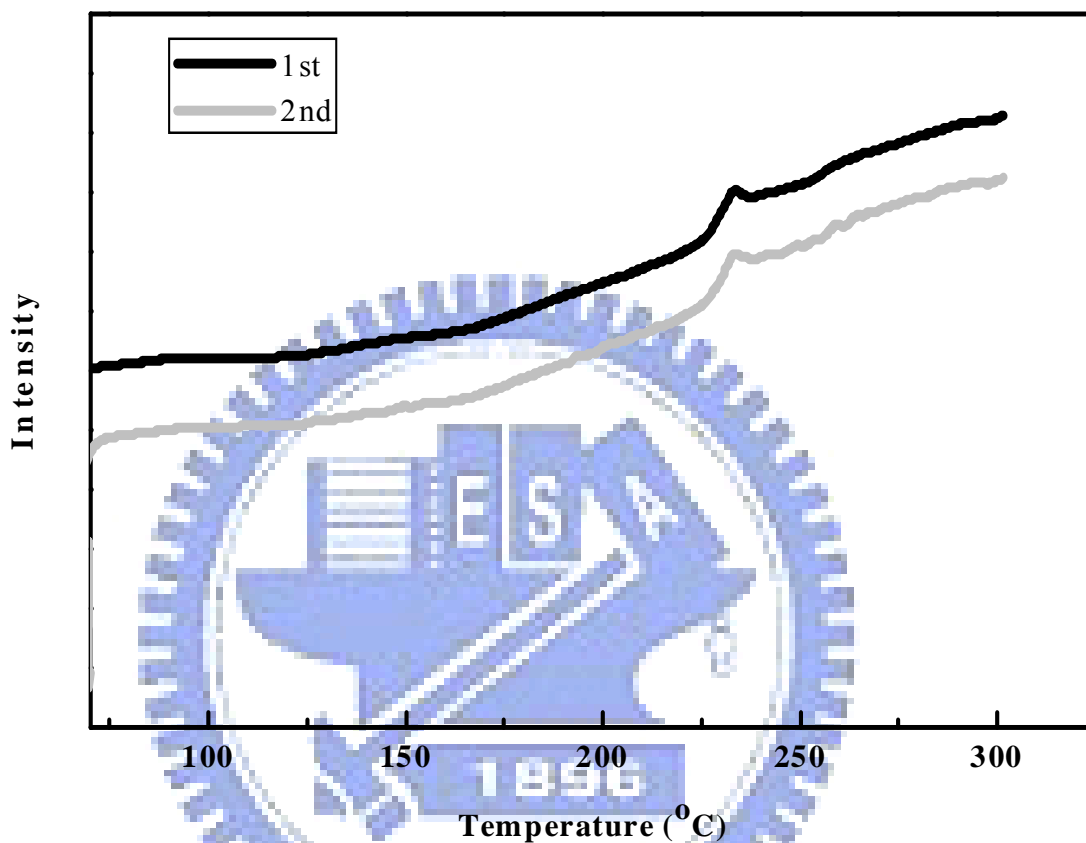


Figure 4.8 DSC curves of BAPP-ODPA polyimide in two heating scans. T_g was determined in 2nd heating scan at a $20\text{ }^{\circ}\text{C}/\text{min}$ heating/cooling rate

4.1.5.2 Thermo-Gravimetric Analysis (TGA)

The thermal stability of BAPP-ODPA polyimide was evaluated by dynamic TGA, which was conducted at a heating rate of $20\text{ }^{\circ}\text{C}/\text{min}$ from room temperature to $900\text{ }^{\circ}\text{C}$. The temperature of 5 % weight loss was defined as the decomposition temperature (T_d). Based on TGA measurement, the T_d value of BAPP-ODPA polyimide was $495\text{ }^{\circ}\text{C}$ as determined from the heating scan up to $900\text{ }^{\circ}\text{C}$ shown in Figure 4.9. The polyimide left

more than a 50 % char yield at 610 °C in nitrogen. The TGA data indicated that BAPP-ODPA polyimide had excellent thermal stability in spite of its relative low Tg of 230 °C.

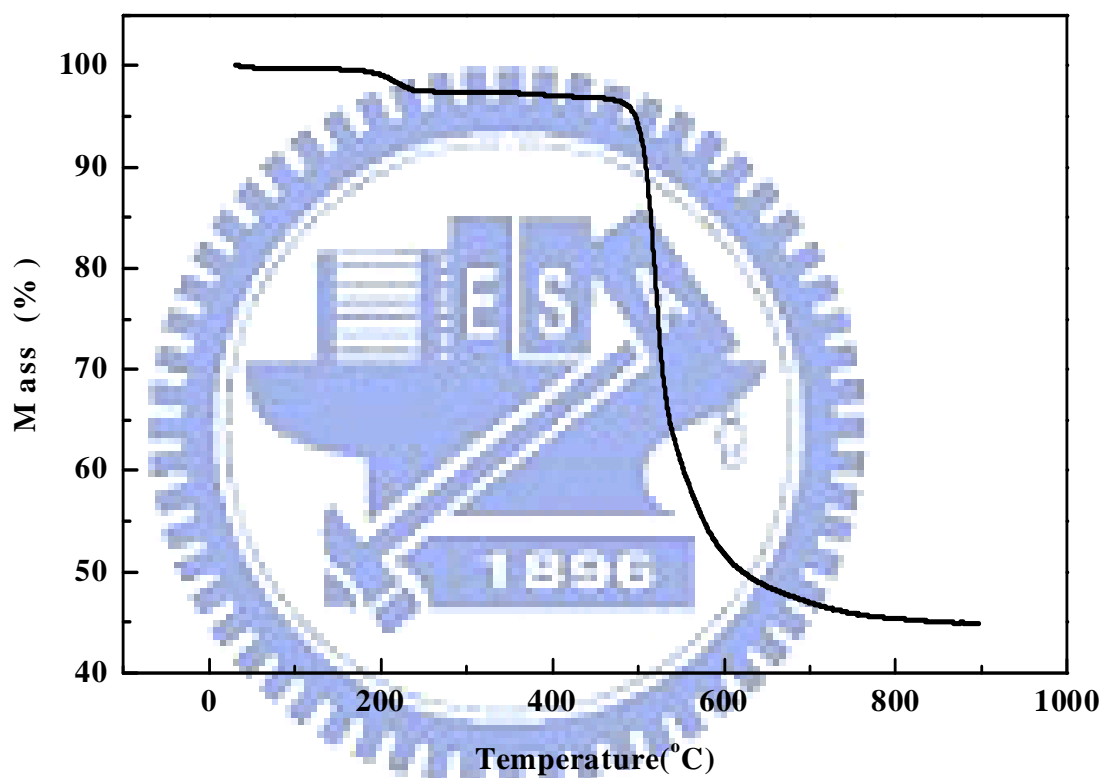


Figure 4.9 The TGA curve of BAPP-ODPA polyimide under nitrogen at a heating rate of 20 °C/min

4.2 XPS analysis of surface chemical states of BAPP-ODPA polyimide

The schematic drawing of the repeating unit of BAPP-ODPA polyimide was shown in Figure 4.10. It contained two types of oxygen and nine types of carbon atoms. The binding energies of the C 1s and O 1s line contributions, from the Scienta database, was summarized and listed in Table 4.2. [64] The separation of the C 1s signal into nine main components, as suggested by Beamson [64], was fully justified by the resolution of the XPS spectra. Therefore, we limited the fitting of the C 1s line to three main carbon components by treating the C1-C3 and C4-C8 as the same chemical states.

The surface chemical states of BAPP-ODPA polyimides under different experimental parameters were characterized by XPS and summarized in Table 4.3 through Table 4.9. Their corresponding XPS C 1s and O 1s spectra were shown in Figures 4.11 through Figure 4.16. The binding energy scale was corrected by setting the lowest component of carbon 1s as 285.0 eV, which was the binding energy of carbon in an aromatic compound. [65] The component ratios were determined from the integral intensities of these component peaks in carbon and oxygen 1s spectra.

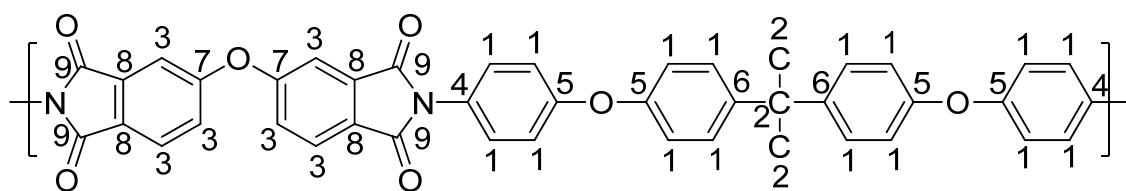
The C 1s integrated areas of these peaks, and their binding energies were summarized in Table 4.4 through Table 4.6. The surface component ratio of un-plasma-treated BAPP-ODPA polyimide was listed in Table 4.4 which consisted of three components, namely C-C, C-O-C, and C=O. The components ratio of C-C, C-O-C, and C=O were 66.8, 27.9, and 5.3 %, respectively. Table 4.5 listed the surface components of BAPP-ODPA polyimide modified by oxygen plasma at a RF power of 50W, where a new component, C-OH appeared. After oxygen plasma treatment, the components ratio of C-C and C=O decreased from 66.8 to 42.5 % and 27.9 to 32.5%. In contrast, the component ratio of C-O-C increased from 27.9 to 32.5%. The ratio of new

component, C-OH increased from 0 to 11.5%. Table 4.6 summarized the surface components of BAPP-ODPA polyimide modified by oxygen plasma at a RF power of 100W. When the RF power increased from 50 to 100W, the components ratio were similar as the RF power at about 50W. The obvious change was the component ratio of C-OH increased from 11.5 to 14.3 %.

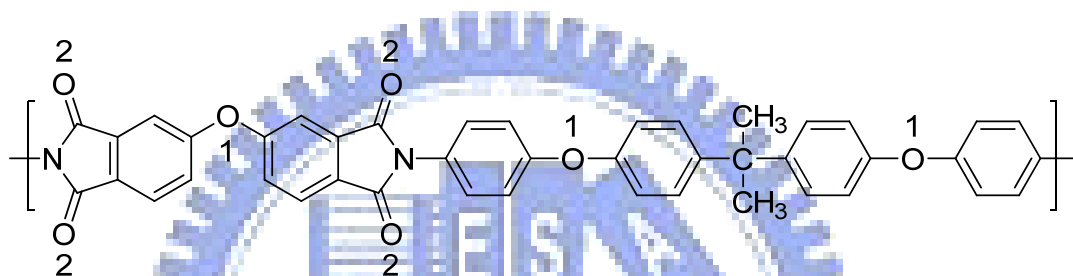
The peaks and binding energies of O 1s spectra for varying RF power were summarized in Table 4.7 through Table 4.9. The binding energy of oxygen element 1s was fixed as 532 eV. [63] The surface component ratio of un-treated BAPP-ODPA polyimide was listed in Table 4.7, which had two components. The components ratio of C-O-C and C=O were 43.1 and 56.9 %, respectively. After oxygen plasma treatment at a RF power of 50W, the components ratio of C-O-C and C=O decreased from 43.1 to 23.7 % and 56.9 to 31.2 %. In contrast, a new component ratio of C-OH was generated after oxygen plasma and its ratio increased from 0 to 45.1 % as listed in Table 4.8. The surface chemical states change of BAPP-ODPA polyimide modified by oxygen plasma at a RF power of 100W was listed in Table 4.9. The surface chemical states were similar to that treated at 50W.

The C 1s spectra and fitted peaks of BAPP-ODPA films plasma treated at RF power of 50W and 100W were shown in Figures 4.12 and 4.13, respectively. In addition to the binding states based on the chemistry of the repeating unit, the plasma modified polyimide surface showed a carbon-hydroxyl bond in C 1s signal, designated as C10. Similarly, a new contribution O3 to the O 1s signal was found, which could be assigned in accordance with C10 in the C 1s. The binding energies and component ratio of untreated BAPP-ODPA and plasma treated at RF power of 50W and 100W were summarized in Table 4.2. The surface chemical states of both untreated and plasma-treated BAPP-ODPA polyimides, can be deduced by fitting their XPS C1s and

O 1s spectra according to the chemical bonding types listed in Table 4.2.



(a)



(b)

Figure 4.10 Binding states of the (a) carbon and (b) oxygen atoms in the repeating unit of BAPP-ODPA.

Table 4.2 Main components and their binding energies in C 1s and O 1s XPS signals of BAPP-ODPA polyimide

Signal	Component	BE (eV)
C 1s	C1 (arom. in BAPP)	284.75
	C2	284.70
	C3 (arom. in ODPA)	284.68
	C4 (C-N)	285.68
	C5 (C-O-C in BAPP)	285.82
	C6	286.19
	C7 (C-O-C in ODPA)	285.69
	C8	285.76
	C9 (C=O)	288.57
	C10 (C-OH)	287.30
O 1s	O1 (C-O-C)	533.29
	O2 (C=O)	531.98
	O3 (C-OH)	532.45

Table 4.3 Experimental conditions for plasma pre-treatment surface of BAPP-ODPA polyimides

Gas	Flow rate (sccm)	Pressure (mtorr)	Power (W)	Time (min)
Oxygen	20	50	100	5
	20	50	50	5

Table 4.4 Carbon 1s spectrum: binding energies and composition quantification of untreated BAPP-ODPA polyimide film.

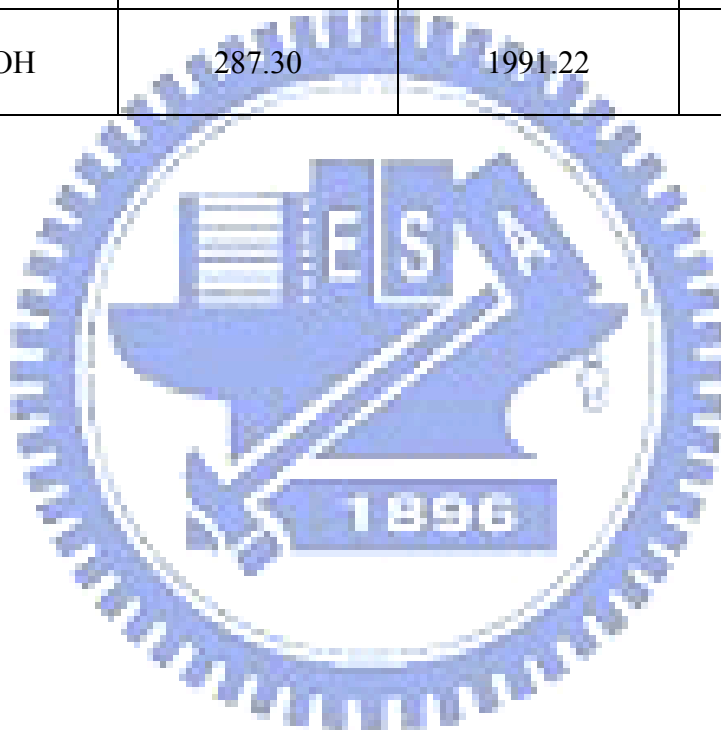
Component	Peak BE (eV)	Area	%
C-C	284.75	12010.52	66.8
C-O-C	285.82	5012.57	27.9
C=O	288.57	947.33	5.3

Table 4.5 Carbon 1s spectrum: binding energies and composition quantification of BAPP-ODPA polyimide film modified by oxygen plasma at a RF Power of 50W.

Component	Peak BE (eV)	Area	%
C-C	284.75	6740.06	42.5
C-O-C	285.82	5166.73	33.5
C=O	288.57	2146.22	12.5
C-OH	287.30	1832.72	11.5

Table 4.6 Carbon 1s spectrum: binding energies and composition quantification of BAPP-ODPA polyimide film modified by oxygen plasma at a RF Power of 100W.

Component	Peak BE (eV)	Area	%
C-C	284.75	5786.65	41.5
C-O-C	285.82	4529.78	32.5
C=O	288.57	1628.00	11.7
C-OH	287.30	1991.22	14.3



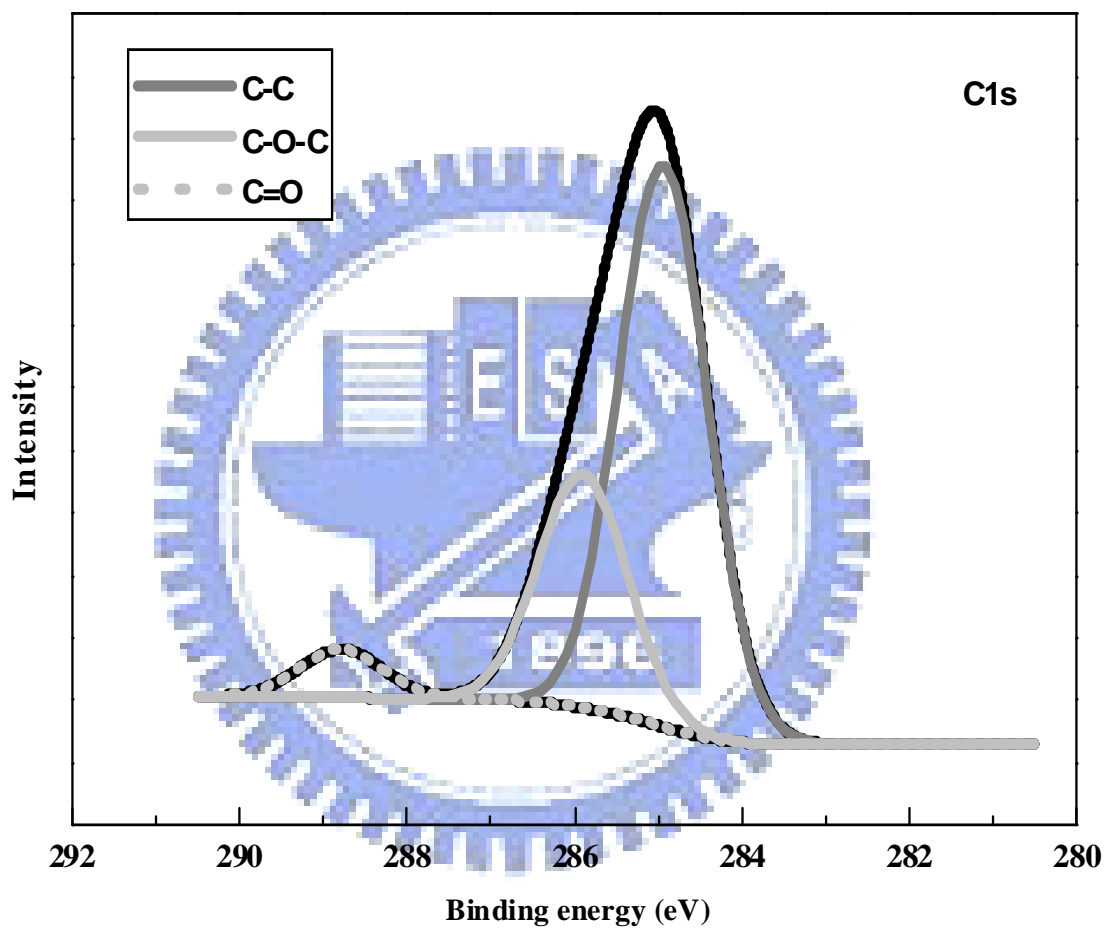


Figure 4.11 The XPS C 1s spectra of untreated BAPP-ODPA polyimide films

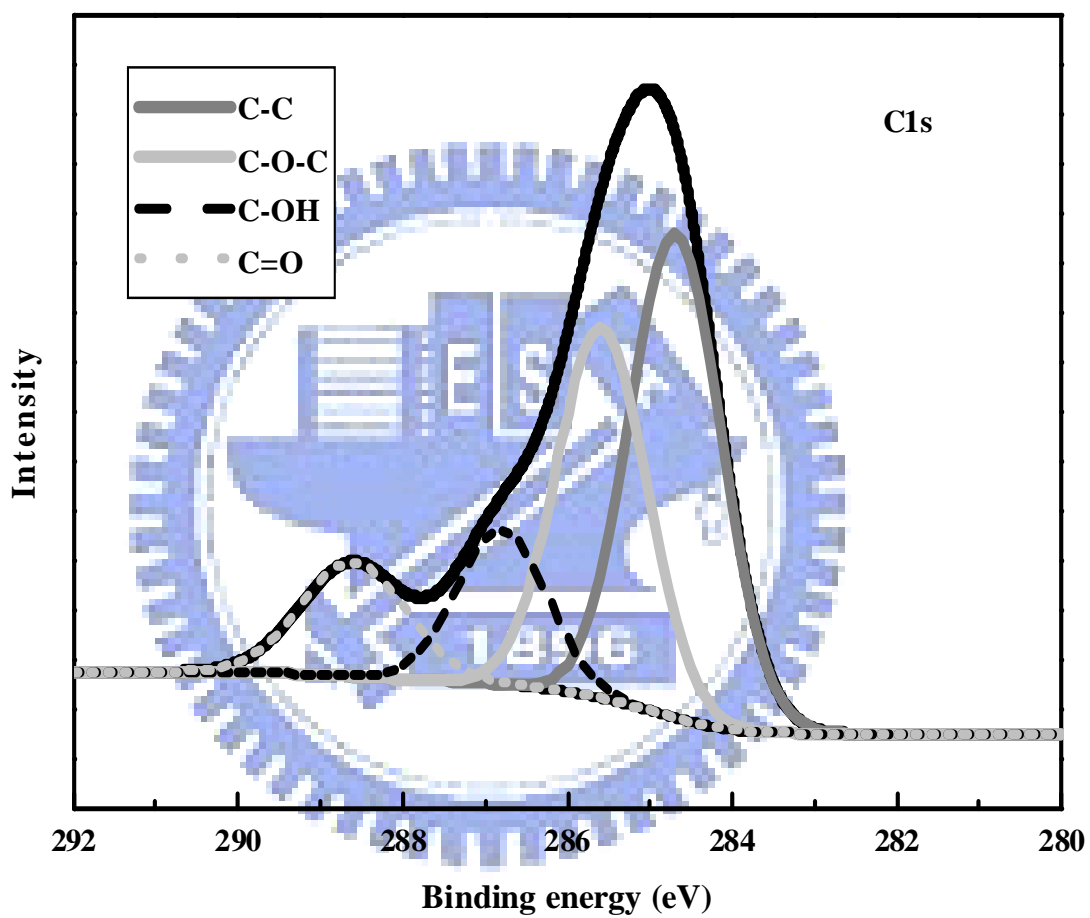


Figure 4.12 The XPS C 1s spectra of BAPP-ODPA polyimide film plasma modified at a RF power of 50W.

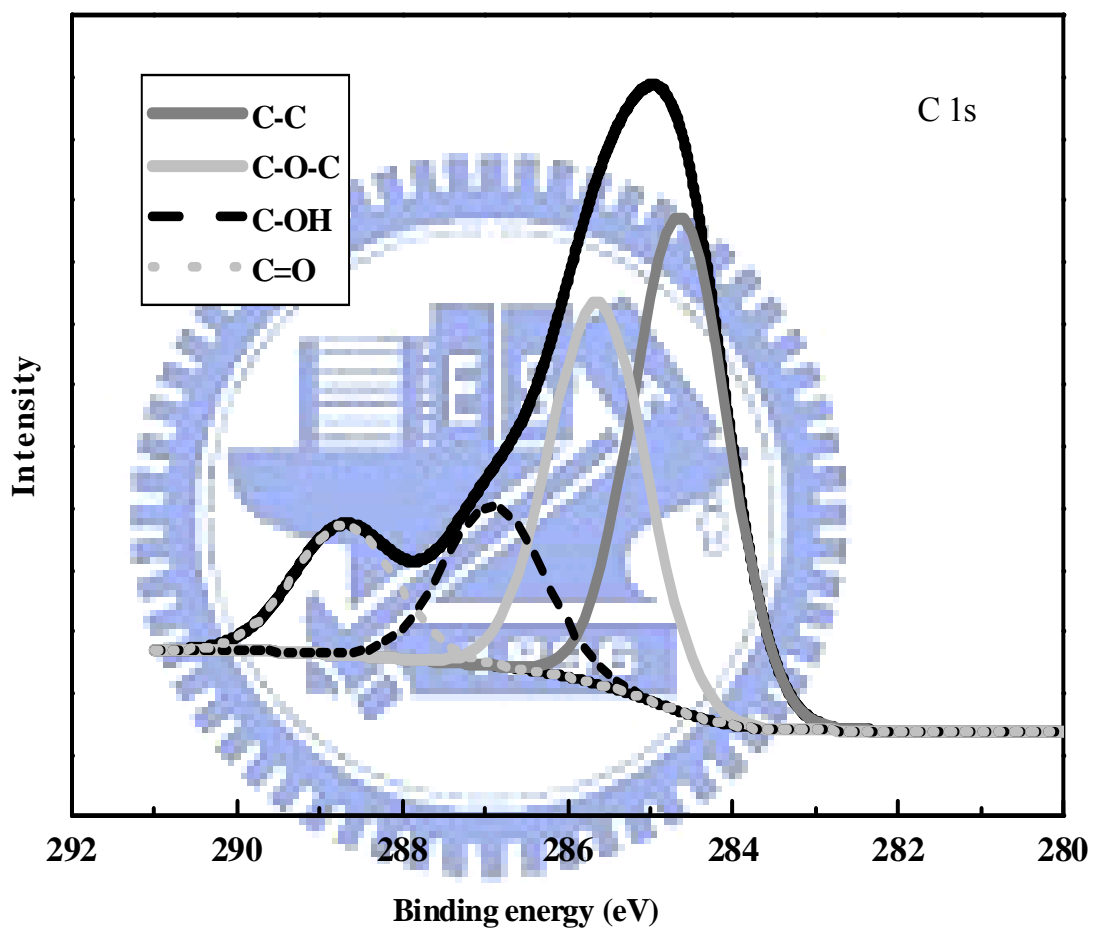


Figure 4.13 The XPS C 1s spectra of BAPP-ODPA polyimide film plasma modified at a RF power of 100W.

Table 4.7 Oxygen 1s spectrum: binding energies and composition quantification of untreated BAPP-ODPA polyimide film.

Component	Peak BE (eV)	Area	%
C-O-C	533.29	3550.97	43.1
C=O	531.98	4688.05	56.9

Table 4.8 Oxygen 1s spectrum: binding energies and composition quantification of BAPP-ODPA polyimide film modified by oxygen plasma at a RF Power of 50W.

Component	Peak BE (eV)	Area	%
C-O-C	533.29	3723.26	23.7
C=O	531.98	4469.17	31.2
C-OH	532.45	7354.04	45.1

Table 4.9 Oxygen 1s spectrum: binding energies and composition quantification of BAPP-ODPA polyimide film modified by oxygen plasma at a RF Power of 100W.

Component	Peak BE (eV)	Area	%
C-O-C	533.29	4085.14	23.2
C=O	531.98	5443.86	29.3
C-OH	532.45	8042.23	47.5

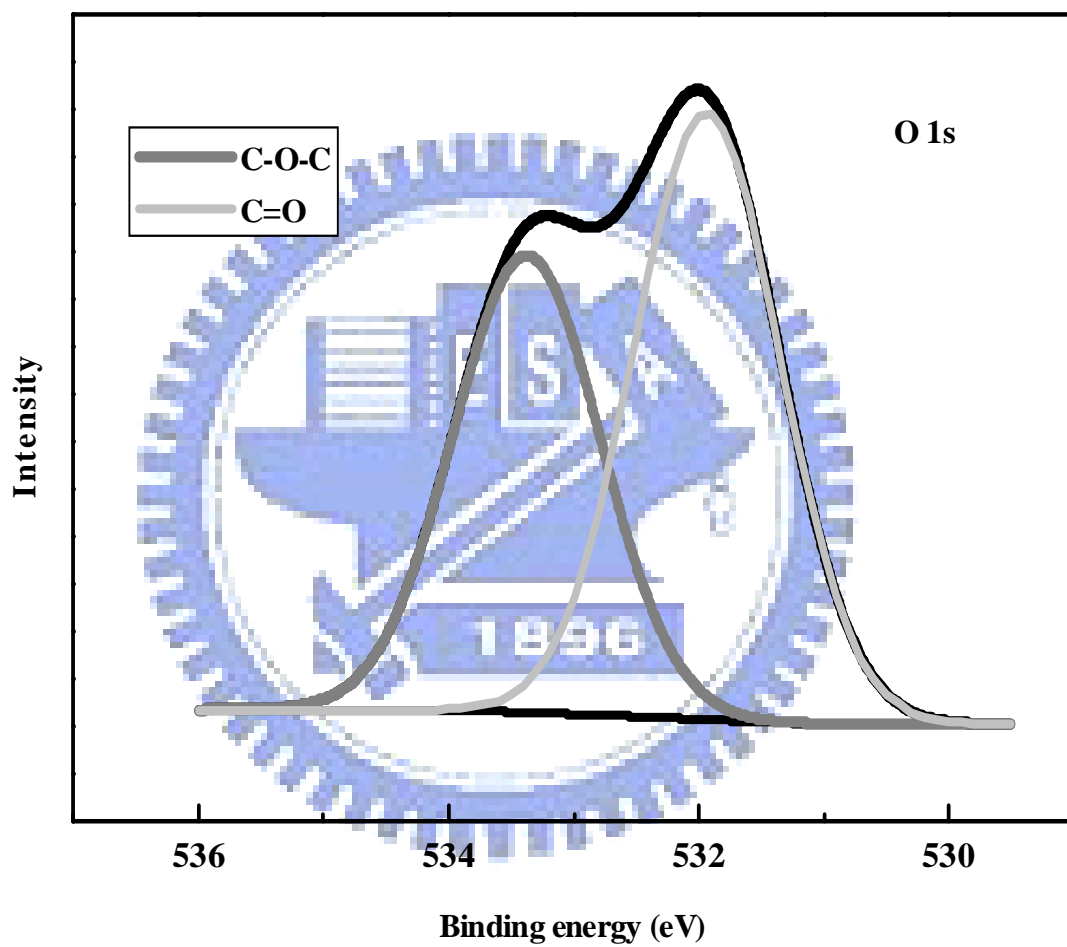


Figure 4.14 The XPS O 1s spectra of untreated BAPP-ODPA polyimide films

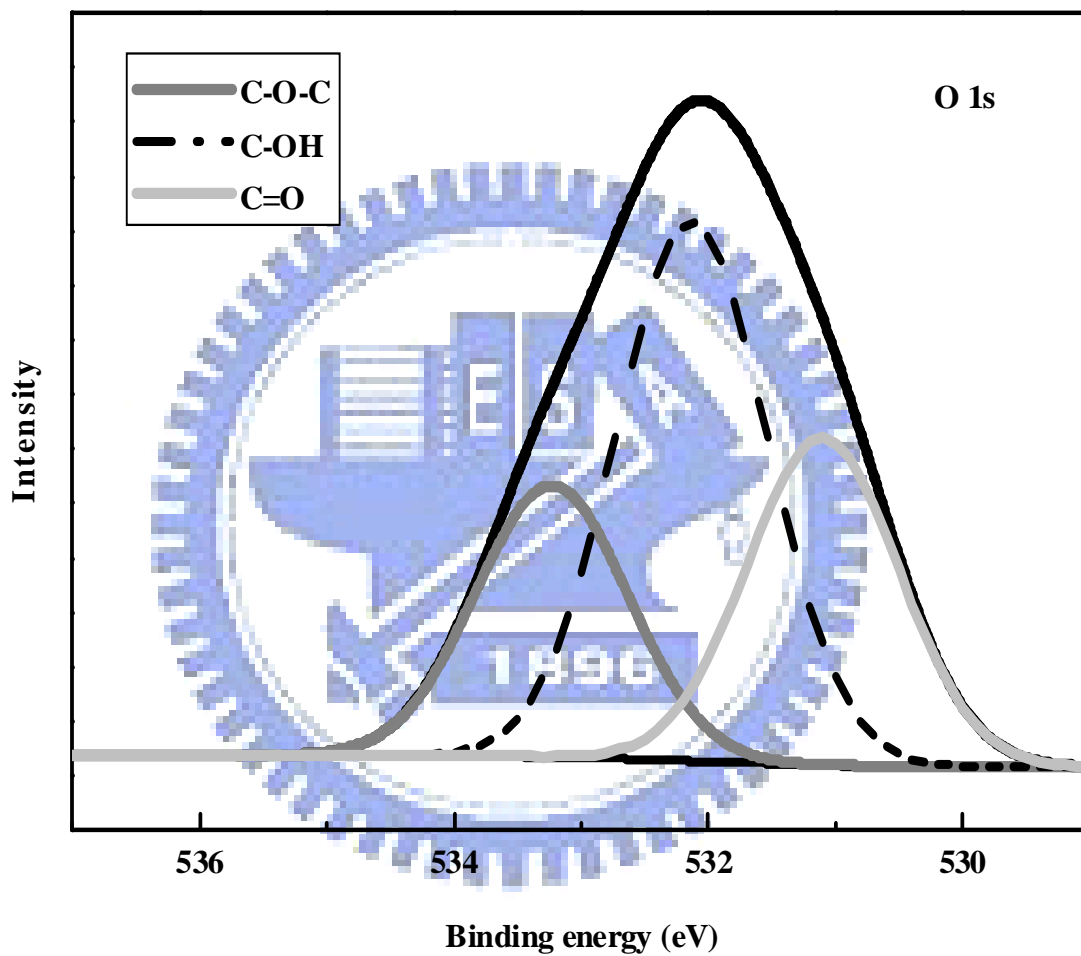


Figure 4.15 The XPS O 1s spectra of BAPP-ODPA polyimide film at a RF power of 50W.

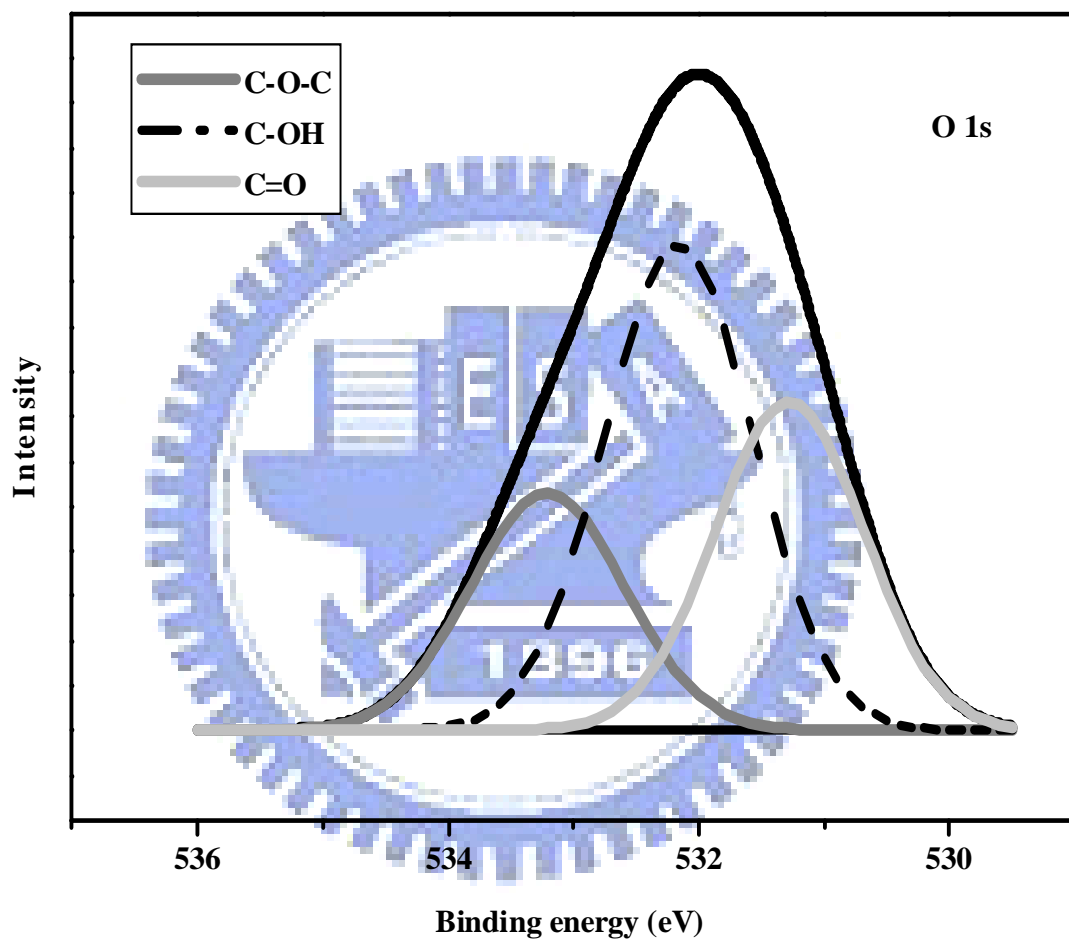


Figure 4.16 The XPS O 1s spectra of BAPP-ODPA polyimide film at a RF power of 100W.

4.3 Adhesion of ITO/Polyimide Interface

Next, the adhesion strength between ITO and BAPP-ODPA polyimide was investigated using 4-point bending test. The effect of plasma surface modification of polyimide on the adhesion at ITO/polyimide interface was addressed. The fracture resistance of the interface, G_c , which was defined as the adhesion strength at ITO/untreated BAPP-ODPA polyimide interface, could be calculated from the Eq. 3.1. The critical load, P_c , was obtained from the load-displacement curve under four-point bending test as shown in Figure 4.17. However, the identification of fracture interface of samples after testing was critical to ensure correct measurement. Figures 4.18 (a)-(c) showed the fractured surface of three separate ITO/PI/epoxy/Si samples. Upon a successful 4-point bending test, the surface morphology of ITO film was shown by a photograph in Figure 4.18 (a), while the opposite side *i.e.* BAPP-ODPA polyimide film was shown by a photograph in Figure 4.18(b). Their identities were further confirmed by a simple multi-meter based on their electric conduction. Figure 4.18 (c) showed a fracture interface at epoxy resin, which was not a valid 4-point bending measurement. Combining optical inspection and electric conduction test of fractured interfaces, the locus of fracture was determined to be at ITO/BAPP-ODPA polyimide interface, instead of epoxy resin or other interface. The adhesion strength values shown for five reasonable samples which the interface made sure between ITO and BAPP-ODPA polyimide prepared for plasma treatment in different RF power as listed in Table 4.10. The average and standard deviation values for three different RF power of samples with ITO/ polyimide interface delamination were as illustrated by Figure 4.19 and showed in Table 4.11. The measured fracture energies of relevant interfaces were 3.0 J/m^2 , 8.0 J/m^2 and 8.7 J/m^2 for untreated BAPP-ODPA polyimide/ITO, BAPP-ODPA polyimide (modified by oxygen plasma at RF Power of 50W)/ITO and BAPP-ODPA polyimide

(modified by oxygen plasma at RF Power of 50W)/ITO interfaces, respectively. Hence, the interfacial adhesion strength increased with increasing of RF power. In this study, the results showed BAPP-ODPA polyimide had the low adhesion strength to the ITO. But the interfacial strength could be improved by oxygen plasma surface modification.

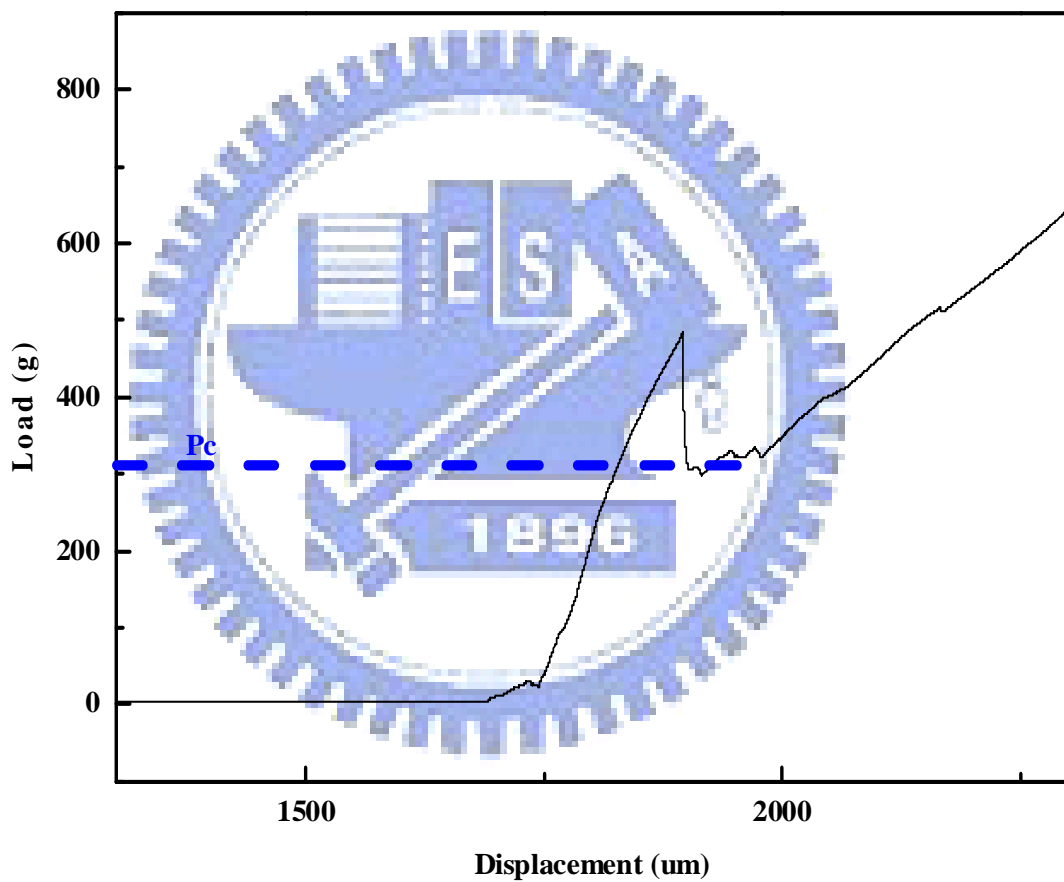
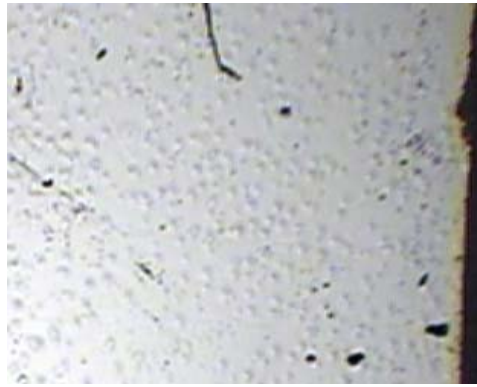
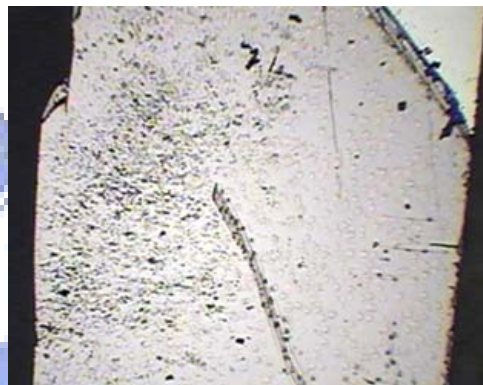


Figure 4.17 Load-displacement graph of ITO/untreated PI sample under 4-point bending test



(a)



(b)



(c)

Figure 4.18 Surface morphology of (a) ITO (b) BAPP-ODAP polyimide thin film (c) Epoxy resin in samples after 4-point bending test

Table 4.10 The critical loads and adhesion strength of various ITO/BAPP-ODPA polyimide samples (untreated and plasma-treated) based on 5 valid measurement data

Parameters of oxygen plasma	Untreated		50W		100W	
	P _c	G _c	P _c	G _c	P _c	G _c
Critical load P _c : g	350.88	3.19	575.26	8.58	550.42	7.86
	325.62	2.75	525.92	7.17	580.62	8.74
	320.06	2.65	573.26	8.52	590.03	9.03
Adhesion strength G _c : J/m ²	380.54	3.75	550.00	7.84	600.40	9.35
	360.32	3.36	530.45	7.30	575.87	8.60

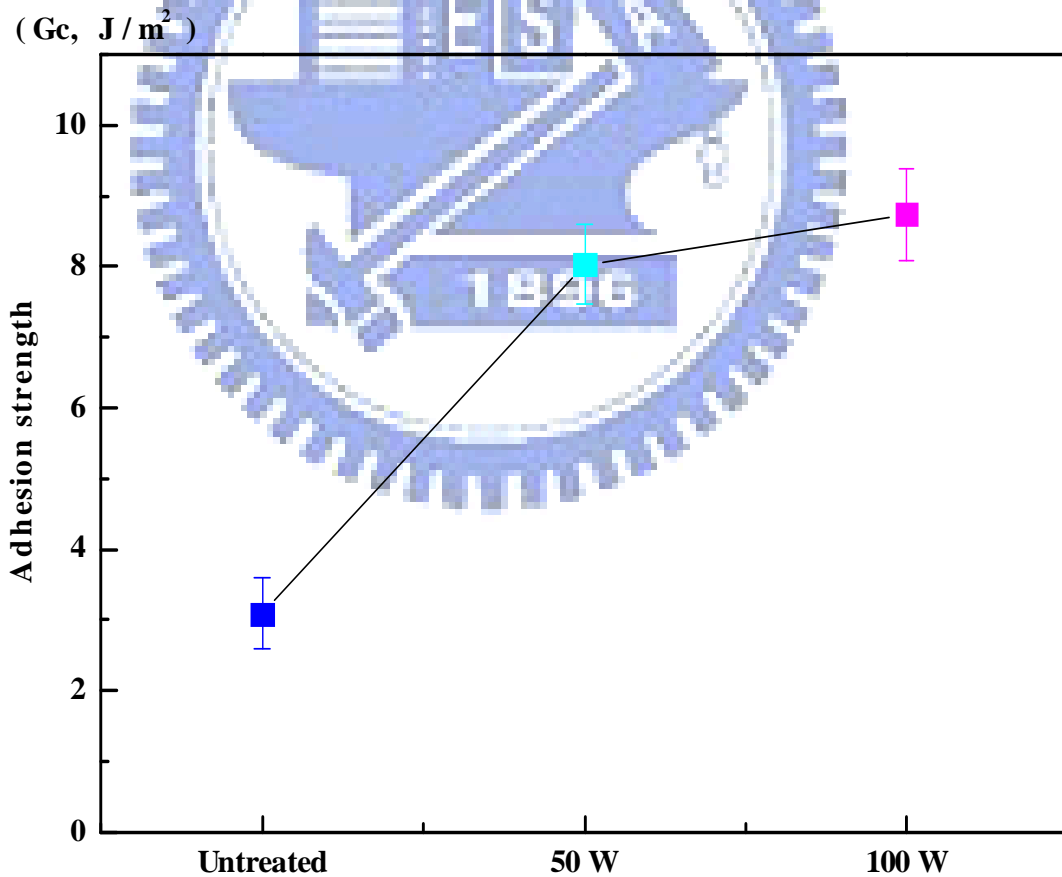


Figure 4.19 Adhesion strength values for ITO/untreated BAPP-ODPA and for ITO/plasma-treated BAPP-ODPA samples

Table 4.11 The average and standard deviation values for three different ITO/PI samples

Sample	G_c (J/m ²)
Untreated PI	3.1 ± 0.5
P : 50 W	8.0 ± 0.6
P : 100 W	8.7 ± 0.6

4.4 Discussion

4.4.1 Characteristic properties of BAPP-ODPA polyimide

4.4.1.1 Transparency

The key factors affecting the coloration of polyimide were two folds: (1) The charge of π electrons in diamine was transferred to dianhydride inter-molecularly and intra-molecularly (2) It had higher light absorption at 400 nm due to the conjugation of benzene rings in stacked packing. [6] The most familiar method was to vary the molecular structure so as to separate the diamine and dianhydride in different polymer chains. For the purpose, it could reduce the charge transferred and destroy the conjugation of benzene rings in stacked packing to obtain transparent polyimide. Hence, it was very important to choose the applicable monomers for synthesizing transparent polyimides. In the thesis, the BAPP was chosen as a monomer due to its alkyl group (H₃C-C-C₃H) as bulky block to destroy the benzene structures stack and efficiently decrease the charge transferred. However, the BAPP and ODPA both had the ether linkage in their structure. The function of ether linkage made the polyimide more flexibility and easily manufactured. Another advantage of the ether linkage could decrease the charge transfer because its structure had presented 106 °C so as to be bulky group. Figure 4.20 had showed the obviously different molecular structures between

commercial and BAPP-ODPA polyimide. According to the experimental data, the transparency certainly had improved. This can be attributed to the hindrance and decreased stacking degree resulting from the ether linkage, the insertion of the bulky group or side chain in BAPP and ODPA. Commercial polyimide (ex. PMDA-(44')BP) generally exhibited lower optical transparency and intense yellow color. [reference]

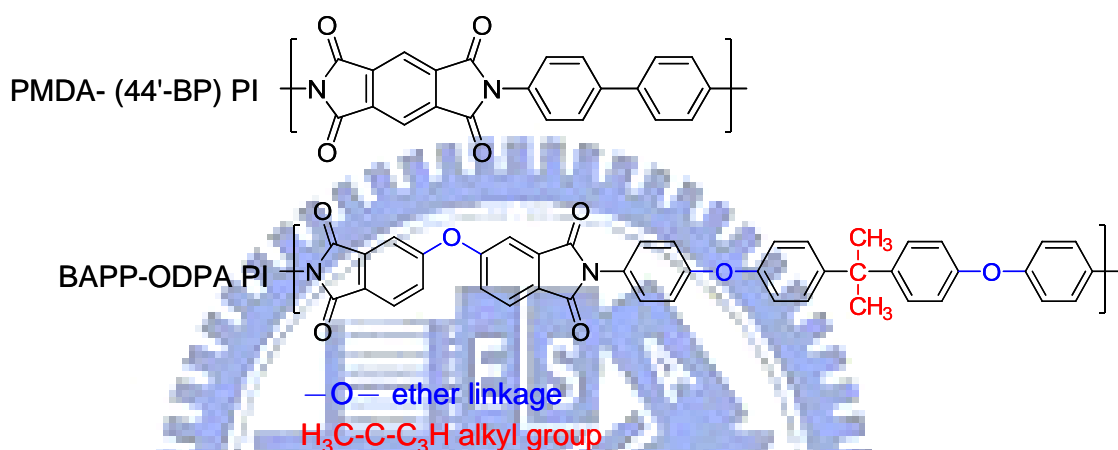


Figure 4.20 The different molecular structures between commercial and transparent PI.

4.4.1.2 Thermal stability

Slightly lower T_g values for the BAPP-ODPA polyimide in comparison with commercial polyimide might be a result of reduced chain-chain interaction and increased free volume due to ether linkage and alkyl group. The T_g value of the BAPP-ODPA polyimide was 230°C, and diamine components, and decreasing due the flexibility of the polymer backbones and bulky block. In order to obtain the high transmission rate, the thermal property such as T_g was compromised. Nevertheless, the TGA data shown that the T_d value of BAPP-ODPA polyimide about 495 °C and left more than a 50 % char yield at 610 °C in nitrogen. The TGA data indicated that BAPP-ODPA polyimide still possessed excellent thermal stability in spite of its relative low T_g of 230 °C.

4.4.1.3 Transparency vs. Thermal stability

Although BAPP-ODPA polyimide had high transparent, the Tg of BAPP-ODPA polyimide was lower than other transparent polyimide. According to Hasanain *et al.* [53] reported, DDS-6FDA and ODA-BTDA polyimides had high Tg at 254 and 276 °C. The Tg of BAPP-ODPA polyimide was 230 °C which was lower than the past report. The reason was attributed that BAPP-ODPA polyimide possessed more ester linkage to make polyimide more flexibility and decreased the Tg. We could see the different polyimides structures as showed in Figure 4.21. The BAPP-ODPA absolutely possessed more ester linkage. In terms of the literature reviews and experimental results, though BAPP-ODPA polyimide had high transparent, the Tg was lower than other transparent polyimide due to ester linkage to decrease Tg.

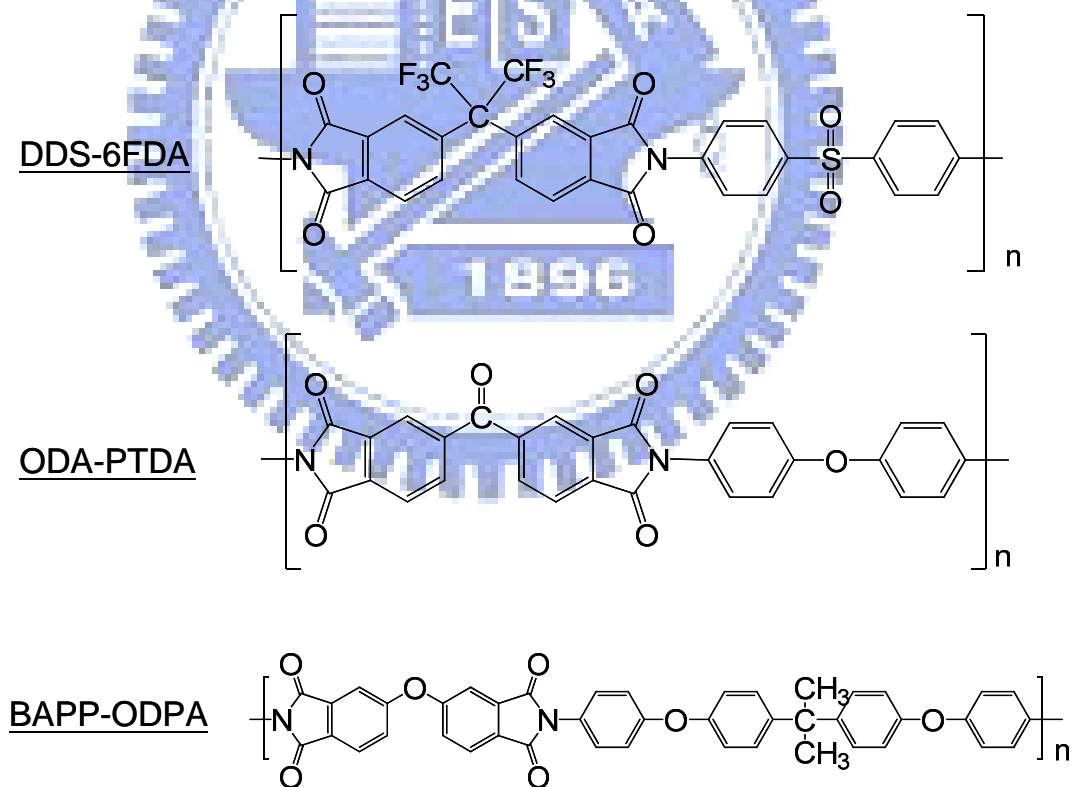


Figure 4.21 The different polyimides' structures : DDS-6FDA, ODA-PTDA, and BAPP-ODPA polyimides.

4.4.2 Surface chemical states of BAPP-ODPA polyimide

The component ratios (relative ratios of components on the surface within the XPS region) of the BAPP-ODPA polyimide surface after modification by oxygen plasma treatment of various RF power were calculated from the integral intensities of the peaks of each component and shown in Table 4.12 for C 1s spectra and Table 4.13 for O 1s spectra.

Several reaction mechanisms of surface chemical states modified by plasma treatment were proposed and illustrated in Figure 4.22. The reaction mechanisms were proposed based on their each bonding energy listed in Table 4.14. [65-68]

Reaction 1: The C-N bond was broken and the process was the selective binding of hydroxyl to carbon, leading to the formation of a new functional group, C-OH as evidenced from new XPS peak. This reaction path led to an increase of C-OH.

Reaction 2: The ether linkage was broken into two parts. One was to form a functional group, C-OH as evidenced from new XPS peak. The other to form a carbonyl group because the C-O-C became C=O with a free radical by oxygen plasma and the free radical had resonance with carbon in the benzene. [64] However, the component ratio of C-O-C decreased, while the C-OH and C=O both increased in the reaction path.

Reaction 3: The alkyl group was broken the methyl to form the lone pair of carbon element, but the lone pair of C might be bonded with hydroxyl to form C-OH. At all events, the component ratio of C-OH increased, while C-C decreased.

In the C 1s signal, the component ratio of C-C decreased from 66.8% in the un-treat PI film to 42.5 and 41.5% when the RF power was 50w and 100w. The reason was the alkyl group broken up and the results had been explained by Reaction 3 in Figure 4.22. Table 4.14 [65-67] listed the binding energies of typical chemical bonds and proposed surface reaction mechanisms in BAPP-ODPA polyimide thin films

modified by oxygen plasma could be judge by it. XPS was detected to the different atom bond with carbon and the C-C and C=O had easier broken than C-O-C depended on different degrees of bond energy as listed at Table 4.14. When the decreased ratio of C-C and C=O had contributed to generate the C-OH, the C-O-C could be observed to have the slight increased. However, the component ratio of C-OH had increased with the RF power. The proposed reason was that all the reaction paths mechanisms helped C-OH increased from 0 to 14.3% showed in the Figure 4.19.

In the O 1s signal, the component ratio of C-O-C had decreased from 43.1% in the untreated PI film to 23.7 and 23.2% when the RF power was 50w and 100w. The results could be explained by Reaction 2 due to the ether linkage broken up. The C=O, as the same, had decreased from 56.9% to 31.2 and 29.3%. The formation of C=O due to electric resonance might explain the results as the Reaction 2. The results of C-OH increased in the O 1s signal was the same with the construction in the C 1s signal. Furthermore, the C-OH in the O 1s had a great increased from 0% to 45.1 and 47.5%. According to above the results, the surface chemical states of BAPP-ODPA polyimide thin films had certainly modified by oxygen plasma treatment.

Table 4.12 The component ratios of BAPP-ODPA polyimide surface of untreated film and modified films under various conditions in carbon 1s.

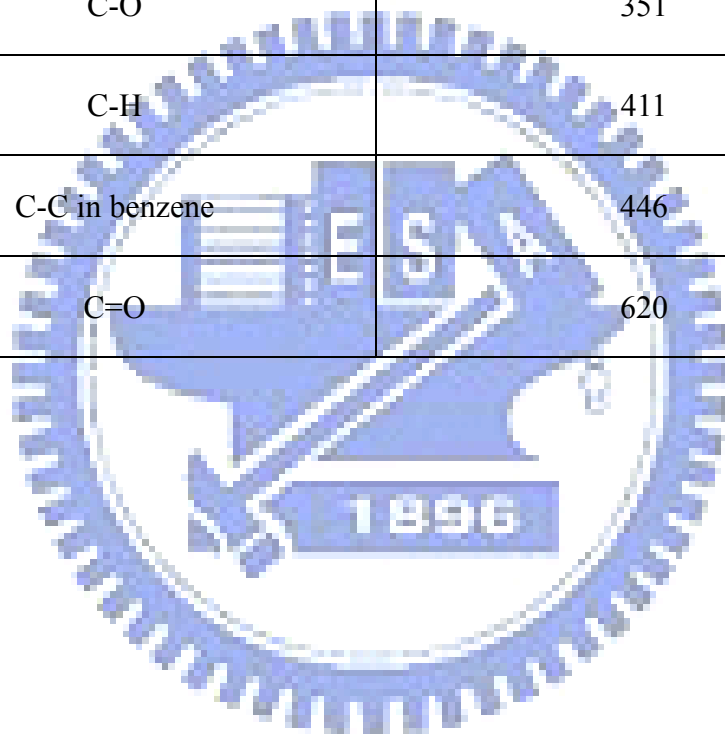
Unit : %	Untreated	50 W	100 W
C-C	66.8	42.5	41.5
C-O-C	27.9	33.5	32.5
C=O	5.3	12.5	11.7
C-OH	0	11.5	14.3

Table 4.13 The component ratios of BAPP-ODPA polyimide surface of un-treat film and modified films under various conditions in oxygen 1s.

Unit : %	Un-treated	50 W	100 W
C-O-C	43.1	23.7	23.2
C=O	56.9	31.2	29.3
C-OH	0	45.1	47.5

Table 4.14 Binding energies of typical chemical bonds.

Bond	Bond Energy (kJ/mole)
C-N	305
C-C	347
C-O	351
C-H	411
C-C in benzene	446
C=O	620



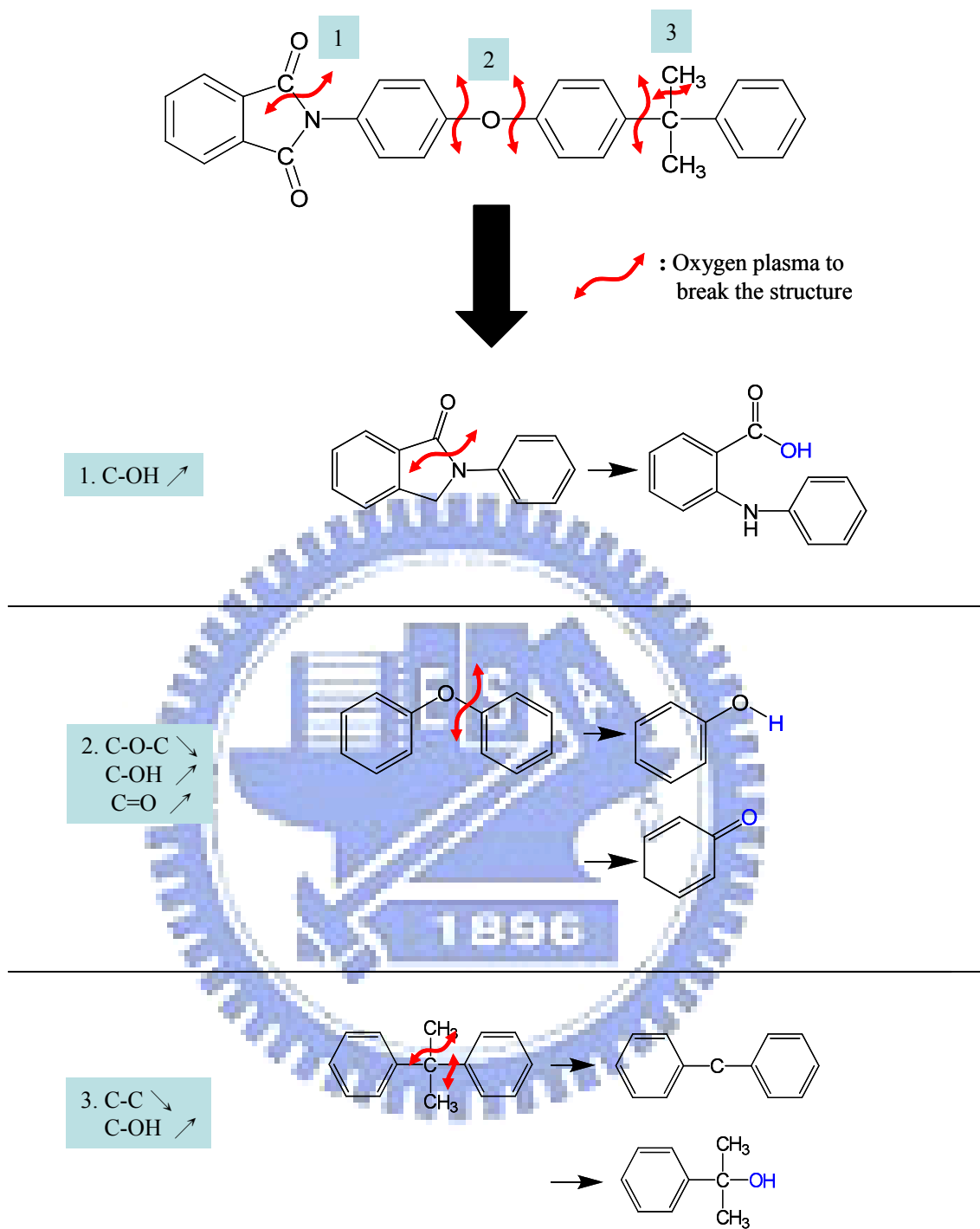


Figure 4.20 Proposed surface reaction mechanisms in BAPP-ODPA polyimide thin films were modified by oxygen plasma.

4.4.3 Surface chemical states vs. interfacial adhesion

Excellent correlation between the adhesion of ITO/BAPP-ODPA polyimide interface and the content of surface C-OH bonding was found for untreated and O₂-plasma treated BAPP-ODPA polyimide films. Based on the surface chemical states from XPS and interfacial adhesion summarized in Table 4.14, the interfacial adhesion strength showed improvement with increasing C-OH bond after O₂-plasma surface modification. However, neither attraction force between positively/ negatively charged each other nor sharing of pairs of electrons between atoms could be accountable for such significant improvement in adhesion strength, hence, the bonding force between C-OH and the metal (Sn and In) in ITO was attributed to not only the ionic bond but also covalent bond. Based on these results, a coordinate covalent bonding was expected to form between metal in ITO and C-OH, in addition to the bonding and interaction between ITO and untreated BAPP-ODPA polyimide.

Example: $\text{Metal} \leftarrow \text{:X}$ (X is N, O etc.)

A coordinate covalent bond was a description of covalent bonding between two atoms in which both electrons shared in the bond come from the same atom. The distinction from ordinary covalent bonding is artificial, but the terminology is popular in textbooks, especially those describing coordination compounds. Once the bonds have been formed using this, its strength and description is no different from that of other polar covalent bonds. [68]

The oxygen element in the C-OH provided a lone pair as donor to attract that the metal element (In, Sn) in ITO provided empty orbit as acceptor. Therefore, we could say that the attraction force had existed between ITO and C-OH. The force was attributed to the coordinate covalent bond and the force indeed had improved the

adhesion by oxygen plasma treatment.

Table 4.14 The component ratios of C-OH in C and O 1s versus adhesion strength

Component ratio		RF power of oxygen plasma		
		Un-plasma-treat BAPP-ODPA PI	50W	100W
C-OH	C 1s	0	11.5%	14.3%
	O 1s	0	45.1%	47.5%
Adhesion strength (J/m ²)		3.1 ± 0.5	8.0 ± 0.6	8.7 ± 0.5

Chapter 5 Conclusions

With the invention of conducting polymers, trend for flexible devices has extended into optoelectronics and; for example, involving the organic polymers for organic light-emitting diode (OLED) and flexible OLED (FOLED) applications, organic transistor for RFID (radio-frequency identification) applications, or even organic solar cell such as DSSC, which are still in the infancy stage. While these materials offer many attractive features, they also impose limitations and challenges such as high CTE, lower T_g, low processing temperatures, adhesive strength in multiple films stacking (with barrier, hard coat, or conductive transparent oxides), high O₂ and water permeation, and device degradation.

A novel and transparent polyimide has been synthesized via a straightforward, high-yielding two-step thermal imidization method. In the thesis, the polyimide was prepared by using 4,4'-oxydiphthalic anhydride (ODPA) and 2,2'-bis[4-(4-aminophenoxy)phenyl]propane (BAPP) in N,N-Dimethyl-acetamide. FTIR analysis showed that condensation reaction led to dehydrate and transform poly(amic-acid) into polyimide. The transparency of the BAPP-ODPA polyimide in the visible region was found to be 98 % when the thickness of polyimide was 80 μm because the ether linkage and bulky group destroyed benzene stacking to minimize or eliminate charge transfer and the light absorption by benzene rings.

Moreover, the BAPP-ODPA polyimide demonstrated superior thermal stability with T_d at 495 °C. The glass transition temperature of BAPP-ODPA was 230°C primarily resulting from the flexible ether linkage and alky group in the backbone, which was a tradeoff between transmittance and mechanical rigidity. In summary, BPPA-ODPA with T_g about 230 °C, high optical transparency, and excellent thermal stability is an excellent polymer substrate for flexible devices applications.

In the other hand, the adhesive strength between ITO and BAPP-ODPA polyimide had been investigated in order to improve the reliability of flexible devices. The surface of polyimide was modified by oxygen plasma in the different RF power and the changes of surface chemical states were characterized by XPS. The interfacial adhesive strength was determined by four-point bending system and the adhesive values shown for a large number of samples had prepared for plasma treatment in different RF power. The electric conductive of ITO and PI films measured by circuit tester were used to judge whether the crack interface occurred at the ITO/PI interface or not. According to the experimental results, the adhesion between ITO and BAPP-ODPA polyimide had improved from 3.01 to 8.7 J/m² due to the component ratio of C-OH increased from 0 to 47.5%. The force of coordinate covalent bond was explained to help the improvement of adhesion. Because the oxygen element in C-OH bond provided a lone pair as donor to attract the metal elements in ITO structure, the interfacial adhesive strength between ITO and BAPP-ODPA polyimide had definitively improved.

In the thesis, we had successfully developed a high T_g and transparent of BAPP-ODPA polyimide. Furthermore, its adhesive strength with ITO had improved by oxygen plasma. The BAPP-ODPA polyimide had excellent thermal properties, high transparency and outstanding reliability; however, it could be applied in flexible devices such as solar cell, e-paper, display, and RFID, etc.

References

- [1] C. J. Brabec, N. S. Sariciftci, and J. C. Hummelen, *Adv. Funct. Mater.* **11**, 1 (2001).
- [2] E. Abada, S. Zampolli, S. Marroc, A. Scorzoni, B. Mazzolai, A. Juarros, D. Gómez, I. Elmi, G. C. Cardinali, J. M. Gómez, F. Palacio, M. Cicioni, A. Mondini, T. Becker, and I. Sayhan, *Sensors and Actuators B.* **127**, 2 (2007).
- [3] F. X. Qiu, Y. M. Zhou, and J. Z. Liu, *Eur. Polym. J.* **40**, 713 (2004).
- [4] P. C. Chiang and W. T. Whang, *Polymer* **44**, 2249 (2003).
- [5] I. K. Spiliopoulos and J. A. Mikroyannidis, *Polymer* **37**, 3331 (1996).
- [6] T. Yamamoto, T. Morikita, T. Maruyama, K. Kubota, and M. Katada, *Macromolecules* **30**, 5390 (1997).
- [7] T. Ade and H. Fukuro, *J. Synth. Org. Chem.* **49**, 506 (1991).
- [8] M. Asegawa, N. Nsui, Y. Hindo, and R. Okota, *Photopolym. Sci. Technol.* **9**, 2 (1996).
- [9] G. Lawton, *Computer* **39**, 1 (2008).
- [10] A. Sugimoto, H. Ochi, S. Fujimura, A. Yoshida, T. Miyadera, and M. Tsuchida, *IEEE Journal of Selected Topics in Quantum Electronics* **1**, 10 (2004).
- [11] C. C. Wu, S. D. Theiss, G. Gu, M. H. Lu, J. C. Sturm, S. Wagner, and S. R. Forrest, *IEEE Electron Device Lett.* **18**, 12 (1997).
- [12] S. E. Shaheen, C. J. Brabec, N. S. Sariciftci, Franz Padinger, T. Fromherz, and J. C. Hummelen, *Appl. Phys. Lett.* **78**, 6 (2001).
- [13] K. Nomura, H. Hideo, A. Takagi, T. Kamiya, M. Hirano, and H. Hosono, *NATURE* **432**, 25 (2004).
- [14] Y. Li, L. W. Tan, X. T. Hao, K. S. Ong, and F. Zhu, *Appl. Phys. Lett.* **86**, 153508 (2005).
- [15] E. L. Bedia, S. Murakami, T. Kitade, and S. Kohjiya, *Polymer* **42**, 7299 (2001).

- [16] J. Si and T. Mitsuyu, *Appl. Phys. Lett.* **72**, 762 (1998).
- [17] A. Miyake, T. Yamada, H. Makino, N. Yamamoto, and T. Yamamoto, *Thin Solid Films* **517**, 1037 (2008).
- [18] H. Suzuki, T. Abe, K. Takaishi, M. Narita, and F. Hamada, *J Polym Sci Part B: Polym Phys.* **38**, 1 (2000).
- [19] F. Wu, N. Deng, and H. Hua, *Chemosphere* **41**, 1233 (2000).
- [20] P. E. Burrows, G. L. Graff, M. E. Gross, P. M. Martin, M. K. Shi, M. Hall, E. Mast, C. Bonham, W. Bennett, and M. B. Sullivan, *Display* **22**, 65 (2001).
- [21] C. D. Sheraw, L. Zhou, J. R. Huang, D. J. Gundlach, T. N. Jackson, M. G. Kane, I. G. Hill, M. S. Hammond, J. Campi, B. K. Greening, *Appl. Phys. Lett.* **80**, 1088 (2002).
- [22] C. J. Drury, C. M. J. Mutsaers, C. M. Hart, M. Matters, and D. M. de Leeuw, *Appl. Phys. Lett.* **73**, 108 (1998).
- [23] G. Binnig, M. Despont, U. Drechsler, W. Häberle, M. Lutwyche, P. Vettiger, H. J. Mamin, B. W. Chui and T. W. Kenny, *Appl. Phys. Lett.* **74**, 1329 (1999).
- [24] H. Ito, W. Oka, H. Goto, and H. Umeda, *Jpn. J. Appl. Phys.* **45**, 4325 (2006).
- [25] S. Elomari, M. D. Skibo, A. Sundarajan, H. Richard, *Compos. Sci. Technol.* **58**, 369 (1998).
- [26] J. Xu, L. Yu, Y. Azuma, T. Fujimoto, H. Umehara, and I. Kojima, *Appl. Phys. Lett.* **81**, 4139 (2002).
- [27] G. Maier, *Prog. Polym. Sci.* **26**, 3 (2001).
- [28] R. A. Dine-Hart and W. W. Wright, *Makromol. Chem.* **143**, 189 (1971).
- [29] S. Ando, T. Matsuura, and S. Sasaki, *Polym. J.* **29**, 69 (1997).
- [30] M. Hasegawa and K. Horie, *Prog. Polym. Sci.* **26**, 259 (2001).
- [31] S. Ando, Y. Terui, Y. Aiki, and T. Ishizuka, *J. Photopolym. Sci. Technol.* **18**, 233

- (2005).
- [32] W. Volksen, H. J. Cha, M. I. Sanchez, and D. Y. Yoon, *React. Funct. Polym.* **30**, 61 (1996).
- [33] T. Matsumoto and T. Kurosaki, *Macromolecules*, **30**, 993 (1997).
- [34] T. Matsumoto, *Macromolecules*, **32**, 4933 (1999).
- [35] H. Seino, A. Mochizuki, and M. Ueda, *J. Polym. Sci. Part A: Polym. Chem.* **37**, 3584 (1999).
- [36] J. Li, J. Kato, K. Kudo, and S. Shiraishi, *Macromol. Chem. Phys.* **201**, 2289 (2000).
- [37] M. Goyal, T. Inoue, M. A. Kakimoto, and Y. Imai, *J. Polym. Sci. Part A: Polym. Chem.* **36**, 39 (1998).
- [38] H. Suzuki, T. Abe, K. Takaishi, M. Narita, and F. Hamada, *J. Polym. Sci. Part A: Polym. Chem.* **38**, 108 (2000).
- [39] J. Yin, W. Zhang, H. J. Xu, J. H. Fang, Y. Sui, Z. Zhu, and Z. G. Wang, *J. Polym. Sci. Part A: Polym. Chem.* **40**, 524 (2002).
- [40] C. P. Yang, S. H. Hsiao, and M. F. Hsu, *J. Polym. Sci. Part A: Polym. Chem.* **40**, 524 (2002).
- [41] D. Wolany, T. Fladung, L. Duda, J. W. Lee, T. Gantenfort, L. Wiedmann, and A. Benninghoven, *Surf. Interface Anal.* **27**, 609 (1999).
- [42] P. N. Sanda, J. W. Bartha, J. G. Clabes, J. L. Jordan, C. Feger, B. D. Silverman, and P. S. Ho, *J. Vac. Sci. Technol. A* **4**, 1035 (1985).
- [43] R. Haight, R. C. White, B. D. Silverman, and P. S. Ho, *J. Vac. Sci. Technol. A* **6**, 2188 (1988).
- [44] Y. Nakamura, Y. Suzuki, and Y. Watanabe, *Thin Solid Films* **290**, 367 (1996).
- [45] Y. S. Lin, H. M. Liu, and H. T. Chen, *J. Appl. Polym. Sci.* **99**, 744 (2006).

- [46] K.L. Mittal, Adhesion Measurement of Films and Coatings. The Netherlands (1995).
- [47] Y. S. Thio, A. S. Argon, and R. E. Cohen, *Polymer*, **45**, 3139 (2004).
- [48] I.B. Yoon, *Jpn. J. Appl. Phys.* **2**, 849 (1974).
- [49] X. Li, B. Bhushan, K. Takashima, C.W. Baek, and Y.K. Kim, *Ultramicroscopy*, **97**, 481 (2003).
- [50] A. A. Volinsky, N.R. Moody, and W. W. Gerberich, *Acta Mater.* **50**, 441 (2002).
- [51] X. Dai, Dissertation of The University of Texas at Austin, 1998.
- [52] X. Li, T. Abe, and M. Esashi, *Sensors and Actuators A*, **87**, 139 (2001)
- [53] F. Hasanaina and Z. Y. Wang, *Polymer* **49**, 831 (2008)
- [54] M. Lane, *Ann. Rev. Mater. Res.* **33**, 27 (2003).
- [55] G. Beamson and D. Briggs, *Chichester* 184 (1992).
- [56] M. R. Elizalde, J. M. Sáncheza, J. M. Martínez-Esnaola, D. Pantuso, T. Scherban, B. Sun, and G. Xu, *Acta Mater.* **51**, 4295 (2003).
- [57] W. H. Lin, R. H. Vora, and T. S. Chung, *J. Polym. Sci. Part B: Polym. Phys.* **38**, 2703 (2000).
- [58] T. Aarii, A. Kishi, and Y. Kobayashi, *Thermochim. Acta* **325**, 151 (1999).
- [59] H. Janseny, H. Gardeniers, M. de Boer, M. Elwenspoek, and J. Fluitman, *J. Micromech. Microeng.* **6**, 14 (1996).
- [60] C. C. Chang, *Surf. Sci.* **25**, 53 (1971).
- [61] T. K. Lin, Dissertation of the University of Science and Technology Yunlin at Taiwan, 2003.
- [62] R. W. M. Kwok, Ph. D. Dissertation: Fabrication of InP MISFET. Canada: Western University of Ontario, 1993.
- [63] L. Wang, Y. Tian, H. Ding, and J. Li, *Eur. Polym. J.* **42**, 2921 (2006).

- [64] D. Wolany, T. Fladung, L. Duda, and J. W. Lee, Surf. Interface Anal. **27**, 609 (1999).
- [65] N. Yasui, H. Nomura, and A. Ide-Ektessabi, Thin Solid Films **447**, 377 (2004).
- [66] M. P. Hughey, D. J. Morris, R. F. Cook, S. P. Bozeman, B. L. Kelly, S. L. N. Chakravarty, D. P. Harkens, and L. C. Stearns, Eng. Fract. Mech. **71**, 245 (2004).
- [67] T. L. Cottrell, The Strengths of Chemical Bonds, 2nd ed. (Butterworths Scientific, London, 1958).
- [68] S. Benson, J. Chem. Educ. **42**, 502 (1965).

